

NONLINEAR DYNAMICS AND SYSTEMS THEORY

An International Journal of Research and Surveys

Volume 22                      Number 4                      2022

CONTENTS

Functional Differential Inclusions with Unbounded Right-hand Side in Banach Spaces.....	355
<i>H. Chouial and M. F. Yarou</i>	
SOF-C-PV System with Storage Battery Based on Cuckoo Search Algorithm .....	367
<i>Hamidia Fethia and Abbad Amel</i>	
Application of Accretive Operators Theory to Linear SIR Model .....	379
<i>Mariam El Hassnaoui, Said Melliani and Mohamed Oukessou</i>	
Design of Navigation and Guidance Control System of Mobile Robot with Position Estimation Using Ensemble Kalman Filter (EnKF) and Square Root Ensemble Kalman Filter (SR-EnKF) .....	390
<i>T. Herlambang, F. A. Susanto, D. Adzkiya, A. Suryowinoto and K. Oktafanto</i>	
On the Dynamics of a Class of Planar Differential Systems .....	400
<i>A. Kina and A. Bendjeddou</i>	
Chaos Synchronization between Fractional-Order Lesser Date Moth Chaotic System and Integer-Order Chaotic System via Active Control.....	407
<i>M. Labid and N. Hamri</i>	
New Design of Stability Study for Linear and Nonlinear Feedback Control of Chaotic Systems .....	414
<i>W. Laouira and N. Hamri</i>	
Control of a Shunt Active Power Filter by the Synchronous Referential Method Connected with a Photovoltaic Solar Energy.....	424
<i>A. Morsli, A. Tlemcani and H. Nouri</i>	
A Neural Network Approximation for a Model of Micromagnetism.....	432
<i>M. Moumni and M. Tilioua</i>	
A New Fractional-Order Three-Dimensional Chaotic Flows with Identical Eigenvalues .....	447
<i>S. Rouar and O. Zehrou</i>	
Estimation of Closed Hotels and Restaurants in Jakarta as Impact of Corona Virus Disease (Covid-19) Spread Using Backpropagation Neural Network .....	457
<i>F. A. Susanto, M. Y. Anshori, D. Rahmalia, K. Oktafanto, D. Adzkiya, P. Katias and T. Herlambang</i>	
Stabilization of Chaotic $h$ -Difference Systems with Fractional Order .....	468
<i>Hasna Youf, Ahlem Gasri and Adel Ouannas</i>	

NONLINEAR DYNAMICS & SYSTEMS THEORY

Volume 22, No. 4, 2022

# Nonlinear Dynamics and Systems Theory

An International Journal of Research and Surveys

**EDITOR-IN-CHIEF A.A.MARTYNYUK**

*S.P.Timoshenko Institute of Mechanics  
National Academy of Sciences of Ukraine, Kiev, Ukraine*

**MANAGING EDITOR I.P.STAVROULAKIS**

*Department of Mathematics, University of Ioannina, Greece*

**REGIONAL EDITORS**

P.BORNE, Lille, France  
M.FABRIZIO, Bologna, Italy  
*Europe*

M.BOHNER, Rolla, USA  
HAO WANG, Edmonton, Canada  
*USA and Canada*

T.A.BURTON, Port Angeles, USA  
C.CRUIZ-HERNANDEZ, Ensenada, Mexico  
*USA and Latin America*

M.ALQURAN, Irbid, Jordan  
*Jordan and Middle East*

K.L.TEO, Perth, Australia  
*Australia and New Zealand*

# Nonlinear Dynamics and Systems Theory

An International Journal of Research and Surveys

## EDITOR-IN-CHIEF A.A.MARTYNYUK

The S.P.Timoshenko Institute of Mechanics, National Academy of Sciences of Ukraine,  
Nesterov Str. 3, 03680 MSP, Kiev-57, UKRAINE / e-mail: journalndst@gmail.com

## MANAGING EDITOR I.P.STAVROULAKIS

Department of Mathematics, University of Ioannina  
451 10 Ioannina, HELLAS (GREECE) / e-mail: ipstav@cc.uoi.gr

## ADVISORY EDITOR A.G.MAZKO

Institute of Mathematics of NAS of Ukraine, Kiev (Ukraine)  
e-mail: mazko@imath.kiev.ua

## REGIONAL EDITORS

M.ALQURAN (Jordan), e-mail: marwan04@just.edu.jo  
P.BORNE (France), e-mail: Pierre.Borne@ec-lille.fr  
M.BOHNER (USA), e-mail: bohner@mst.edu  
T.A.BURTON (USA), e-mail: taburton@olympen.com  
C. CRUZ-HERNANDEZ (Mexico), e-mail: ccruz@cicese.mx  
M.FABRIZIO (Italy), e-mail: mauro.fabrizio@unibo.it  
HAO WANG (Canada), e-mail: hao8@ualberta.ca  
K.L.TEO (Australia), e-mail: K.L.Teo@curtin.edu.au

## EDITORIAL BOARD

Aleksandrov, A.Yu. (Russia)	Jafari, H. (South African Republic)
Artstein, Z. (Israel)	Khusainov, D.Ya. (Ukraine)
Awrejcewicz, J. (Poland)	Kloedon, P. (Germany)
Benrejeb, M. (Tunisia)	Kokologiannaki, C. (Greece)
Braiek, N.B. (Tunisia)	Kouzou, A. (Algeria)
Chen Ye-Hwa (USA)	Krishnan, E.V. (Oman)
D'Anna, A. (Italy)	Limarchenko, O.S. (Ukraine)
De Angelis, M. (Italy)	Okninski, A. (Poland)
Denton, Z. (USA)	Peterson, A. (USA)
Vasundhara Devi, J. (India)	Radziszewski, B. (Poland)
Djemai, M. (France)	Shi Yan (Japan)
Dshalalow, J.H. (USA)	Sivasundaram, S. (USA)
Eke, F.O. (USA)	Sree Hari Rao, V. (India)
Gajic Z. (USA)	Staicu V. (Portugal)
Georgiev, S.G. (France)	Stavarakakis, N.M. (Greece)
Georgiou, G. (Cyprus)	Vatsala, A. (USA)
Herlambang T. (Indonesia)	Zuyev, A.L. (Germany)
Honglei Xu (Australia)	

## ADVISORY COMPUTER SCIENCE EDITORS

A.N.CHERNIENKO and A.S.KHOROSHUN, Kiev, Ukraine

## ADVISORY LINGUISTIC EDITOR

S.N.RASSHYVALOVA, Kiev, Ukraine

## INSTRUCTIONS FOR CONTRIBUTORS

**(1) General.** Nonlinear Dynamics and Systems Theory (ND&ST) is an international journal devoted to publishing peer-refereed, high quality, original papers, brief notes and review articles focusing on nonlinear dynamics and systems theory and their practical applications in engineering, physical and life sciences. Submission of a manuscript is a representation that the submission has been approved by all of the authors and by the institution where the work was carried out. It also represents that the manuscript has not been previously published, has not been copyrighted, is not being submitted for publication elsewhere, and that the authors have agreed that the copyright in the article shall be assigned exclusively to InforMath Publishing Group by signing a transfer of copyright form. Before submission, the authors should visit the website:

<http://www.e-ndst.kiev.ua>

for information on the preparation of accepted manuscripts. Please download the archive Sample\_NDST.zip containing example of article file (you can edit only the file Samplefilename.tex).

**(2) Manuscript and Correspondence.** Manuscripts should be in English and must meet common standards of usage and grammar. To submit a paper, send by e-mail a file in PDF format directly to

Professor A.A. Martynyuk, Institute of Mechanics,  
Nesterov str.3, 03057, MSP 680, Kiev-57, Ukraine  
e-mail: journalndst@gmail.com

or to one of the Regional Editors or to a member of the Editorial Board. Final version of the manuscript must typeset using LaTeX program which is prepared in accordance with the style file of the Journal. Manuscript texts should contain the title of the article, name(s) of the author(s) and complete affiliations. Each article requires an abstract not exceeding 150 words. Formulas and citations should not be included in the abstract. AMS subject classifications and key words must be included in all accepted papers. Each article requires a running head (abbreviated form of the title) of no more than 30 characters. The sizes for regular papers, survey articles, brief notes, letters to editors and book reviews are: (i) 10-14 pages for regular papers, (ii) up to 24 pages for survey articles, and (iii) 2-3 pages for brief notes, letters to the editor and book reviews.

**(3) Tables, Graphs and Illustrations.** Each figure must be of a quality suitable for direct reproduction and must include a caption. Drawings should include all relevant details and should be drawn professionally in black ink on plain white drawing paper. In addition to a hard copy of the artwork, it is necessary to attach the electronic file of the artwork (preferably in PCX format).

**(4) References.** Each entry must be cited in the text by author(s) and number or by number alone. All references should be listed in their alphabetic order. Use please the following style:

Journal: [1] H. Poincare, Title of the article. *Title of the Journal* **volume**  
(issue) (year) pages. [Language]

Book: [2] A.M. Lyapunov, *Title of the Book*. Name of the Publishers, Town, year.

Proceeding: [3] R. Bellman, Title of the article. In: *Title of the Book*. (Eds.).  
Name of the Publishers, Town, year, pages. [Language]

**(5) Proofs and Sample Copy.** Proofs sent to authors should be returned to the Editorial Office with corrections within three days after receipt. The corresponding author will receive a sample copy of the issue of the Journal for which his/her paper is published.

**(6) Editorial Policy.** Every submission will undergo a stringent peer review process. An editor will be assigned to handle the review process of the paper. He/she will secure at least two reviewers' reports. The decision on acceptance, rejection or acceptance subject to revision will be made based on these reviewers' reports and the editor's own reading of the paper.

# NONLINEAR DYNAMICS AND SYSTEMS THEORY

An International Journal of Research and Surveys  
Published by InforMath Publishing Group since 2001

Volume 22

Number 4

2022

## CONTENTS

Functional Differential Inclusions with Unbounded Right-hand Side in Banach Spaces .....	355
<i>H. Chouial and M. F. Yarou</i>	
SOFC-PV System with Storage Battery Based on Cuckoo Search Algorithm .....	367
<i>Hamidia Fethia and Abbadi Amel</i>	
Application of Accretive Operators Theory to Linear SIR Model .....	379
<i>Mariam El Hassnaoui, Said Melliani and Mohamed Oukessou</i>	
Design of Navigation and Guidance Control System of Mobile Robot with Position Estimation Using Ensemble Kalman Filter (EnKF) and Square Root Ensemble Kalman Filter (SR-EnKF) .....	390
<i>T. Herlambang, F. A. Susanto, D. Adzkiya, A. Suryowinoto and K. Oktafianto</i>	
On the Dynamics of a Class of Planar Differential Systems .....	400
<i>A. Kina and A. Bendjeddou</i>	
Chaos Synchronization between Fractional-Order Lesser Date Moth Chaotic System and Integer-Order Chaotic System via Active Control .....	407
<i>M. Labid and N. Hamri</i>	
New Design of Stability Study for Linear and Nonlinear Feedback Control of Chaotic Systems .....	414
<i>W. Laouira and N. Hamri</i>	
Control of a Shunt Active Power Filter by the Synchronous Referential Method Connected with a Photovoltaic Solar Energy .....	424
<i>A. Morsli, A. Tlemcani and H. Nouri</i>	
A Neural Network Approximation for a Model of Micromagnetism .....	432
<i>M. Moumni and M. Tilioua</i>	
A New Fractional-Order Three-Dimensional Chaotic Flows with Identical Eigenvalues .....	447
<i>S. Rouar and O. Zehrou</i>	
Estimation of Closed Hotels and Restaurants in Jakarta as Impact of Corona Virus Disease (Covid-19) Spread Using Backpropagation Neural Network .....	457
<i>F. A. Susanto, M. Y. Anshori, D. Rahmalia, K. Oktafianto, D. Adzkiya, P. Katias and T. Herlambang</i>	
Stabilization of Chaotic $h$ -Difference Systems with Fractional Order .....	468
<i>Hasna Yousfi, Ahlem Gasri and Adel Ouannas</i>	

Founded by A.A. Martynyuk in 2001.

Registered in Ukraine Number: KB No 5267 / 04.07.2001.

# NONLINEAR DYNAMICS AND SYSTEMS THEORY

An International Journal of Research and Surveys

*Impact Factor from SCOPUS for 2020: SJR – 0.360, SNIP – 1.040 and CiteScore – 1.4*

**Nonlinear Dynamics and Systems Theory** (ISSN 1562–8353 (Print), ISSN 1813–7385 (Online)) is an international journal published under the auspices of the S.P. Timoshenko Institute of Mechanics of National Academy of Sciences of Ukraine and Curtin University of Technology (Perth, Australia). It aims to publish high quality original scientific papers and surveys in areas of nonlinear dynamics and systems theory and their real world applications.

## AIMS AND SCOPE

**Nonlinear Dynamics and Systems Theory** is a multidisciplinary journal. It publishes papers focusing on proofs of important theorems as well as papers presenting new ideas and new theory, conjectures, numerical algorithms and physical experiments in areas related to nonlinear dynamics and systems theory. Papers that deal with theoretical aspects of nonlinear dynamics and/or systems theory should contain significant mathematical results with an indication of their possible applications. Papers that emphasize applications should contain new mathematical models of real world phenomena and/or description of engineering problems. They should include rigorous analysis of data used and results obtained. Papers that integrate and interrelate ideas and methods of nonlinear dynamics and systems theory will be particularly welcomed. This journal and the individual contributions published therein are protected under the copyright by International InforMath Publishing Group.

## PUBLICATION AND SUBSCRIPTION INFORMATION

**Nonlinear Dynamics and Systems Theory** will have 5 issues in 2022, printed in hard copy (ISSN 1562–8353) and available online (ISSN 1813–7385), by InforMath Publishing Group, Nesterov str., 3, Institute of Mechanics, Kiev, MSP 680, Ukraine, 03057. Subscription prices are available upon request from the Publisher, EBSCO Information Services (<mailto:journals@ebSCO.com>), or website of the Journal: <http://e-ndst.kiev.ua>. Subscriptions are accepted on a calendar year basis. Issues are sent by airmail to all countries of the world. Claims for missing issues should be made within six months of the date of dispatch.

## ABSTRACTING AND INDEXING SERVICES

Papers published in this journal are indexed or abstracted in: Mathematical Reviews / MathSciNet, Zentralblatt MATH / Mathematics Abstracts, PASCAL database (INIST–CNRS) and SCOPUS.



# Functional Differential Inclusions with Unbounded Right-hand Side in Banach Spaces

H. Chouial\* and M. F. Yarou

*LMPA Laboratory, Department of Mathematics, Jijel University, Algeria.*

Received: March 27, 2022; Revised: September 15, 2022

**Abstract:** In this work, we provide a reduction method that solve functional differential inclusion in Banach spaces, that is, when the right-hand side contains a finite delay. We consider the case when the set-valued mapping takes nonempty closed non-convex and unnecessarily bounded values, we use the notion of  $\lambda - H$  Lipschitzness assumption instead of the standard Lipschitz condition, known as a truncation. An application to a dynamical system governed by a delayed perturbed sweeping process is given, such problems are well-posed for differential complementarity systems and vector hysteresis problems.

**Keywords:** *nonconvex differential inclusion; reduction; delay; unboundedness;  $\lambda$ -Hausdorff distance.*

**Mathematics Subject Classification (2010):** 93C10, 34A60.

## 1 Introduction

Let  $\tau, T$  be two non-negative real numbers,  $E$  be a separable Banach space equipped with the norm  $\|\cdot\|$ ,  $\mathcal{C}_0 := \mathcal{C}_E([-\tau, 0])$  (resp.  $\mathcal{C}_T := \mathcal{C}_E([-\tau, T])$ ) be the Banach space of all continuous mappings from  $[-\tau, 0]$  (resp.  $[-\tau, T]$ ) to  $E$  equipped with the norm of uniform convergence. Let  $\Pi : [0, T] \times \mathcal{C}_0 \rightrightarrows E$  be a set-valued mapping with nonempty closed values. In this work, we study the existence of solutions for the following differential inclusion with delay:

$$(DP) \quad \begin{cases} \dot{u}(t) \in \Pi(t, Z(t)u) & \text{a.e. } t \in [0, T], \\ u(t) = \psi(t), & t \in [-\tau, 0], \end{cases}$$

where  $\psi \in \mathcal{C}_0$  and  $Z(t) : \mathcal{C}_T \rightarrow \mathcal{C}_0$  is defined by  $(Z(t)u)(s) = u(t+s), \forall s \in [-\tau, 0]$ . In [9], Fryszkowski proved an existence result for (DP) when  $\Pi$  is an integrably bounded

---

\* Corresponding author: <mailto:hananechouial@yahoo.com>

and lower semicontinuous set-valued mapping with nonconvex values, the proof is based on the construction of a continuous selection for a class of nonconvex decomposable sets. Many other results have been obtained using a fixed point or discretization approach, see for instance [2, 4–6, 8] and the references therein. In [5], a discretization technique was initiated, it consists to subdivide the interval  $[0, T]$  in a sequence of subintervals and to reformulate the problem with delay to a sequence of problems without delay and then apply the results known in this case. Our goal in this work is to prove the existence of a global solution to (DP) for a general class of unbounded sets thanks to a recent result for the undelayed problem due to Tolstonogov [11]. We weaken the standard Lipschitz condition by a truncated one. Then, we use this result to present an application for functional differential inclusions governed by time and state dependent nonconvex sweeping process. This kind of problems corresponds to several important mechanical problems and nonsmooth dynamical systems. When external forces (perturbations) are applied to the system described by the sweeping process, the problem found many applications in resource allocation in economics, nonregular electrical circuits, crowd motion modeling and hysteresis. We propose here a new variant of the existence result which generalizes the previous results. The paper is organized as follows. In Section 2, we prepare some material which will be needed later in our proof. Section 3 is devoted to the main result. An application is given in Section 4 for a dynamical system governed by a sweeping process subject to external forces containing a finite delay.

## 2 Preliminaries

Throughout the paper, we will use the following notation and definitions. Let  $E$  be a separable Banach space,  $\|\cdot\|$  its norm and  $\ominus$  its zero element. We denote by  $\mathcal{C}_E([0, T])$  the Banach space of all continuous mappings from  $[0, T]$  to  $E$ ,  $L_E^1([0, T])$  is the Banach space of all measurable mappings from  $[0, T]$  to  $E$ . Let  $\mathcal{B}(\mathcal{C}_0)$  be the  $\sigma$ -algebra of Borel sets of  $\mathcal{C}_0$  and  $\mathcal{L}$  be the  $\sigma$ -algebra of Lebesgue measurable subsets of  $[0, T]$ ,  $d(u, A)$  means the usual distance from a point  $u$  to a set  $A$ , i.e.,  $d(u, A) := \inf_{v \in A} \|u - v\|$ ,  $u \in E$ . We denote by  $\lambda\mathbb{B}$  the closed ball with radius  $\lambda$  in  $E$  centered at  $\ominus$ , and  $\overline{\mathbb{B}}_{\mathcal{C}_0}$  the closed unit ball of  $\mathcal{C}_0$  with center 0. A set-valued mapping  $\Lambda : [0, T] \times E \rightarrow E$  is integrally bounded if there exists an integrable function  $\xi : [0, T] \rightarrow \mathbb{R}^+$  such that

$$\|\Lambda(t, u)\| := \sup\{\|v\|; v \in \Lambda(t, u)\} \leq \xi(t), t \in [0, T], u \in E.$$

A set-valued mapping with closed values, is measurable whenever  $\Lambda^{-1}(U) = \{t \in [0, T] : \Lambda(t) \cap U \neq \emptyset\}$  belongs to  $\mathcal{L}$  for every closed set  $U \subset E$ .

Following [3], for any set  $A \subset E$  and  $\lambda > 0$ , we put  $A_\lambda = A \cap \lambda\overline{\mathbb{B}}$ . For  $A, B \subset E$ , the excess, the Hausdorff distance and the  $\lambda$ -Hausdorff distance between  $A$  and  $B$  are defined respectively by  $e(A, B) := \sup_{a \in A} d(a, B)$ ,  $haus(A, B) = \max\{e(A, B), e(B, A)\}$  and

$$haus_\lambda(A, B) = \max\{e(A_\lambda, B), e(B_\lambda, A)\}.$$

If  $A$  is a nonempty closed subset of  $E$ , then  $\delta^*(u, A) = \sup_{v \in A} \langle u, v \rangle$  is the support function of  $A$  at  $u \in E$ , and  $\overline{\text{co}}(A)$  stands for the closed convex hull of  $A$ , characterized by

$$\overline{\text{co}}(A) = \{u \in E : \forall v \in E, \langle v, u \rangle \leq \delta^*(v, A)\}.$$

The projection of  $u$  on  $A$  is the element of  $A$  denoted by  $Proj_A(u)$  and satisfying  $Proj_A(u) = \{v \in A : d(u, A) = \|u - v\|\}$ .

Let  $g : E \rightarrow \mathbb{R} \cup \{+\infty\}$  be a proper convex continuous function on  $E$  and  $u \in E$  with  $g(u) < +\infty$ , the subdifferential of  $g$  is the set defined by

$$\partial g(u) = \{z \in E : \langle z, v - u \rangle \leq g(v) - g(u), \forall v \in E\},$$

if  $g(u)$  is not finite, we set  $\partial g(u) = \emptyset$ ,  $\partial g(u)$  is a closed convex set if  $g$  is convex.

Let  $A \subset E$  and  $u \in A$ , the normal cone to  $A$  at  $u$  is defined by

$$N_A(u) = \{v \in E : \langle v, c - u \rangle \leq 0, \text{ for all } c \in A\}.$$

A vector  $\omega \in E$  is said to be in the Fréchet subdifferential of  $g$  at  $u$ , denoted by  $\partial^F g(u)$ , if for every  $\varepsilon > 0$  there exists  $\delta > 0$  such that for all  $u' \in B(u, \delta)$ , we have

$$\langle \omega, u' - u \rangle \leq g(u') - g(u) + \varepsilon \|u' - u\|.$$

The Fréchet normal cone  $N_A^F(u)$  of  $A$  at  $u \in A$  is given by  $N_A^F(u) = \partial^F \chi_A(u)$ , where  $\chi_A$  is the indicator function of  $A$ , so we have the inclusion  $N_A^F(u) \subset N_A(u)$  for all  $u \in A$ .

On the other hand, the Fréchet normal cone is also related to the Fréchet subdifferential of the distance function since for all  $u \in A$ ,

$$N_A^F(u) = \mathbb{R}_+ \partial^F d(u, A); \text{ and } \partial^F d_A(u) = N^F(A; u) \cap \mathbb{B}.$$

We now recall the definition of subsmooth sets.

**Definition 2.1** Let  $A$  be a closed subset of  $E$ , we say that  $A$  is subsmooth at  $u_0 \in A$  if for every  $\epsilon > 0$ , there exists  $\delta > 0$  such that

$$\langle \zeta_2 - \zeta_1; u_2 - u_1 \rangle \geq -\epsilon \|u_2 - u_1\| \tag{1}$$

whenever  $u_1, u_2 \in B(u_0; \delta) \cap A$  and  $\zeta_i \in N_A(u_i) \cap \mathbb{B}$ . The set  $A$  is subsmooth if it is subsmooth at each point of  $A$ .

Let  $A$  be a closed subset in  $E$  and  $u_0 \in A$ . Then, if  $A$  is subsmooth at  $u_0$ , then it is normally Fréchet regular at  $u_0$ , that is,  $N_A^F(u_0) = N_A(u_0)$  and  $\partial d(u_0, A) = \partial^F d(u_0, A)$ .

**Definition 2.2** A family  $(S(q))_{q \in Q}$  of closed sets in  $E$  with parameter  $q \in Q$ , is called equi-uniformly subsmooth if for every  $\epsilon > 0$ , there exists  $\delta > 0$  such that for each  $q \in Q$ , the inequality (1) holds for all  $u_1, u_2 \in S(q)$  satisfying  $\|u_1 - u_2\| < \delta$  and all  $\zeta_i \in N(S(q); u_i) \cap \mathbb{B}$ .

**Proposition 2.1** [10] Let  $\{C(t, u) : (t, u) \in [0; T] \times E\}$  be a family of nonempty closed sets of  $E$  which is equi-uniformly subsmooth and let  $\nu \geq 0$ , assume that there exist positive real constants  $L_1, L_2$  such that for any  $t, s \in [0, T]$  and  $u, v, z \in E$ ,

$$|d(z, C(t, u)) - d(z, C(s, v))| \leq L_1 |t - s| + L_2 \|u - v\|.$$

Then the following assertions hold:

- (a) For all  $(t, u, v) \in \text{gph}(C)$ , we have  $\nu \partial d(v, C(t, u)) \subset \nu \mathbb{B}$ ;
- (b) For any sequences  $(t_n)_n$  in  $[0, T]$  converging to  $t$ ,  $(u_n)_n$  converging to  $u$ ,  $(v_n)_n$  converging to  $v \in C(t, u)$  with  $v_n \in C(t_n, u_n)$ , and any  $\zeta \in H$ , we have

$$\limsup_{n \rightarrow +\infty} \sigma(\zeta, \nu \partial d(v_n, C(t_n, u_n))) \leq \sigma(\zeta, \nu \partial d(v, C(t, u))) .$$

**Lemma 2.1** [1] Let  $m > 0$ ,  $(\omega_i)$  and  $(v_i)$  be nonnegative sequences satisfying  $\omega_i \leq m + \sum_{j=0}^{i-1} v_j \omega_j$  for any  $i \in \mathbb{N}$ , then  $\omega_i \leq m \exp\left(\sum_{j=0}^{i-1} v_j\right)$ ,  $\forall i \in \mathbb{N}$ .

### 3 Main Result

We begin this section by listing the hypotheses used throughout the paper.

**Hypotheses  $\mathcal{H}_{(\Pi)}$ :** For every  $\beta > 0$  and  $\mathcal{C}_0^\beta = \mathcal{C}_0 \cap \beta \overline{\mathbb{B}}_{\mathcal{C}_0}$ , let  $\Pi : [0, T] \times \mathcal{C}_0^\beta \rightarrow E$  be a set-valued mapping with nonempty closed values satisfying:

- (i) for every  $\psi \in \mathcal{C}_0^\beta$ ,  $\Pi(\cdot, \psi)$  is measurable;
- (ii) for some functions  $\eta(\cdot), \xi(\cdot) \in L^1_{\mathbb{R}^+}([0, T])$  such that for all  $t \in [0, T]$  and for all  $\psi \in \mathcal{C}_0^\beta$ ,

$$d(\ominus, \Pi(t, \psi)) < \xi(t) + \eta(t)\|\psi\|_{\mathcal{C}_0},$$

and  $d(\ominus, \Pi(t, \ominus)) = 0$  for  $\xi(t) = 0$ ;

- (iii)  $\forall \psi, \phi \in \mathcal{C}_0^\beta$ , with  $\phi \neq \psi$ , we have

$$\text{haus}_\lambda(\Pi(t, \phi), \Pi(t, \psi)) \leq \eta(t)\|\phi - \psi\|_{\mathcal{C}_0}.$$

For the proof of our theorem we need the following result for the undelayed problem.

**Theorem 3.1** [11] *For every  $\beta > 0$ , let  $\Lambda : [0, T] \times \beta \overline{\mathbb{B}} \rightarrow E$  be a set-valued mapping with nonempty closed values satisfying:*

- (1) for every  $u \in \mathcal{C}_E([0, T])$  and  $t \in [0, T]$ , the mapping  $t \rightarrow \Lambda(t, u(t))$  is measurable;
- (2) for some functions  $\eta(\cdot), \xi(\cdot) \in L^1_{\mathbb{R}^+}([0, T])$ ,

$$d(\ominus, \Lambda(t, u(t))) < \xi(t) + \eta(t)\|u(t)\| \text{ a.e.}, \|u(t)\| \leq \beta,$$

$d(\ominus, \Lambda(t, \ominus)) = 0$  for  $\xi(t) = 0$ ;

- (3) for  $\|u(t)\| \leq \beta, \|v(t)\| \leq \beta, u(t) \neq v(t)$ , we have

$$\text{haus}_\lambda(\Lambda(t, u(t)), \Lambda(t, v(t))) \leq \eta(t)\|u(t) - v(t)\| \text{ a.e.}$$

with  $0 \leq \lambda \leq \dot{m}(t)$  for  $t \in [0, T]$ , where  $m(\cdot) : [0, T] \rightarrow \mathbb{R}$  is the absolutely continuous solution to the differential equation

$$\begin{cases} \dot{m}(t) &= \eta(t) m(t) + \xi(t) \text{ a.e. in } [0, T], \\ m(0) &= m_0 \geq 0. \end{cases}$$

Then,  $\forall u_0 \in \mathcal{C}_E([0, T])$  with  $\|u_0\| < \beta$ , the problem

$$\begin{cases} \dot{u}(t) \in \Lambda(t, u(t)); & \text{a.e. on } [0, T]; \\ u(0) = u_0; \end{cases} \quad (2)$$

admits a solution  $u$  such that  $\|u(t)\| \leq m(t), \|\dot{u}(t)\| \leq \dot{m}(t)$  a.e. for  $t \in [0, T]$  with  $m(t) \leq \beta$ .

Now, we are able to give the existence result for the delayed problem.

**Theorem 3.2** *Let  $\Pi : [0, T] \times \mathcal{C}_0^\beta \rightarrow E$  be a set-valued mapping satisfying  $\mathcal{H}_{(\Pi)}$ . Then,  $\forall \psi \in \mathcal{C}_0$ , the problem (DP) admits at least one continuous solution  $u : [-\tau, T] \rightarrow E$ , absolutely continuous on  $[0, T]$ . Furthermore,  $\|\dot{u}(t)\| \leq \dot{m}(t)$  a.e.  $t \in [0, T]$ .*

**Proof.** We will reduce our problem to a problem without delay and apply Theorem 3.1. For every  $n \in \mathbb{N}$ , consider a partition of  $[0, T]$  defined by  $t_i^n = i\varpi_n$ ,  $\varpi_n = Tn^{-1}$ ,  $i = 0, 1, \dots, n$ .

**Step 1 (Construction of approximate solutions):** for every  $(t, u) \in [-\tau, t_1^n] \times E$ , we define  $p_0^n : [-\tau, t_1^n] \times E \rightarrow E$  by

$$p_0^n(t, u) = \begin{cases} \psi(t) & \text{if } t \in [-\tau, 0]; \\ \psi(0) + \frac{t}{\varpi_n}(u - \psi(0)) & \text{if } t \in ]0, t_1^n]; \end{cases}$$

clearly,  $p_0^n(t_1^n, u) = u, \forall u \in E$ .

We define the set-valued mapping  $\Lambda_0^n$  on  $[0, t_1^n] \times E$  with closed values in  $E$  by

$$\Lambda_0^n(t, u) := \Pi(t, \mathcal{Z}(t_1^n)p_0^n(\cdot, u)), \quad \forall (t, u) \in [0, t_1^n] \times E.$$

Let's show that  $\Lambda_0^n$  satisfies the conditions of Theorem 3.1. Remark first, that the function  $u \mapsto \mathcal{Z}(t_1^n)p_0^n(\cdot, u)$  is Lipschitz. Indeed, for every  $u, v \in E$ , we have

$$\begin{aligned} \|\mathcal{Z}(t_1^n)p_0^n(\cdot, u) - \mathcal{Z}(t_1^n)p_0^n(\cdot, v)\|_{\mathcal{C}_0} &= \sup_{s \in [-\tau, 0]} \|p_0^n(t_1^n + s, u) - p_0^n(t_1^n + s, v)\| \\ &= \sup_{s \in [-\varpi_n, 0]} \|p_0^n(t_1^n + s, u) - p_0^n(t_1^n + s, v)\| \\ &= \sup_{s \in [-\varpi_n, 0]} \left\| \frac{t_1^n + s}{\varpi_n}(u - v) \right\| \\ &= \|u - v\|. \end{aligned}$$

So the mapping  $t \mapsto \Lambda_0^n(t, u)$  is measurable. On the other hand,

$$\begin{aligned} \|\mathcal{Z}(t_1^n)p_0^n(\cdot, u)\|_{\mathcal{C}_0} &= \sup_{s \in [-\tau + t_1^n, t_1^n]} \|p_0^n(s, u)\| \\ &\leq \max\{\|\psi\|_{\mathcal{C}_0}, \sup_{s \in [0, t_1^n]} \|\psi(0) + \frac{s}{\varpi_n}(u - \psi(0))\|\} \\ &\leq \max\{\|\psi\|_{\mathcal{C}_0}, \sup_{s \in [0, t_1^n]} ((1 - \frac{s}{\varpi_n})\|\psi(0)\| + \frac{s}{\varpi_n}\|u\|)\} \\ &\leq \max\{\|\psi\|_{\mathcal{C}_0}, \|\psi(0)\| + \|u\|\}. \end{aligned}$$

Furthermore, by the condition (ii) of  $\mathcal{H}(\Pi)$ , we have, for every  $t \in [0, t_1^n]$  and  $u \in E$  such that  $\|u\| \leq \beta$ ,

$$\begin{aligned} d(\ominus, \Lambda_0^n(t, u)) = d(\ominus, \Pi(t, \mathcal{Z}(t_1^n)p_0^n(\cdot, u))) &\leq \xi(t) + \eta(t) \|\mathcal{Z}(t_1^n)p_0^n(\cdot, u)\| \\ &\leq \xi(t) + \eta(t)(\|\psi\|_{\mathcal{C}_0} + \|u\|), \\ &\leq \zeta(t)(1 + \|\psi\|_{\mathcal{C}_0}) + \eta(t)\|u\|, \end{aligned}$$

where  $\zeta(t) := \max\{\xi(t), \eta(t)\}$ .

For  $\zeta(t) = 0$ , we have  $d(\ominus, \Lambda_0^n(t, \ominus)) = d(\ominus, \Pi(t, \mathcal{Z}(t_1^n)p_0^n(\cdot, \ominus))) = 0$ . Finally, according to (iii), one obtain

$$\begin{aligned} haus_\lambda(\Lambda_0^n(t, u), \Lambda_0^n(t, v)) &= haus_\lambda(\Pi(t, \mathcal{Z}(t_1^n)p_0^n(\cdot, u)), \Pi(t, \mathcal{Z}(t_1^n)p_0^n(\cdot, v))) \\ &\leq \eta(t) \|\mathcal{Z}(t_1^n)p_0^n(\cdot, u) - \mathcal{Z}(t_1^n)p_0^n(\cdot, v)\| \\ &= \eta(t) \|u - v\|, \end{aligned}$$

$\|u\| \leq \beta$  and  $\|v\| \leq \beta, u \neq v$ . Hence  $\Lambda_0^n$  verifies the conditions of Theorem 3.1, this provides an absolutely continuous solution  $\vartheta_0^n : [0, t_1^n] \rightarrow E$  to the problem

$$\begin{cases} \dot{\vartheta}_0^n(t) \in \Lambda_0^n(t, \vartheta_0^n(t)) & \text{a.e. on } [0, t_1^n]; \\ \vartheta_0^n(t) = \psi(0) + \int_0^t \dot{\vartheta}_0^n(s)ds & \forall t \in ]0, t_1^n]; \\ \vartheta_0^n(0) = \psi(0), \end{cases}$$

with  $\|\vartheta_0^n(t)\| \leq m(t)$  and  $\|\dot{\vartheta}_0^n(t)\| \leq \dot{m}(t)$ . That is,  $\vartheta_0^n$  is a solution to

$$\begin{cases} \dot{\vartheta}_0^n(t) & \in \Pi(t, Z(t_1^n)p_0^n(\cdot, \vartheta_0^n)) & \text{a.e. on } [0, t_1^n]; \\ \vartheta_0^n(0) & = \psi(0). \end{cases}$$

Put

$$u_n(t) = \begin{cases} \psi(t) & \text{if } t \in [-\tau, 0]; \\ \vartheta_0^n(t) & \text{if } t \in ]0, t_1^n]. \end{cases}$$

As before, for every  $(t, u) \in [-\tau, t_1^n] \times E$ , we define  $p_1^n : [-\tau, t_2^n] \times E \rightarrow E$  by

$$p_1^n(t, u) = \begin{cases} u_n(t) & \text{if } t \in [-\tau, t_1^n]; \\ u_n(t_2^n) + \frac{t-t_2^n}{\varpi_n}(u - u_n(t_2^n)) & \text{if } t \in ]t_1^n, t_2^n] \end{cases}$$

with  $p_1^n(t_2^n, u) = u$ ,  $\forall u \in E$ . Hence, we can define similarly the set-valued mapping  $\Lambda_1^n$  on  $[t_1^n, t_2^n] \times E$  with closed values of  $E$  by

$$\Lambda_1^n(t, u) := \Pi(t, Z(t_2^n)p_1^n(\cdot, u)), \quad \forall (t, u) \in [t_1^n, t_2^n] \times E.$$

The function  $u \mapsto Z(t_2^n)p_1^n(\cdot, u)$  is Lipschitz since for all  $u, v \in E$ , we have

$$\begin{aligned} \|Z(t_2^n)p_1^n(\cdot, u) - Z(t_2^n)p_1^n(\cdot, v)\| &= \sup_{s \in [-\tau, 0]} \|p_1^n(t_2^n + s, u) - p_1^n(t_2^n + s, v)\| \\ &= \sup_{s \in [-\varpi_n, 0]} \|p_1^n(t_2^n + s, u) - p_1^n(t_2^n + s, v)\| \\ &= \sup_{s \in [-\varpi_n, 0]} \|u_n(t_1^n) + \frac{t_2^n + s - t_1^n}{\varpi_n}(u - u_n(t_1^n)) \\ &\quad - (u_n(t_1^n) + \frac{t_2^n + s - t_1^n}{\varpi_n}(v - u_n(t_1^n)))\| \\ &= \sup_{s \in [-\varpi_n, 0]} \|\frac{t_2^n + s - t_1^n}{\varpi_n}(u - v)\| \\ &= \|\frac{t_2^n - t_1^n}{\varpi_n}(u - v)\| \\ &= \|u - v\| \end{aligned}$$

and

$$\begin{aligned} \|Z(t_2^n)p_1^n(\cdot, u)\|_{C_0} &= \sup_{s \in [-\tau + t_2^n, t_2^n]} \|p_1^n(s, u)\| \\ &\leq \max\{\|\psi\|_{C_0}, \sup_{s \in [0, t_1^n]} \|v_0^n(s)\|\} + \sup_{s \in [t_1^n, t_2^n]} \left( (1 - \frac{t-s}{\varpi_n})\|u_n(t_2^n)\| + \frac{t-s}{\varpi_n}\|u\| \right) \\ &\leq \max\{\|\psi\|_{C_0}, \sup_{s \in [0, t_1^n]} \|v_0^n(s)\|\} + \|u\|. \end{aligned}$$

For every  $t \in [t_1^n, t_2^n]$  and  $u \in E$ , with  $\|u\| \leq \beta$

$$\begin{aligned} d(\ominus, \Lambda_1^n(t, u)) &= d(\ominus, \Pi(t, Z(t_2^n)p_1^n(\cdot, u))) \leq \xi(t) + \eta(t) \|Z(t_2^n)p_1^n(\cdot, u)\| \\ &\leq \zeta(t)(1 + \max\{\|\psi\|_{C_0}, \sup_{s \in [0, t_1^n]} \|v_0^n(s)\|\}) + \eta(t) \|u\|, \end{aligned}$$

for  $\zeta(t) = 0$

$$d(\ominus, \Lambda_1^n(t, \ominus)) = d(\ominus, \Pi(t, Z(t_2^n)p_1^n(\cdot, \ominus))) = 0.$$

Furthermore, by condition (iii) of  $\mathcal{H}(\Pi)$ , we have for every  $t \in [0, t_1^n]$  and  $u, v \in E$  such that  $\|u\| \leq \beta$ , and  $\|v\| \leq \beta$ ,  $u \neq v$ ,

$$\begin{aligned} \text{haus}_\lambda(\Lambda_1^n(t, u), \Lambda_1^n(t, v)) &= \text{haus}_\lambda(\Pi(t, Z(t_2^n)p_1^n(\cdot, u)), \Pi(t, Z(t_2^n)p_1^n(\cdot, v))) \\ &\leq \eta(t) \|Z(t_2^n)p_1^n(0, u) - Z(t_2^n)p_1^n(0, v)\| \\ &= \xi(t) + \eta(t) \|p_1^n(t_2^n, u) - p_1^n(t_2^n, v)\| \\ &= \xi(t) + \eta(t) \|u - v\|. \end{aligned}$$

Hence  $\Lambda_1^n$  verifies the conditions of Theorem 3.1, this provides an absolutely continuous solution  $\vartheta_1^n : [t_1^n, t_2^n] \rightarrow E$  to the problem

$$\begin{cases} \dot{\vartheta}_1^n(t) &\in \Lambda_1^n(t, \vartheta_1^n(t)) & \text{a. e. on } [t_1^n, t_2^n]; \\ \vartheta_1^n(t) &= u_n(t_2^n) + \int_{t_1^n}^t \dot{\vartheta}_1^n(s) ds & \forall t \in ]t_1^n, t_2^n]; \\ \vartheta_1^n(t_2^n) &= u_n(t_2^n), \end{cases}$$

$\|\vartheta_1^n(t)\| \leq m(t)$  and  $\|\dot{\vartheta}_1^n(t)\| \leq \dot{m}(t)$ . So  $v_1^n$  is a solution of

$$\begin{cases} \dot{\vartheta}_1^n(t) &\in \Pi(t, Z(t_2^n)p_1^n(\cdot, \vartheta_1^n)) & \text{a.e. on } [t_1^n, t_2^n]; \\ \vartheta_1^n(t) &= u_n(t_1^n) + \int_{t_1^n}^t \dot{\vartheta}_1^n(s) ds & \forall t \in ]t_1^n, t_2^n]; \\ \vartheta_1^n(0) &= \psi(0). \end{cases}$$

By induction, suppose that  $u_n$  is defined on  $[-\tau, t_k^n]$ , absolutely continuous on  $[0, t_k^n]$ , and satisfies

$$\begin{cases} \dot{u}_n(t) &\in \Pi(t, Z(t_{k-1}^n)p_{k-1}^n(\cdot, u)) & \text{a.e. on } [t_{k-1}^n, t_k^n]; \\ u_n(t) &= u_n(t_{k-1}^n) + \int_{t_{k-1}^n}^t \dot{u}_n(s) ds & \forall t \in ]t_{k-1}^n, t_k^n]; \end{cases}$$

and build a solution on  $[t_k^n, t_{k+1}^n]$ . For every  $(t, u) \in [-\tau, t_1^n] \times E$ , we defined  $p_k^n : [-\tau, t_{k+1}^n] \times E \rightarrow E$  by

$$p_k^n(t, u) = \begin{cases} u_n(t) & \text{if } t \in [-\tau, t_k^n]; \\ u_n(t_k^n) + \frac{t-t_k^n}{\varpi_n}(u - u_n(t_k^n)) & \text{if } t \in ]t_k^n, t_{k+1}^n]; \end{cases}$$

with  $p_k^n(t_{k+1}^n, u) = u$  and  $p_k^n \in \mathcal{C}_E([-\tau, t_{k+1}^n])$ . The function  $u \mapsto Z(t_{k+1}^n)p_k^n(\cdot, u)$  is Lipschitz. Indeed, for all  $u, v \in E$ , we have

$$\begin{aligned} &\|Z(t_{k+1}^n)p_k^n(\cdot, u) - Z(t_{k+1}^n)p_k^n(\cdot, v)\| = \\ &\sup_{s \in [-\tau, 0]} \|p_k^n(t_{k+1}^n + s, u) - p_k^n(t_{k+1}^n + s, v)\| \\ &= \sup_{t \in [-\tau + t_{k+1}^n, t_{k+1}^n]} \|p_k^n(t, u) - p_k^n(t, v)\|. \end{aligned}$$

We distinguish two cases:

(1) if  $-\tau + t_{k+1}^n \leq t_k^n$ , we have

$$\begin{aligned} \sup_{t \in [-\tau + t_{k+1}^n, t_{k+1}^n]} \|p_k^n(t, u) - p_k^n(t, v)\| &= \sup_{t \in [t_k^n, t_{k+1}^n]} \|p_k^n(t, u) - p_k^n(t, v)\| \\ &= \sup_{t \in [t_k^n, t_{k+1}^n]} \left\| \frac{t-t_k^n}{\varpi_n}(u - v) \right\| \\ &= \|u - v\|. \end{aligned}$$

(2) if  $t_k^n \leq -\tau + t_{k+1}^n \leq t_{k+1}^n$ , we have

$$\begin{aligned} \sup_{t \in [-\tau + t_{k+1}^n, t_{k+1}^n]} \|p_k^n(t, u) - p_k^n(t, v)\| &\leq \sup_{t \in [t_k^n, t_{k+1}^n]} \|p_k^n(t, u) - p_k^n(t, v)\| \\ &= \sup_{t \in [t_k^n, t_{k+1}^n]} \left\| \frac{t - t_k^n}{\varpi_n} (u - v) \right\| \\ &= \|u - v\|. \end{aligned}$$

$$\begin{aligned} \|Z(t_{k+1}^n)p_k^n(\cdot, u)\|_{\mathcal{C}_0} &= \sup_{s \in [-\tau + t_{k+1}^n, t_{k+1}^n]} \|p_k^n(s, u)\| \\ &\leq \max \left\{ \|\psi\|_{\mathcal{C}_0}, \max_{0 \leq k \leq i-1} \sup_{s \in [t_k^n, t_{k+1}^n]} \|v_k^n(s)\| \right\} + \|u\|. \end{aligned}$$

Similarly, we can define  $\Lambda_k^n$  on  $[t_k^n, t_{k+1}^n] \times E$  with closed values of  $E$  by

$$\Lambda_k^n(t, u) := \Pi(t, Z(t_{k+1}^n)p_k^n(\cdot, u)), \quad \forall (t, u) \in [t_k^n, t_{k+1}^n] \times E,$$

satisfying conditions of Theorem 3.1. Hence, there exists an absolutely continuous solution  $\vartheta_k^n : [t_k, t_{k+1}] \rightarrow E$  to

$$\begin{cases} \dot{\vartheta}_k^n(t) \in \Lambda_k^n(t, \vartheta_k^n(t)) & \text{a.e. on } [t_k^n, t_{k+1}^n]; \\ \vartheta_k^n(t) = u_n(t_k^n) + \int_{t_k^n}^t \dot{\vartheta}_k^n(s) ds & \forall t \in ]t_k^n, t_{k+1}^n]; \\ \vartheta_k^n(t_k^n) = u_n(t_k^n), \end{cases}$$

$\|\vartheta_k^n(t)\| \leq m(t)$  and  $\|\dot{\vartheta}_k^n(t)\| \leq \dot{m}(t)$ . So  $\vartheta_k^n$  is a solution of

$$\begin{cases} \dot{\vartheta}_k^n(t) \in \Pi(t, Z(t_{k+1}^n)p_k^n(\cdot, \vartheta_k^n)) & \text{a.e. on } [t_k^n, t_{k+1}^n]; \\ \vartheta_k^n(t) = u_n(t_k^n) + \int_{t_k^n}^t \dot{\vartheta}_k^n(s) ds & \forall t \in ]t_k^n, t_{k+1}^n]; \\ \vartheta_k^n(t_k^n) = u_n(t_k^n). \end{cases}$$

Putting  $u_n(t) = \vartheta_k^n(t)$  on  $[t_k^n, t_{k+1}^n]$ , we obtain

$$u_n(t) = \begin{cases} \vartheta_0^n(t) = \psi(0) + \int_0^t \dot{u}_n(s) ds & \text{if } t \in [0, t_1^n]; \\ \vartheta_1^n(t) = u_n(t_1^n) + \int_{t_1^n}^t \dot{u}_n(s) ds & \text{if } t \in ]t_1^n, t_2^n]; \\ \dots \\ \vartheta_k^n(t) = u_n(t_k^n) + \int_{t_k^n}^t \dot{u}_n(s) ds & \text{if } t \in ]t_k^n, t_{k+1}^n]; \end{cases}$$

and  $\|u_n(t)\| \leq m(t)$ . For every  $t \in [0, T]$ , we set  $\theta_n(t) = t_i^n$ ,  $\delta_n(t) = t_{i+1}^n$ ,  $\forall t \in ]t_i^n, t_{i+1}^n]$  and  $\theta_n(0) = 0$  and define  $p_{\varpi_n \theta_n}^n \in \mathcal{C}_E([-\tau, \delta_n(t)])$  by

$$p_{\varpi_n \theta_n}^n(t, x) = \begin{cases} u_n(t) & \text{if } t \in [-\tau, \theta_n(t)]; \\ u_n(\theta_n(t)) + \frac{t - \theta_n(t)}{\varpi_n} (u - u_n(\theta_n(t))) & \text{if } t \in ]\theta_n(t), \delta_n(t)]. \end{cases}$$

Clearly,  $u_n$  is continuous on  $[-\tau, T]$ , absolutely continuous on  $[0, T]$  and satisfies

$$\begin{cases} \dot{u}_n(t) \in \Pi(t, Z(\delta_n(t))p_{\varpi_n \theta_n}^n(\cdot, u_n(t))) & \text{a. e. on } [0, T]; \\ u_n(t) = \psi(0) + \int_0^t \dot{u}_n(s) ds & \forall t \in [0, T]; \\ u_n(t) = \psi(t) & \forall t \in [-\tau, 0]. \end{cases} \quad (3)$$

**Step 2 (Uniform convergence):** by condition (2) of Theorem 3.1, for almost every  $t \in [0, T]$ , one has

$$\dot{u}_n(t) \in \Pi(t, Z(\delta_n(t))p_{\varpi_n\theta_n(t)}^n(\cdot, u_n(t))) \tag{4}$$

with  $Z(\delta_n(t))p_{\varpi_n\theta_n(t)}^n(0, u_n(t)) = u_n(t)$  and

$$d(\ominus, \Pi(t, Z(\delta_n(t))p_{\varpi_n\theta_n(t)}^n(\cdot, u_n(t)))) \leq \xi(t) + \eta(t)\|u_n(t)\|.$$

Further, since  $\|u_n(t)\| \leq m(t)$ , we have

$$d(\ominus, \Pi(t, Z(\delta_n(t))p_{\varpi_n\theta_n(t)}^n(\cdot, u_n(t)))) \leq \xi(t) + \eta(t)m(t).$$

Hence for almost every  $t \in [0, T]$ ,

$$\|\dot{u}_n(t)\| \leq \dot{m}(t). \tag{5}$$

This shows that  $\dot{u}_n(\cdot)$  is uniformly bounded by  $\dot{m}(\cdot)$ . By extracting a subsequence, we may assume that  $(\dot{u}_n)_n$  converges  $\sigma(L^1, L^\infty)$  to some  $v \in L^1_E([0, T])$ . So  $(u_n(\cdot))$  is a bounded sequence of  $\mathcal{C}_E([0, 1])$  since for every  $t \in [0, T]$ ,

$$\|u_n(t)\| = \|\psi(0)\| + \int_0^t \|\dot{u}_n(s)\| ds \leq \|\psi(0)\| + \int_0^t \dot{m}(s) ds = \gamma(t)$$

and it is clear that  $(u_n(\cdot))$  is equicontinuous. By Ascoli’s theorem, we get that  $(u_n)_n$  is relatively compact. By extracting a subsequence (that we do not relabel), we conclude that  $(u_n)_n$  converges uniformly to some mapping  $u$  and

$$u(t) = \psi(0) + \int_0^t v(s) ds, \forall t \in [0, T],$$

hence  $\dot{u}(t) = v(t)$  almost everywhere.

Now, let’s show that

$$\begin{aligned} & \|Z(\delta_n(t))p_{\varpi_n\theta_n(t)}^n(\cdot, u_n(t)) - Z(t)u\| \longrightarrow 0, \text{ when } n \longrightarrow \infty. \\ & \sup_{s \in [-\tau, 0]} \|Z(\delta_n(t))p_{\varpi_n\theta_n(t)}^n(s, u_n(t)) - Z(t)u(s)\|_{C_0} = \\ & \sup_{s \in [-\tau, 0]} \|p_{\varpi_n\theta_n(t)}^n(\delta_n(t) + s, u_n(t)) - u(s + t)\| \\ = & \sup_{s \in [-\tau, 0]} \|p_{\varpi_n\theta_n(t)}^n(\delta_n(t) + s, u_n(t)) - u(\delta_n(t) + s) + u(\delta_n(t) + s) - u(s + t)\| \\ \leq & \sup_{s \in [-\tau, 0]} \|p_{\varpi_n\theta_n(t)}^n(\delta_n(t) + s, u_n(t)) - x(\delta_n(t) + s)\| + \\ & \sup_{s \in [-\tau, 0]} \|u(\delta_n(t) + s) - u(s + t)\|. \end{aligned}$$

First,

$$\begin{aligned} & \sup_{s \in [-\tau, 0]} \|p_{\varpi_n\theta_n(t)}^n(\delta_n(t) + s, u_n(t)) - x(\delta_n(t) + s)\| \\ \leq & \sup_{s \in [-\tau, -\varpi_n]} \|p_{\varpi_n\theta_n(t)}^n(\delta_n(t) + s, u_n(t)) - u(\delta_n(t) + s)\| \end{aligned}$$

$$\begin{aligned}
 & + \sup_{s \in [-\varpi_n, 0]} \|p_{\varpi_n \theta_n(t)}^n(\delta_n(t) + s, u_n(t)) - u(\delta_n(t) + s)\| \\
 & = \sup_{s \in [-\tau, -\varpi_n]} \|u_n(\delta_n(t) + s) - u(\delta_n(t) + s)\| + \\
 & \sup_{s \in [-\varpi_n, 0]} \|u_n(\theta_n(t)) + \frac{\delta_n(t) + s - \theta_n(t)}{\mu_n}(u_n(t) - u_n(\theta_n(t)) - u(\delta_n(t) + s))\| \\
 & = \sup_{s \in [-\tau, -\varpi_n]} \|u_n(\delta_n(t) + s) - u(\delta_n(t) + s)\| \\
 & + \sup_{s \in [-\varpi_n, 0]} \left\| \frac{s}{\varpi_n}(u_n(t) - u_n(\theta_n(t))) + u_n(t) - u(\delta_n(t) + s) \right\| \\
 & = \|u_n(\theta_n(t)) - u(\theta_n(t))\| + \|u_n(t) - u_n(\delta_n(t))\|.
 \end{aligned}$$

On the other hand,

$$\begin{aligned}
 \sup_{s \in [-\tau, 0]} \|u(\delta_n(t) + s) - u(s + t)\| & \leq \sup_{s \in [-\tau, -\varpi_n]} \|u(\delta_n(t) + s) - u(s + t)\| \\
 & + \sup_{s \in [-\varpi_n, 0]} \|u(\delta_n(t) + s) - u(s + t)\| \\
 & = \sup_{s \in [-\tau, -\varpi_n]} \|u(\delta_n(t) + s) - u(s + t)\| \\
 & + \|u(\delta_n(t)) - u(t)\|.
 \end{aligned}$$

Then

$$\begin{aligned}
 \sup_{s \in [-\tau, 0]} \|Z(\delta_n(t))p_{\varpi_n \theta_n(t)}^n(s, u_n(t)) - Z(t)u(s)\|_{\mathcal{C}_0} & \leq \\
 & \|u_n(\theta_n(t)) - u(\theta_n(t))\| + \|u_n(t) - u_n(\delta_n(t))\| + \\
 & \sup_{s \in [-\tau, -\varpi_n]} \|u(\delta_n(t) + s) - u(s + t)\| + \|u(\delta_n(t)) - u(t)\|.
 \end{aligned}$$

As  $|\theta_n(t) - t| \leq \varpi_n$  and  $|\delta_n(t) - t| \leq \varpi_n, \forall t \in [0, T]$ , then  $\theta_n(t) \rightarrow t$  and  $\delta_n(t) \rightarrow t$  for  $n$  large enough. Furthermore,  $(u_n)_n$  converges uniformly to  $u, \|u(\delta_n(t)) - u(t)\| \rightarrow 0, \|u_n(\delta_n(t)) - u_n(t)\| \rightarrow 0$  and  $\|u_n(\theta_n(t)) - u(\theta_n(t))\| \rightarrow 0$ . As  $u$  is uniformly continuous, there is  $\lambda > 0$  such that  $|s - t| \leq \lambda$  implies  $\|u(s) - u(t)\| \leq \epsilon$ . But we have  $|\delta_n(t) + s - (s + t)| \leq \varpi_n$  for all  $s \in [-\tau, \varpi_n]$ . Hence

$$\sup_{s \in [-\tau, -\varpi_n]} \|u(\delta_n(t) + s) - u(s + t)\| \leq \epsilon \text{ for } \lambda \leq \varpi_n.$$

We can conclude that

$$Z(\delta_n(t))p_{\varpi_n \theta_n(t)}^n(\cdot, u_n(t)) \rightarrow Z(t)u \text{ in } \mathcal{C}_0. \tag{6}$$

Finally,  $\dot{u}(t) \in \Pi(t, Z(t)u)$ . Indeed, by (4), (6) and condition (iii), we infer that

$$d(\dot{u}_n(t), \Pi(t, Z(t)u)) \leq \eta(t)\|Z(\delta_n(t))p_{\varpi_n \theta_n(t)}^n(\cdot, u_n(t)) - Z(t)u\| \text{ a.e.}$$

Passing to the limit in this inequality as  $n \rightarrow \infty$ , we have

$$d(\dot{u}(t), \Pi(t, Z(t)u)) = 0 \text{ a.e.}$$

So,  $u$  satisfies

$$\begin{cases} \dot{u}(t) & \in \Pi(t, Z(t)u) & \text{a.e. on } [0, T]; \\ u(t) & = \psi(0) + \int_0^t \dot{u}(s)ds & \forall t \in [0, T]; \\ u(t) & = \psi(t) & \forall t \in [-\tau, 0]. \end{cases}$$

The proof is then complete.

#### 4 Application: a Delay Perturbed Sweeping Process

In this section, we present an application for functional differential inclusions governed by time and state-dependent nonconvex sweeping process. The sweeping process is a constrained differential inclusion involving normal cones, which appears naturally in several applications such as elastoplasticity, electrical circuits, hysteresis, crowd motion, etc. This kind of problems corresponds to several important mechanical problems, planning procedures in mathematical economy and nonsmooth dynamical systems. We propose here a new variant of the existence result which generalizes the previous results.

**Theorem 4.1** *Let  $H$  be a separable Hilbert space and let  $C : [0, T] \times H \rightrightarrows H$  be a set-valued mapping with nonempty closed values satisfying the following assumptions:*

$(\mathcal{H}_1^C)$  *for all  $(t, u) \in [0, T] \times H, C(t, u)$  is uniformly subsmooth;*

$(\mathcal{H}_2^C)$  *there are real constants  $L_1 > 0$  and  $0 < L_2 < 1$  such that for all  $t, s \in [0, T]$ , and  $u, v, z \in H$ ,*

$$|d(z, C(t, u)) - d(z, C(s, v))| \leq L_1|t - s| + L_2\|u - v\|;$$

$(\mathcal{H}_3^C)$  *for any bounded subset  $A \in H$ , the set  $C(t, A)$  is ball-compact.*

*Assume that  $(\mathcal{H}_1^C)$ ,  $(\mathcal{H}_2^C)$ ,  $(\mathcal{H}_3^C)$  and hypotheses  $\mathcal{H}_{(\Pi)}$  are satisfied. Then, for any  $\psi \in \mathcal{C}_0$  with  $\psi(0) = u_0 \in C(0, u_0)$ , there exists a continuous solution  $u : [-\tau, T] \rightarrow H$ , Lipschitz on  $[0, T]$  to the problem*

$$(R) \quad \begin{cases} \dot{u}(t) \in -N_{C(t, u(t))}(u(t)) + \Pi(t, Z(t)u), & \text{a.e. in } [0, T]; \\ u(t) \in C(t, u(t)), \quad \forall t \in [0, T]; \\ \psi(s) = Z(0)u(s), \quad \forall s \in [-\tau, 0]. \end{cases}$$

**Proof.** By using the discretization approach based on Moreau’s catching-up algorithm, the proof is a careful adaptation of Theorem 3.5 in [7].

#### 5 Conclusion

In this paper, we established an existence result to first order functional differential inclusions for a general class of unbounded nonconvex sets. The approach used is an adaptation of a reduction method which consists of replacing the problem with delay with a problem without delay and applying the known results in this case. As an application, we stated also a new version of the existence result for a first order perturbed nonconvex sweeping process that finds several applications in nonsmooth dynamical systems such as differential complementarity systems and vector hysteresis problems. This will be the subject of forthcoming works.

#### Acknowledgment

Research supported by the General direction of scientific research and technological development (DGRSDT) under project PRFU No. C00L03UN180120180001.

**References**

- [1] D. Affane and M. F. Yarou. Perturbed first-order state dependent Moreau's sweeping process. *Int. J. Nonlin. Anal. Appl.* **12** (2021) 605–615.
- [2] D. Affane and M. F. Yarou. General second order functional differential inclusions driven by the sweeping process with subsmooth sets. *J. Nonlin. Funct. Anal.* **26** (2020) 1–18.
- [3] H. Attouch and R. J. B. Wets. Quantitative stability of variational system: I. The epigraphical distance. *Amer. Math. Soc.* **328** (1991) 695–729.
- [4] M. Bounkhel and M. F. Yarou. Existence results for first and second order nonconvex sweeping process with delay. *Portugaliae Mathematica.* **61** (2004) 207–230.
- [5] C. Castaing and A. G. Ibrahim. Functional differential inclusion on closed sets in Banach spaces. *Adv. Math. Econ.* **2** (2000) 21–39.
- [6] C. Castaing, A. G. Ibrahim and M. F. Yarou. Existence problems in second order evolution inclusions: discretization and variational approach. *Taiwanese J. Math.* **12** (2008) 1435–1477.
- [7] C. Castaing, A. G. Ibrahim and M. F. Yarou. Some contributions to nonconvex sweeping process. *J. Nonl. Conv. Anal.* **10** (2009) 1–20.
- [8] H. Chouial and M. F. Yarou. Reduction method for functional nonconvex differential inclusions. *Maltepe J. Math.* **3** (2021) 6–14.
- [9] A. Fryszkowski. Existence of solutions of function-differential inclusion in nonconvex case. *Anal. Polonici Math.* **45** (1985) 121–124.
- [10] T. Haddad, J. Noel and L. Thibault. Perturbed sweeping process with a subsmooth set depending on the state. *Linear Nonlin. Anal.* **2** (2016) 155–174.
- [11] A. A. Tolstonogov. Existence and relaxation of solutions to differential inclusions with unbounded right-hand side in a Banach space. *Siberian Math. J.* **58** (2017) 727–742.
- [12] M. F. Yarou. Reduction approach to second order perturbed state-dependent sweeping process. *Crea. Math. Infor.* **28** (2019) 215–221.



# SOFC-PV System with Storage Battery Based on Cuckoo Search Algorithm

Hamidia Fethia\* and Abbadi Amel

*LREA Laboratory, Yahia Feres University, Medea, Algeria.*

Received: March 9, 2022; Revised: September 13, 2022

**Abstract:** Each panel had an operating point (current, voltage) which allowed it to deliver its maximum power. It is therefore necessary to try to control the choppers in order to stay as close as possible to the requested operating point. For this, we use the search algorithms for the optimal operating point (Maximum Power Point Tracker or MPPT). Lately, the MPPT technique has become the focus for a significant number of researches in order to improve the dynamic performance of the PV system, so we can distinguish several algorithms of the MPPT such as the P&O (Perturb & Observe) and those based on intelligent techniques such the meta-heuristic approach.

We will study and discuss in this work, the use of the Cuckoo Search (CS) algorithm to determine the maximum power point by using in the first section, the PV with a resistance load; in the second section, the same algorithm is used also to tune the PI controllers' gains of rotor speed and the DC-DC controller to adjust the DC Voltage coming from the PV/SOFC-Battery with an alternative load, in order to be able to supply the inverter which is connected to the induction motor and controlled by the Direct Torque Control (DTC), driving a centrifugal pump. The simulation results show the effectiveness of the proposed technique using the pumping system supplied by a hybrid source.

**Keywords:** *DTC; IM; hybrid SOFC-PV system; MPPT; battery storage; CSA.*

**Mathematics Subject Classification (2010):** 70Kxx, 93C10, 93-XX.

---

\* Corresponding author: [mailto:fe\\_hamidia@yahoo.fr](mailto:fe_hamidia@yahoo.fr)

## 1 Introduction

Optimization is a branch of mathematics, seeking to analyze and solve analytically or numerically the problems which consist in determining the best element of a set. Optimization methods are currently occupying a very important place in the scientific field given the complexity of industrial problems. The researchers thought about finding the solutions of these problems by flexible methods to integrate various specific constraints.

The algorithms of the first class are those of the conventional methods. These include the Newton-Raphson method, Nonlinear Programming (NLP), Quadratic Programming (QP), the Newton Method, Mixed Integer Programming and Dynamic Programming. All these mathematical methods are fundamentally based on the convexity of the objective function to find the minimum. According to the limits of conventional methods, the need to introduce new optimization techniques capable of overcoming the problem posed by classical methods is imperative. The methods which offer this possibility are the intelligent methods called “metaheuristic”.

Metaheuristics are recently developed stochastic optimization methods. For this concern, numerous mathematical programming approaches for metaheuristic optimization have been proposed for example ‘Particle Swarm Optimization’ (PSO) is proposed by Kennedy and Eberhart [1]. They inspire the social behavior of swarming animals, such as flocks of birds and schools of fish. An individual in the swarm has only local knowledge of his situation in the swarm. It uses this local information, as well as its own memory, to decide where to move. Ant Colony Optimisation (ACO) is proposed by Dorigo [2], it results from the observation of social insects, especially ants, which naturally solve complex problems. This ability is found to be possible due to the ability of ants to communicate with each other indirectly, by depositing chemicals on the ground which are called pheromones. This type of indirect communication is called stigmergy. We have also the artificial bee colony (ABC) proposed by Dervis Karaboga [3], genetic algorithms (GA) proposed by Holland [4] and the Bat algorithm proposed by Xin-She Yang [5], etc. In a difficult energy context, marked by the foreseeable exhaustion of fossil fuels and their impacts on the environment, expectations in terms of renewable energies in general and solar energy in particular, are increasingly important. These energies and, more particularly, solar energy are considered to be the future energy solution. Indeed, solar energy is one of the most environmentally friendly energy, an economical and sustainable source. Lately, the MPPT technique has become the focus for a significant number of researches in order to improve the dynamic performance of the PV system, mainly in terms of the ability to rapidly pursue the global power point (GMPP) in the presence of other local maximums power point (LMPP). Researchers have been interested in another type of the MPPT technique which is based on the meta-heuristic approach, for example the MPPT-ABC [6], MPPT-GA [7] and MPPT-ACO [8].

The CS algorithm was first proposed by Yang and Deb [9], the Cuckoo Search (CS) is a recent metaheuristic which is inspired by the mode of reproduction of certain species of cuckoos. In fact, their reproduction strategy is unique in that the females lay their eggs in the nests of other species (whose eggs look similar). These eggs can then be incubated by surrogate parents. On the other hand, when cuckoo eggs manage to hatch in the host nest (they hatch faster), cuckoo chicks have the reflex to eject the host species eggs out of the nest and even mimic the call of the host chicks, for the purpose of being fed by the host species. However, it can happen that cuckoo eggs are discovered; in this case, the surrogate parents remove them from the nest, or abandon the nest and start their brood

elsewhere. This meta-heuristic is therefore based on this parasitic behavior of cuckoo species associated with a “Levy flight” type of movement logic specific to certain birds and certain species of flies.

This work proposes the use of the cuckoo search algorithm to track the MPP and get the desired DC Voltage needed later by using the boost converter, so the first part proposes the PV as a source and resistance as a load. In the second part, we propose the CS algorithm to tune the gains of PI controllers of speed and the DC-DC Voltage controller connected to the battery of hybrid system (SOFC-PV with storage battery), so we have hybrid system as source and the induction motor driving a centrifugal pump as a load.

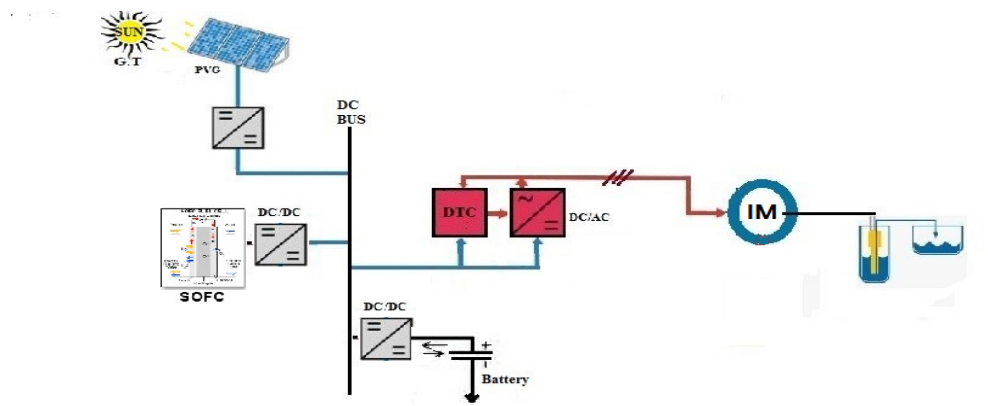


Figure 1: Scheme of SOFC-PV with a storage battery for the pumping system.

## 2 PV Module

Solar panels are intended to recover energy from solar radiation to transform it into heat or electricity. PV modules (usually presented in the form of panels) consist of a number of elementary cells placed in series in order to make the voltage at the output usable. These modules are then associated in a network (series-parallel) so as to obtain the desired voltages / currents. An equivalent circuit model for a solar cell is shown in Figure 2. The model consists of a current source, a diode, a shunt resistor  $R_P$  and a series resistance  $R_S$ .

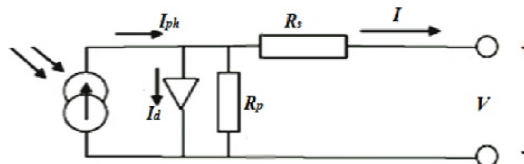


Figure 2: PV cell model.

The topology of the boost converter is shown in Figure 3. For this converter, the

output voltage is always higher than the input PV voltage. Power flow is controlled by the on/off duty cycle of the switching transistor. This converter topology can be used in conjunction with lower PV voltages. No extra blocking diode is necessary when the boost topology is used. For sizing a photovoltaic system, we need to know in the first the motor consumption energy (as in our case we need to get  $U_{dc}=514V$ ). Then, we must take in account the obtained results and also the meteorological data as the input parameters of the photovoltaic installation of the input program.

The data sheet information on the PV panel is presented in Table 1. The commercialized solar modules are formed generally by a number of cells assembled in parallel  $N_p$  or /and in series  $N_s$ . The relationship between the cell terminal current and voltage is given by

$$I = I_{ph} + I_0 \left[ \exp\left(\frac{V + I.R_s}{\alpha.V_{th}} - 1\right) \right] - \frac{V + I.R_s}{R_p}, \quad (1)$$

where  $V_{th}$  is the thermal voltage of the cell,  $I_{ph}$  is the photocurrent, it depends mainly on the radiation and cell's temperature.

### 3 MPPT Based on Cuckoo Search Algorithm

Both P&O and INC algorithms may have difficulty in finding the optimum when used in large arrays where multiple local maxima occur [9]. In this section, we propose a cuckoo search algorithm to track the maximum power point. A boost converter, or parallel chopper, is used when it is desired to increase the available voltage of a DC source by controlling the duty cycle of the switching transistor. In photovoltaic systems, this converter can be used as a source-load adapter, when the operating point in direct coupling is on the right-hand of the MPP.

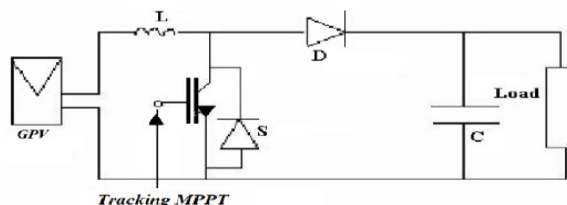


Figure 3: Boost Converter DC/DC.

#### 3.1 Cuckoo Search principle

The Cuckoo Search (CS) algorithm is based on the following rules:

- Each cuckoo lays only one egg at a time and places it in a randomly chosen nest.
- The best nests with high quality eggs (solutions) are kept for the next generations.
- The number of host nests is fixed and the egg laid by a cuckoo can be discovered by the host species with a probability  $P_a \in [0, 1]$ . In this case, the host bird either takes the egg out of the nest or leaves the nest and builds a new one.

To simplify, this last hypothesis can be approached by replacing a fraction  $P_a$  of nests with new ones. In CS, each egg in a nest represents a solution and each cuckoo can lay a single egg, the goal is to use the new and potentially better solution to replace a poorer solution in a nest. Although the algorithm can be extended to a more complex case where each nest contains several eggs representing a set of solutions, here we use a simpler version where each nest contains only one egg. In this case, there is no longer any distinction between the egg, nest or cuckoo, and each nest corresponds to an egg which also represents a cuckoo.

### 3.2 Levy Flight

In the context of CS, the cuckoo movement pitch is determined by the Levy Flight (Figure 4). The Levy flight is a random walk in which the steps have a length having a certain probability distribution (Levy distribution), the direction of the steps being isotropic and random. Levy Flight is a class of random walk in which the jumps are distributed according to the Levy distribution which consists of a power law with an infinite variance and a mean of the type:  $Levy(\beta) \sim (y) = x^{-\beta}$ ,  $1 < \beta < 3$ .

In the case of CS, the use of the Levy Flight improves and optimizes the search: new solutions are generated by a random Levy walk around the best solution obtained so far, which speeds up the overall search. From an implementation point of view, generating

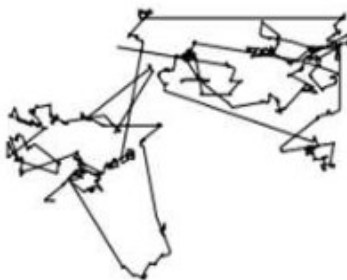


Figure 4: Levy Flight.

a random number with the Levy Flight follows two steps: choosing a random direction and generating the step that should obey the Levy distribution. The generation of a direction can be achieved from a uniform distribution, while the generation of steps is more delicate. There are several methods to achieve this, but one of the simplest and most efficient is to use Mantegna's formulas to determine the step  $s$ :

$$s = \frac{u}{|v|^{\frac{1}{\beta}}}. \quad (2)$$

### 3.3 MPPT-CSA

In general, the Lévy flight is characterized by using the following relation

$$x_j^{i+1} = x_j^i + \alpha \oplus Levy \quad (3)$$

and the operator  $\oplus$  represents the entry-wise multiplication [10] for the multidimensional problem. For MPPT, it can be simplified to

$$D_j^{i+1} = D_j^i + \alpha \cdot Levy = D_j^i + s, \quad (4)$$

where

$$s \approx k \cdot \frac{u}{|v|^{\frac{1}{\beta}}} (D_{best} - D), \quad (5)$$

where  $u$  and  $v$  are the centered Gaussian distributions such that

$$u = N(0, \delta_u^2), \quad v = N(0, \delta_v^2) \quad (6)$$

with

$$\delta_u = \left[ \frac{\gamma(1+\beta) \times \sin \pi \times (\frac{\beta}{2})}{\gamma(\frac{1+\beta}{2}) \times \beta \times 2^{\frac{\beta-1}{2}}} \right]^{\frac{1}{\beta}}. \quad (7)$$

Figure 5 represents the schematic diagram of the DC-DC converter of a Photovoltaic panel using the MPPT based on the Cuckoo Search Algorithm and connected to the resistance load.

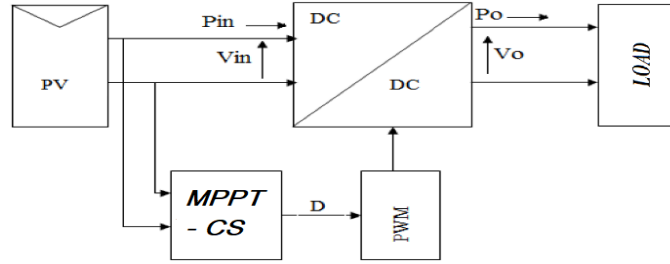


**Figure 5:** MPPT based on the Cuckoo Search Algorithm.

#### 4 Solid Oxide Fuel Cell

The electrolyte must be an electronic insulator and an ionic conductor. It can be either liquid or solid. The bipolar plates allow the access of gases to the reaction sites by the presence of channels.

There are six types of fuel cells which, depending on the electrolyte, operate at different temperatures. They are the Alkaline Fuel Cell (AFC), Proton Exchange Membrane Fuel Cell, Direct Methanol Fuel Cell (DMFC), Phosphoric Acid Fuel Cell (PAFC), Molten carbonate battery (MCFC Molten Carbonate Fuel Cell), Solid Oxid Fuel Cell (SOFC (this type is used in our work)) as shown in Figure 6.

Fuel cells therefore allow the direct transformation of the chemical energy of the reaction of a hydrogen fuel with an oxidant oxygen into electrical energy. The electrical energy comes from the electronic exchange of the chemical reaction and not from the heat given off by the latter. To do this, two compartments containing the oxidant and the fuel, respectively, are produced on either side of the electrolyte, thus avoiding the mixing of the gases and therefore, the direct chemical reaction.

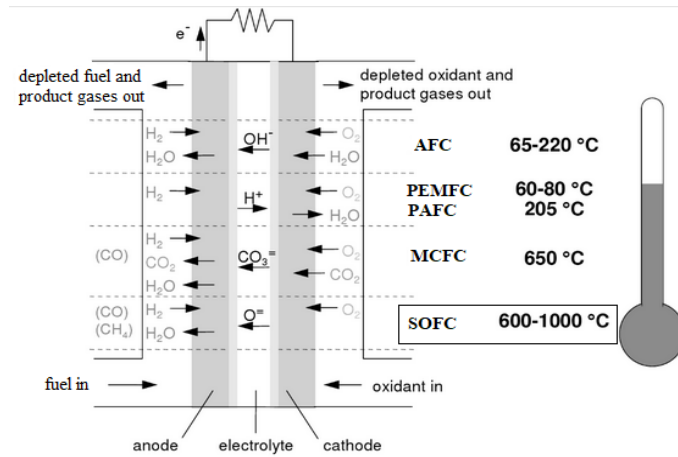
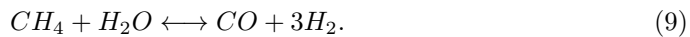
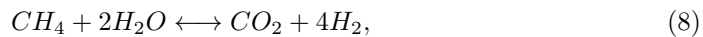


**Figure 6:** Fuel cells types; their reaction and operation temperatures [11].

On both sides of the electrolyte in each gas compartment electrodes are arranged which at the same time ensure the transport of electrons and ionic species (Figure 6). The fuel cell stack is composed of numerous single fuel cells in a series. Thus, the total voltage of the stack is approximately equal to the sum of every single cell voltage [12].

Reactions occurring in the SOFC are as follows [13].

Reforming reactions



Water-gas shift reaction



Electrochemical reactions Anode



Cathode



## 5 Direct Torque Control DTC

The direct torque control has many advantages that are already well known over conventional techniques: the fast torque response; it is considered as a sensor-less control, robust against the variation of machines parameters; relatively simple without the Park transformation and without pulse width modulation (PWM). It also allows decoupling between the control of the flux and the torque. Thus, several research works have been developed for the application of this technique to synchronous and asynchronous machines.

The first application of the DTC to the asynchronous machine appeared in the 1985s, and was proposed by Takahachi and Bepenbrock [14]. The stator flux vector can be estimated using the measured current and voltage vectors [15–17]

$$\frac{d\varphi_s}{dt} = V_s - R_s I_s \quad (14)$$

or

$$\varphi_s = \int (V_s - R_s I_s) dt. \quad (15)$$

The DTC is based on the use of the hysteresis controllers, to control the estimated stator flux and electromagnetic torque. These two variables are controlled by a hysteresis controller with two-level.

The output of the comparators and the stator flux angle are used to index a switch table of optimum voltage vectors, in order to determine the suitable voltage vectors. The sector of the stator flux is divided into six sectors. It indicates that the appropriate voltage vector should be chosen in a particular sector, either to increase the stator flux or to decrease the stator flux and either to increase torque or to decrease torque.

## 6 Pumping System

The proposed hybrid system is shown in Figure 1. The battery is also connected to dc link through a DC-DC converter. Figure 7 represents the controller of a DC-DC converter used to maintain the dc voltage constant that is needed to feed our pumping system.

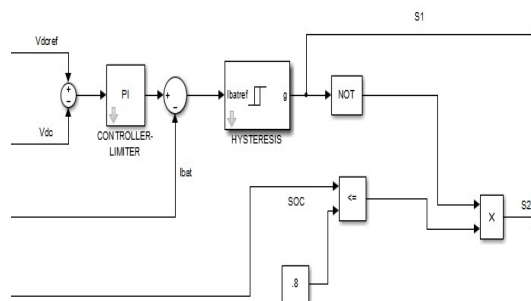


Figure 7: DC-DC Converter Controller.

## 7 Battery Storage

The battery control is an essential element for the success of autonomous systems. The batteries used in autonomous systems are generally of the lead-acid (Pb) type. Cadmium-nickel (NiCd) batteries are rarely used anymore because their price is much higher and they contain cadmium (toxic). Their replacements, nickel-metal hydride batteries (NiMH) are interesting and used in this paper.

Treating the controller output as the reference current for the battery, a hysteresis band approach is adapted to switch either Q1 or Q2 of the DC-DC converter as shown in Figure 8.

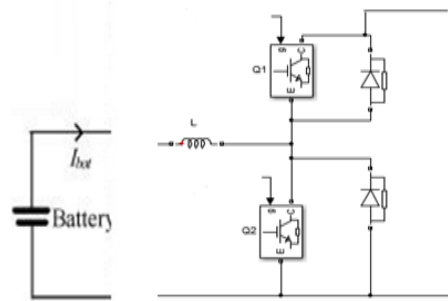


Figure 8: Controller battery.

In this work, the battery acts as a source or sink, the depth of discharge is equal to 60%.

## 8 Tuning PI Gains by Cuckoo Search Algorithm

The input of our PI controller is used the error calculated by the difference between the reference and instantaneous values ( $e_1 = w^* - w$ ) of the PI speed controller and ( $e_2 = V_{dc}^* - V_{dc}$ ) of the PI-DC Voltage source. The PI controller for the above system can be presented as the following expression

$$u = k_p e(t) + k_i \int e(t) dt. \quad (16)$$

Cost-function is presented by calculation of the error between the reference and estimated values; and the numbers of iterations and population used in this work are the same;  $it=50$ ,  $N_{po}=15$ .

## 9 Digital Simulation

The pumping system is built using MATLAB/SIMULINK. In this simulation, the induction machine parameters are listed in Table 2. The centrifugal pump performances used in this work for speed of 2900 tr/min are:  $Q=30 \text{ m}^3/h$ ,  $H=80\text{m}$ ,  $P=1.5 \text{ KW}$ . SOFC with 200 cells in a series. We observe the performance of the proposed supply system with 11 PV solar panels to get 514V.

## 10 Discussion of Results

In the first part, as shown in Figure 9, the DC Voltage and Duty Cycle responses (of the output of the DC-DC converter connected to the resistance load) are presented using the system presented in Figure 5. In the second part, we propose to add a SOFC with a storage battery to supply an alternative load (IM-Pump). The pumping system is simulated with constant load torque (10N.m) applied between 0.6sec and 0.8 sec and the variation of irradiation and temperature as shown in Figure 10, and a simulation was run in a closed loop as shown in Figures 10 and 11, where it can be observed that the DC Voltage, flux and rotor speed track their references ( $V_{dc}^*=514\text{V}$ ,  $\text{Flux}^*=1.1\text{Wb}$ ,  $w^*=126 \text{ rad/ sec}$ ). To get the desired value of voltage, we have used 11 panels.

The nominal open-circuit voltage	42.1V
The nominal short-circuit current	3.87A
The voltage at the MPP	33.7V
The maximum experimental peak output power	120W
The current at the MPP	3.56A
The open-circuit voltage/ $T^{\circ}$ coefficient	$(80 \pm 10)mV\%C^{\circ}$
The short circuit current/ $T^{\circ}$ coefficient	$(0065 \pm 0.015)mV\%C^{\circ}$
Parallel resistance $R_s$	$0.473\Omega$
Serie resistance $R_p$	$1367\Omega$

**Table 1:** Data sheet information of PV panel “BP MSX120”.

Power	3.5Kw
Stator resistance	4.85 Ohm
Rotor resistance	3.805 Ohm
Inertia	$0.031Kg.m^2$
Friction	0.001136
Frequency	50 Hz
Stator inductance	0.274H
Rotor inductance	0.274 H
Mutual Inductance	0.258 H
Poles	2

**Table 2:** Data sheet information on the Induction Motor.

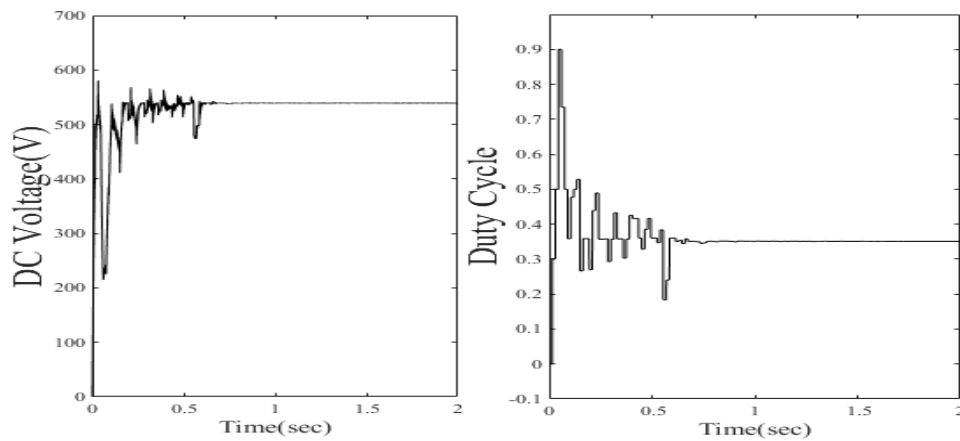


**Figure 9:** DC Voltage response using PV connected to the resistance load and based on the MPPT-CS method ( $G=1000W/m^2$ ,  $T=298K$ ).

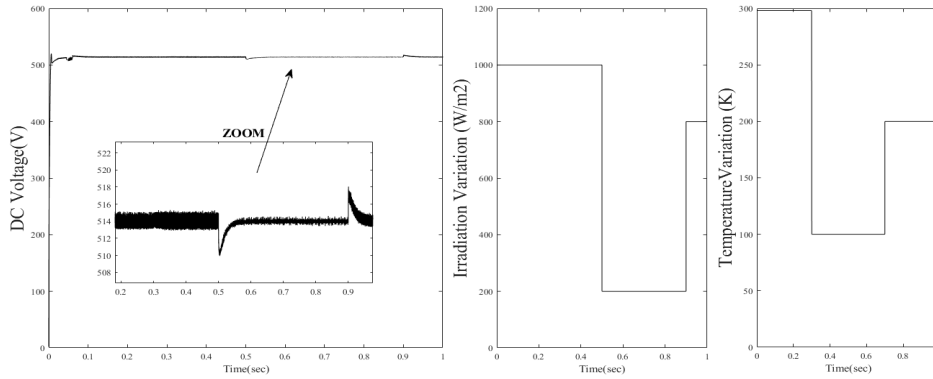


**Figure 10:** DC Voltage response using Hybrid System (PV-SOFC-Battery-IM-Pump) based on the CS method with irradiation, temperature and torque variation.

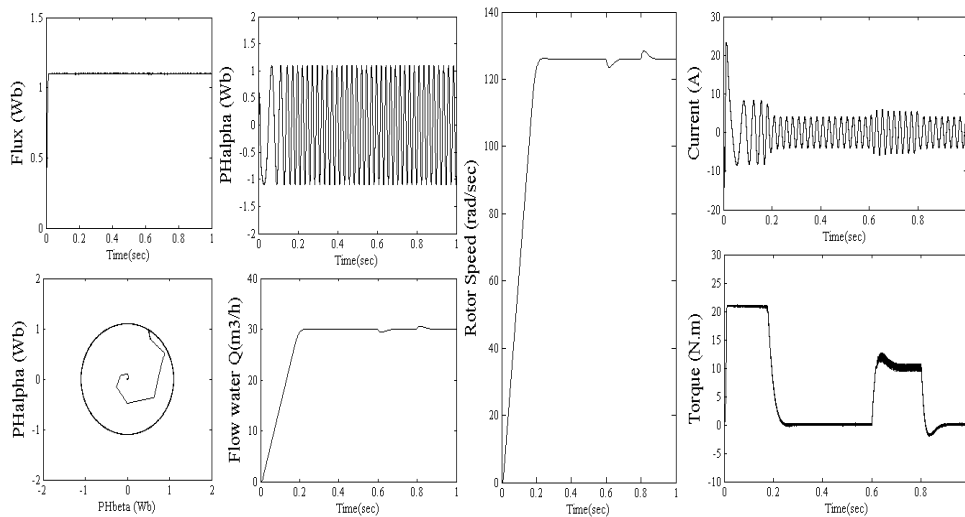


**Figure 11:** Current, Flow of water, Flux, Torque and Rotor Speed responses of a hybrid (PV-SOFC-battery-IM-Pump) System based on the CS method with irradiation, temperature and torque variation.

### 11 Conclusion

The aim of this study is to resolve the drawback of power loss caused by oscillations around the maximum power point (MPP) and the relatively low response time to rapid changes in weather conditions. This paper proposes another type of the control named a meta-heuristic algorithm (Cuckoo Search Algorithm), which is used on one hand to track the maximum power point, and in second hand, the same metaheuristic algorithm is used to tune the PI gains to get the desired value that we need to supply our system (514V).

The obtained simulation results show the effectiveness of the proposed algorithms using in the first section the load resistance supplied by PV and in the second part the induction motor driving pump fed by a hybrid system.

## References

- [1] J. Kennedy and R. Eberhart. Particle Swarm Optimization. *IEEE Proceeding of the Sixth International Symposium on Neural Networks* **4** (1995) 1942–1948.
- [2] M. Dorigo and T. Stützle. The Ant Colony Optimization Metaheuristic: Algorithms, Applications and Advances. *Handbook of Metaheuristics*, Chapter 9, 2009, 250–285.
- [3] K. Karaboga and B. Basturk. Artificial Bee Colony (ABC) Optimization Algorithm for Solving Constrained Optimization Problems. *Foundations of Fuzzy Logic and Soft Computing* (2007) 789–798.
- [4] K. Sastry, D. Goldberg and G. Kendall. Genetic Algorithms. *Search Methodologies*, Chapter 4, 2005, 97–125.
- [5] X. S. Yang and X. He. Bat algorithm: literature review and applications. *International Journal Bio-Inspired Computation* **5** (3) (2013) 141–149.
- [6] N. Li, M. Mingxuan, W. Yihao, C. Lichuang, Z. Lin and Z. Qianjin. Maximum Power Point Tracking Control Based on Modified ABC Algorithm for Shaded PV System. In: *AEIT International Conference of Electrical and Electronic Technologies for Automotive*, 2019.
- [7] P. Kumar, G. Jain and D. K. Palwalia. Genetic algorithm based maximum power tracking in solar power generation. In: *15 International Conference on Power and Advanced Control Engineering (ICPACE)*, 2015.
- [8] K. Rajalashmi and C. Monisha. Maximum Power Point Tracking Using Ant Colony Optimization for Photovoltaic System Under Partially Shaded Conditions. *International Journal of Engineering and Advanced Technology (IJEAT)* **8** (2C2) (2018) 82–87.
- [9] D. A. Nugraha, K. L. Lian and L. Suwarno. Novel MPPT Method Based on Cuckoo Search Algorithm and Golden Section Search Algorithm for Partially Shaded PV System. *Canadian Journal Of Electrical and Computer Engineering* **42** (3) (2019) 173–182.
- [10] J. Y. Shi, F. Xue, Z. J. Qin, W. Zhang, L. T. Ling and T. Yang. Improved Global Maximum Power Point Tracking for Phtovoltaic System Via Cuckoo Search Under Partial Shaded Conditions. *Journal of power Electronics* **16** (1) (2016) 287–296.
- [11] F. Babir. *PEM Fuel Cells: Theory and Practice*. Elsevier Academic Press, 2005.
- [12] W. J. Zou and Y. B. Kim. Temperature Control for a 5 kW Water-Cooled PEM Fuel Cell System for a Household Application. *IEEE Access* **7** (2019) 144826–144835.
- [13] J. Li, N. Gao, J. Y. Cao, H. Y. Tu, M. R. Hu, X. J. Zhui and J. Li. Predictive control of a direct internal reforming SOFC using a self-recurrent wavelet network model. *Journal of Zhejiang University-SCIENCE A (Applied Physics & Engineering)* **11** (1) (2010) 61–70.
- [14] M. Depenbrock. Direct self-control (DSC) of inverter fed induction machine. *IEEE Power Electronics Specialists Conference* (1987) 632–641.
- [15] S. Bentouati, A. Tlemçani, M. S. Boucherit and L. Barazane. A DTC Neurofuzzy Speed Regulation Concept for a Permanent Magnet Synchronous Machine. *Nonlinear Dynamics and Systems Theory* **13** (4) (2013) 344–358.
- [16] F. Hamidia, A. Larabi, A. Tlemceni and M. S. Boucherit. AIDTC Techniques for Induction Motors. *Nonlinear Dynamics and Systems Theory* **13** (2) (2013) 147–156.
- [17] F. Hamidia, A. Abbadi, A. Tlemceni and M. S. Boucherit. Dual Star Induction Motor supplied with double Photovoltaic Panels Based on Fuzzy Logic Type-2. *Nonlinear Dynamics and Systems Theory* **18** (4) (2018) 359–371.



# Application of Accretive Operators Theory to Linear SIR Model

Mariam El Hassnaoui\*, Said Melliani and Mohamed Oukessou

*Laboratory of Applied Mathematics and Scientific Computing  
Sultan Moulay Slimane University B.P. 523, 23000 Beni-Mellal, Morocco.*

Received: September 8, 2021; Revised: July 8, 2022

**Abstract:** In this paper, we discuss the existence and uniqueness results for a linear SIR (Susceptible-Infected-Recovered) model on  $L^p$ -spaces, for  $1 \leq p < +\infty$ . This work represents two extensions of the basic static linear model presented in [4]. Our analysis is fundamentally based on the accretive operators theory.

**Keywords:** *SIR; epidemic models; accretive operators; existence result; mild solution.*

**Mathematics Subject Classification (2010):** 92D30, 47H06, 35F10.

## 1 Introduction

In epidemiology, mathematical models have become important tools in analyzing the spread and control of infectious diseases caused by bacteria, viruses and fungi through a direct transmission from individual-to-individual: through a sneeze, cough, skin-skin contact and exchange of body fluids. Some examples of the diseases are Coronavirus disease (Covid-19), Acquired Immune Deficiency Syndrome (AIDS), Ebola, Dengue fever, etc. The first mathematician who proposed a mathematical model describing an infectious disease is Daniel Bernoulli. In 1760, he modelled the spread of smallpox [8]. In our case, we are interested in the SIR model which can model Coronavirus disease. This model was first used by Kermack and McKendrick in 1927, and has subsequently been applied to a variety of diseases [13]. They have considered a constant total population and assumed that the interaction between the groups was determined by the disease transmission and removal rates. They have classified the population into three groups: susceptible (S), infected (I) and recovered (R). There have been many variations such as

---

\* Corresponding author: <mailto:mariam.hassnaoui@gmail.com>

classical epidemiological models. These models are based on the standard Susceptible-Infectious-Recovered (SIR) compartments segmented in the model. Susceptible is a group of people who are vulnerable to infection when contacting with infectious people, see [11] and the references therein.

The SIR model was discussed by many authors. Diekmann et al. [10] studied epidemic models with one strain. However, Ackleh and Allen [1] studied SIR-type models of disease with  $n$  strains and vertical transmission. In 2009, Hina Khan et al. [14] solved the SIR model by means of an analytic technique for nonlinear problems and the homotopy analysis method. After two years, Bain et al. studied the existence of at least two positive periodic solutions of the SIR model in [5]. They based on the continuation theorem of coincidence degree theory. Moreover, in 2016, I. Al-Darabsah and Y. Yuan proposed the mathematical model for the transmission by SIR for Ebola [2]. In the same year, I. Ameen and P. Novati studied the fractional SIR model with constant population [3], they obtained a numerical solution using discrete methods.

The aim of this paper is to study the problem (1) on  $L^p$  spaces, for  $1 \leq p < \infty$ . We note that our SIR model is linear because we have ignored the transmission of the epidemic disease from one person to another person. We note that this model was investigated theoretically in a number of papers. For example, in [16], the authors studied a stochastic epidemic-type model with enhanced connectivity, and they obtained an exact solution of the model. Our objective in this work is to discuss the existence and uniqueness result for the problem (1). In fact, although this model is standard, in our situation, we have encountered some difficulties lying in the fact that the problem is composed of three equations that are strongly coupled. To overcome these difficulties, we first rewrite our system as a Cauchy problem involving two matrix operators, and we show that the latter one has a unique solution using the accretive theory. We note that the solution of this system gives more information on the propagation of the epidemic. In general, it is difficult to compute the analytical solution of the problem. On the other hand, it is usually impossible to obtain the exact solution for the general case. Therefore, our approach guarantees the existence and uniqueness of the solution, we can approximate the solution using numerical methods.

The rest of this paper is organized as follows. In the next section we present the mathematical formulation of the SIR model. In Section 3, we introduce the functional setting and gather some preliminary facts in connection with the problem. The existence and uniqueness for the problem (Theorem 4.1) is stated in Section 4 by the accretive theory.

## 2 Model Formulation

In this section, we give the mathematical formulation describing the mechanism of the SIR model. The following diagram represents the SIR model. In this diagram:

- $b$  : Immigration rate of susceptible.
- $c$  : Specific rate of contact with pathogen.
- $\beta$  : Probability of infection when there is direct contact.
- $\mu$  : Probability of illness in case of infection.
- $\xi$  : 1/shedding period.

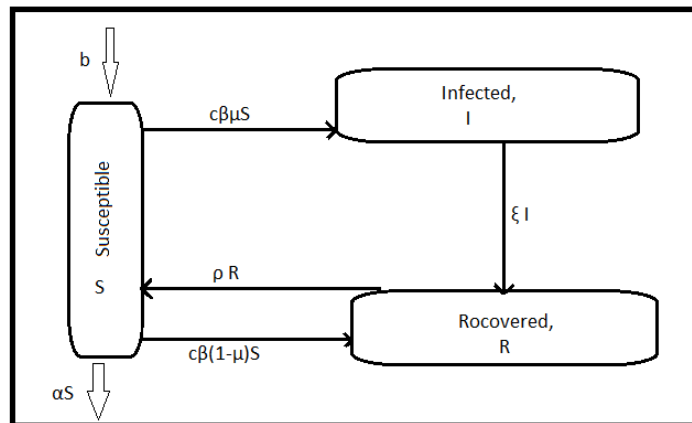


**Figure 1:** The mechanism of SIR model.

- $\alpha$  : Specific death rate in population.
- $\rho$  : Specific immunity loss rate.

We denote the total population size by  $N$ , i.e.,  $N(t, a) = I(t, a) + S(t, a) + R(t, a)$ . Now, in order to formulate the dynamics of the above diagram mathematically, the following assumptions have been adopted:

1. There is a constant number of the host populations entering into the system with the immigration rate  $b > 0$ .
2. Person-to-person transmission can be ignored.
3.  $\alpha$  is the same for all  $S - I - R$  classes.
4. The parameters  $\xi$  and  $\rho$  are constants.
5. Individuals can become infected and ill and then recover to become immune, or, on exposure, they may pass directly into the immune class.

**Remark 2.1** a) Assumption (3) dictates a linear system, whereas much of the SIR model literature is concerned with nonlinear models, including an SI interaction term [15].

- b) Assumption (4) is permissible because many zoonotic pathogens, and campylobacter in particular, cause much more mild illness rather than death.
- c) Under these assumptions, our system represents an extension of the basic linear model presented in [4].

According to these assumptions, the SIR model can be represented mathematically by the following coupled system of partial differential equations:

$$\begin{cases} \frac{\partial S}{\partial t}(t, a) = t \cdot \frac{\partial S}{\partial a}(t, a) + b(t, a) - (\alpha + c\beta)S(t, a) + \rho R(t, a), \\ \frac{\partial I}{\partial t}(t, a) = c\beta\mu S(t, a) - (\alpha + \xi)I(t, a), \\ \frac{\partial R}{\partial t}(t, a) = \xi I(t, a) + c\beta(1 - \mu)S(t, a) - (\alpha + \rho)R(t, a), \\ S(0, a) = S_0(a), \quad I(0, a) = I_0(a) \quad \text{and} \quad R(0, a) = R_0(a), \end{cases} \quad (1)$$

where  $t \in [0, T]$ ,  $a \in [0, L]$ ,  $L > 0$  and  $b(t, a) = \alpha N(t, a) = \alpha(S(t, a) + I(t, a) + R(t, a))$ . The functions  $S$ ,  $I$  and  $R$  are dependent on time  $t$  and age "a", and all others parameters are independent of time and age.

### 3 Notations and Preliminaries

In this section, we shall fix on the notations and introduce the functional framework, which will be used throughout this paper. Let  $X$  be a real Banach space with norm  $\|\cdot\|$  and dual  $X^*$ .

We are going to introduce now the class of operators for which we could obtain existence and uniqueness results for solutions. Accretive operators were introduced by Browder [9] and Kato [12] independently.

**Definition 3.1** • An operator  $A : D(A) \subset X \rightarrow 2^X$  is said to be accretive if the inequality  $\|u - v + \lambda(\hat{u} - \hat{v})\| \geq \|u - v\|$  holds for all  $\lambda \geq 0$ ,  $u, v \in D(A)$  and  $\hat{u} \in Au$ ,  $\hat{v} \in Av$ . If, in addition,  $R(I + \lambda A)$  (i.e., the range of the operator  $I + \lambda A$ ), is for some, hence for all,  $\lambda > 0$ , precisely  $X$ , then  $A$  is called m-accretive.

• An operator  $A$  is said to be quasi-accretive (quasi-m-accretive) if there exists  $\omega \in \mathbb{R}$  such that  $A + \omega I$  is accretive (respectively, m-accretive), in this case, we say also that  $A$  is  $\omega$ -accretive ( $\omega$ -m-accretive, respectively).

**Remark 3.1** An operator  $A$  is accretive if and only if  $A$  is quasi-accretive with  $\omega = 0$ .

In order to verify accretivity of a given operator, it is useful to take into account alternative characterizations of this property. To do that, we need to introduce the bracket and the duality map.

Let  $u \in X$ . We denote by  $[v, u]_s$  the function defined from  $X \times X$  into  $\mathbb{R}$  by

$$[v, u]_s = \sup\{u^*(v) : u^* \in \Gamma_1(u)\},$$

where  $\Gamma_1(\cdot)$  denotes the duality map from  $X$  into  $2^{X^*}$  given by

$$\Gamma_1(u) = \{u^* \in X^* : \langle u^*, u \rangle = \|u\| \text{ and } |u^*| = 1\}.$$

We also define the duality map  $\Gamma$  from  $X$  into  $2^{X^*}$  by

$$\Gamma(u) = \{u^* \in X^* : \langle u^*, u \rangle = \|u\|^2 \text{ and } |u^*| = \|u\|\}.$$

We recall that the function  $sgn_0(\cdot)$  is defined by

$$sgn_0(x) = \begin{cases} 1 & \text{if } x > 0, \\ 0 & \text{if } x = 0, \\ -1 & \text{if } x < 0. \end{cases}$$

Now, we recall some important facts regarding accretive operators which will be used in our paper, we have the following proposition [6].

**Proposition 3.1** *Let  $A : D(A) \subset X \rightarrow 2^X$  be an operator on  $X$ . The following conditions are equivalent:*

1.  $A$  is an  $\omega$ -accretive operator.
2. the inequality  $[\hat{u} - \hat{v}, u - v]_s \geq -\omega\|u - v\|$  holds for every  $u, v \in D(A)$  and  $\hat{u} \in Au, \hat{v} \in Av$ .
3. for each  $\lambda > 0$  with  $\lambda\omega < 1$ , the resolvent  $(I + \lambda A)^{-1} : R(I + \lambda A) \rightarrow D(A)$  is a single-valued  $\frac{1}{1-\lambda\omega}$ -Lipschitzian mapping.

The quasi-m-accretive operators play an important role in the study of the Cauchy problem.

Consider the following Cauchy problem:

$$\begin{cases} u'(t) + A(u(t)) \ni f(t), & t \in (0, T), \\ u(0) = u_0 \in \overline{D(A)}, \end{cases} \tag{2}$$

where  $A$  is quasi-m-accretive on  $X$  and  $f \in L^1(0, T, X)$ .

Let  $\epsilon > 0$ . An  $\epsilon$ -discretization on  $[0, T]$  of the equation  $u'(t) + A(u(t)) \ni f(t)$  consists of a partition  $0 = t_0 \leq t_1 \leq \dots \leq t_N$  of the interval  $[0, t_N]$  and a finite sequence  $(f)_{i=1}^N \subseteq X$  such that

$$\begin{cases} t_i - t_{i-1} < \epsilon & \text{for } i = 1, \dots, N, \quad T - \epsilon < t_N \leq T, \\ \sum_{i=1}^N \int_{t_{i-1}}^{t_i} \|f(s) - f_i\| ds < \epsilon. \end{cases}$$

A  $D_{A;\epsilon} = (t_0 \leq t_1 \leq \dots \leq t_N; f_1, \dots, f_N)$  solution of (2) is a piecewise constant function  $x : [0, t_N] \rightarrow X$  whose values  $x_i$  on  $(t_{i-1}, t_i]$  satisfy the finite difference equation

$$\frac{x_i - x_{i-1}}{t_i - t_{i-1}} + A(x_i) \ni f_i, \quad i = 1, \dots, N.$$

Such a function  $x = (x)_{i=1}^N$  is called an  $\epsilon$ -approximate solution to the Cauchy problem (2) if it further satisfies

$$\|x(0) - u_0\| \leq \epsilon.$$

The following theorem is known (see [4, Theorem 4.5] or [7, p.108]) and deals with the existence of strong solutions.

**Theorem 3.1** *If  $X$  is a Banach space with the Radon-Nikodym property,  $A : D(A) \subseteq X \rightarrow 2^X$  is a quasi-m-accretive operator, and  $f \in BV(0, T; X)$ , i.e.,  $f$  is a function of bounded variation on  $[0, T]$ , then problem (2) has a unique strong solution whenever  $u_0 \in D(A)$ .*

Let  $f, g \in L^1(0, T; X)$  and  $A$  be a  $\omega$ -accretive operator; if  $u$  and  $v$  are integral solutions of  $u'(t) + Au(t) \ni f(t)$  and  $u'(t) + Au(t) \ni g(t)$ , respectively, then

$$\|u(t) - v(t)\| \leq e^{\omega t} \|u(0) - v(0)\| + \int_0^t e^{\omega(t-s)} \|f(s) - g(s)\| ds. \quad (3)$$

The following theorem plays an important role in our results.

**Theorem 3.2** *Let  $X$  be a reflexive Banach space and let  $A$  be a quasi- $m$ -accretive operator in  $X$ . Let  $F : X \rightarrow X$  be locally Lipschitz. Then, for each  $u_0 \in D(A)$ , there is a local strong solution to the problem*

$$\begin{cases} u'(t) + A(u(t)) \ni F(u(t)), \\ u(0) = u_0 \in \overline{D(A)}. \end{cases}$$

Assume further that

$$\langle -Fu, w \rangle \geq -k_1 \|u\|^2 + k_2, \quad (u, w) \in \Gamma,$$

then the solution is global.

We have the following definition.

**Definition 3.2** We say that  $u \in C(0, T; X)$  is a weak solution of problem (2) if there are sequences  $(u_n) \subseteq W^{1,\infty}(0, T; X)$  and  $(f_n) \subseteq L^1(0, T; X)$  satisfying the following conditions:

1.  $u'_n(t) + A(u_n(t)) \ni f_n(t)$  for almost all  $t \in [0, T]$ ,  $n = 1, 2, \dots$ ;
2.  $\lim_{n \rightarrow \infty} \|u_n - u\|_\infty = 0$ ;
3.  $u(0) = u_0$ ;
4.  $\lim_{n \rightarrow \infty} \|f_n - f\|_1 = 0$ .

The following result, which is an easy consequence of Theorem 3.1, is important.

**Theorem 3.3** *Let  $X$  be a Banach space with the Radon-Nikodym property. Then problem (2) admits a unique weak solution which is the unique integral solution of this problem.*

**Remark 3.2** The results stated above for quasi- $m$ -accretive operators with  $\omega \neq 0$  are also valid for  $m$ -accretive operators.

Let  $p \in [1, +\infty)$ , we denote by  $X_p$  the following space:

$$X_p := L^p([0, T] \times [0, L], dt da).$$

We also consider the following product space:

$$\mathcal{H}_p := X_p \times X_p \times X_p$$

equipped with the norm

$$\|v\|_{\mathcal{H}_p} = \|(v_0, v_1, v_2)^T\|_{\mathcal{H}_p} = \|v_0\|_{X_p} + \|v_1\|_{X_p} + \|v_2\|_{X_p}.$$

#### 4 Existence Result

In this section, we are concerned with the existence and uniqueness result for problem (1). For our subsequent analysis, we need the following hypothesis:

$\mathcal{A}$  : The parameters  $c, \alpha, \beta, \mu, \xi$  and  $\rho$  are positive.

For  $i = 1, 2, \dots, 5$ , let  $F_i$  denote the bounded multiplication operators from  $X_p$  into itself. We define the matrix operator

$$F = \begin{pmatrix} 0 & F_1 & F_2 \\ F_3 & 0 & 0 \\ F_4 & F_5 & 0 \end{pmatrix},$$

where

$$F_1(u_1) = \alpha u_1, \quad F_2(u_2) = (\alpha + \rho)u_2, \quad F_3(u_3) = c\beta\mu_3, \\ F_4(u_4) = c\beta(1 - \mu)u_4 \quad \text{and} \quad F_5(u_5) = \xi u_5.$$

The operators  $F_i, i = 1, \dots, 5$ , are bounded on the space  $X_p$ , therefore  $F$  is also bounded on the product space  $\mathcal{H}_p$ .

**Remark 4.1** The boundedness of the operator  $F$  implies that it is a Lipschitz operator with a Lipschitz constant  $\|F\|_{\mathcal{L}(\mathcal{H}_p)}$ .

Define the following linear operator  $T$  by

$$T : D(T) \subseteq L^p(D) \longrightarrow L^p(D) \\ \psi \longrightarrow T\psi(t, a) = -t \frac{\partial \psi}{\partial a}(t, a).$$

**Remark 4.2** The operator  $T$  is usually called the free streaming operator. It is a closed densely defined linear operator. Its resolvent set  $\rho(T)$  contains the half plane

$$\{\lambda \in \mathbb{C} : \mathbf{Re}\lambda > 0\}.$$

We also define the matrix operator

$$A = \begin{pmatrix} T + c\beta\mu & 0 & 0 \\ 0 & \alpha + \xi & 0 \\ 0 & 0 & \alpha + \rho \end{pmatrix}$$

with the domain  $D(A)$  given by  $D(A) = D(T) \times X_p \times X_p$ .

Now, we establish some auxiliary results required in the proof of our existence and uniqueness result. In the following lemma, we prove that  $A$  is an  $m$ -accretive operator.

**Lemma 4.1** *If the hypothesis  $\mathcal{A}$  is true, then the operator  $A$  is  $m$ -accretive on  $\mathcal{H}_p$ .*

**Proof.** In the first step, we prove that  $A$  is accretive on  $\mathcal{H}_p$ . Indeed, let  $g_1, g_2 \in D(A)$  and let  $u = (u_0, u_1, u_2) \in \Gamma_1(g_1 - g_2)$ . If we note  $g_1 - g_2 = (g_1^0 - g_2^0, g_1^1 - g_2^1, g_1^2 - g_2^2)$ , then, for  $i = 0, 1, 2$ , we have

$$u_i = \|g_1^i - g_2^i\|^{1-p} |g_1^i - g_2^i| \operatorname{sgn}_0(g_1^i - g_2^i).$$

So, we have

$$\begin{aligned}
& [A(g_1) - A(g_2), u]_s \\
\geq & \|g_1^0 - g_2^0\|^{1-p} \int_0^T \int_0^L |g_1^0 - g_2^0|^{p-1} t \cdot \frac{\partial}{\partial a} (g_1^0 - g_2^0)(t, a) \operatorname{sgn}_0(g_1^0 - g_2^0) da dt \\
& + c\beta\mu \|g_1^0 - g_2^0\|^{1-p} \int_0^T \int_0^L |g_1^0 - g_2^0|^{p-1} ((g_1^0 - g_2^0)(t, a)) \operatorname{sgn}_0(g_1^0 - g_2^0) da dt \\
& + (\alpha + \xi) \|g_1^1 - g_2^1\|^{1-p} \int_0^T \int_0^L |g_1^1 - g_2^1|^{p-1} ((g_1^1 - g_2^1)(t, a)) \operatorname{sgn}_0(g_1^1 - g_2^1) da dt \\
& + (\alpha + \rho) \|g_1^2 - g_2^2\|^{1-p} \int_0^T \int_0^L |g_1^2 - g_2^2|^{p-1} ((g_1^2 - g_2^2)(t, a)) \operatorname{sgn}_0(g_1^2 - g_2^2) da dt \\
= & \|g_1^0 - g_2^0\|^{1-p} \frac{1}{p} \int_0^T \int_0^L t \cdot \frac{\partial}{\partial a} (|(g_1^0 - g_2^0)(t, a)|^p) da dt \\
& + c\beta\mu \int_0^L |(g_1^0 - g_2^0)(t, a)|^p da dt + (\alpha + \xi) \int_0^T \int_0^L |(g_1^1 - g_2^1)(t, a)|^p da dt \\
& + (\alpha + \rho) \int_0^T \int_0^L |(g_1^2 - g_2^2)(t, a)|^p da dt \\
= & c\beta\mu \|g_1^0 - g_2^0\|_{X_p} + (\alpha + \xi) \|g_1^1 - g_2^1\|_{X_p} + (\alpha + \rho) \|g_1^2 - g_2^2\|_{X_p} \geq 0.
\end{aligned}$$

This proves that the operator  $A$  is accretive on  $\mathcal{H}_p$ .

To complete the proof, it suffices to establish that  $R(I + A) = \mathcal{H}_p$ , where  $R(I + A)$  denotes the range of the operator  $I + A$ . Indeed, let  $(v_0, v_1, v_2)$  be an element of  $\mathcal{H}_p$ , we seek for an element  $(u_0, u_1, u_2) \in D(A)$  such that

$$\begin{pmatrix} T + c\beta\mu & 0 & 0 \\ 0 & 1 + (\alpha + \xi) & 0 \\ 0 & 0 & 1 + (\alpha + \rho) \end{pmatrix} \begin{pmatrix} u_0 \\ u_1 \\ u_2 \end{pmatrix} = \begin{pmatrix} v_0 \\ v_1 \\ v_2 \end{pmatrix}$$

or equivalently, we look for a solution of the following system:

$$\begin{cases} Tu_0 + c\beta\mu u_0 = v_0, \\ u_1 + (\alpha + \xi)u_1 = v_1, \\ u_2 + (\alpha + \rho)u_2 = v_2. \end{cases}$$

It is clear that

$$\begin{cases} u_1 = \frac{v_1}{1 + \alpha + \xi}, \\ u_2 = \frac{v_2}{1 + \alpha + \rho}. \end{cases}$$

Hence, it remains to solve the equation

$$Tu_0 + c\beta\mu u_0 = v_0. \quad (4)$$

According to Remark 4.2, equation (4) has a unique solution because  $1 \in \rho(T)$ . This yields that  $R(I + A) = \mathcal{H}_p$  and completes the proof.

We introduce the following lemma which shows that the operator  $F$  is Lipschitzian.

**Lemma 4.2** *If  $F$  maps  $\mathcal{H}_p$  into itself, then there exists a constant  $\lambda > 0$  such that, for all  $u, v \in \mathcal{H}_p$ , we have*

$$\|F(u) - F(v)\|_{\mathcal{H}_p} \leq \lambda \|u - v\|_{\mathcal{H}_p}.$$

**Proof.** Let  $u, v \in \mathcal{H}_p$ , we have

$$\begin{aligned} & \|F(u) - F(v)\|_{\mathcal{H}_p} \\ = & \|(F_1u_1 - F_1v_1 + F_2u_2 - F_2v_2, F_3u_0 - F_3v_0, F_4u_0 - F_4v_0 + F_5u_1 - F_5v_1)\|_{\mathcal{H}_p} \\ = & \|F_1u_1 - F_1v_1 + F_2u_2 - F_2v_2\|_{X_p} + \|F_3u_0 - F_3v_0\|_{X_p} \\ & + \|F_4u_0 - F_4v_0 + F_5u_1 - F_5v_1\|_{X_p} \\ \leq & \alpha \|u_1 - v_1\|_{X_p} + (\alpha + \rho) \|u_2 - v_2\|_{X_p} + c\beta\mu \|u_0 - v_0\|_{X_p} \\ & + c\beta(1 - \mu) \|u_0 - v_0\|_{X_p} + \xi \|u_1 - v_1\|_{X_p} \\ = & c\beta \|u_0 - v_0\|_{X_p} + (\alpha + \xi) \|u_1 - v_1\|_{X_p} + (\alpha + \rho) \|u_2 - v_2\|_{X_p} \\ \lambda \leq & \|u - v\|_{\mathcal{H}_p}, \end{aligned}$$

where  $\lambda = \max(c\beta, \alpha + \xi, \alpha + \rho)$ . This completes the proof.

Now, using the operators  $A$  and  $F$ , problem (1) may be written in the form

$$\begin{cases} U'(t) + AU(t) = FU(t), & t \in [0, T], \\ U(0) = U_0, \end{cases} \tag{5}$$

where

$$U(t) = \begin{pmatrix} S(t) \\ I(t) \\ R(t) \end{pmatrix} \quad \text{and} \quad U_0 = \begin{pmatrix} S_0 \\ I_0 \\ R_0 \end{pmatrix}.$$

In the following result, we try to show that if assumption  $\mathcal{A}$  holds, then equation (5) has a unique solution. Hence the main result of this section reads as follows.

**Theorem 4.1** *Let  $1 \leq p < +\infty$ . We assume that the condition  $\mathcal{A}$  holds true and  $F$  maps  $\mathcal{H}_p$  into itself, then the problem (5) has a unique mild solution for all initial data  $(S_0, I_0, R_0)$  belonging to  $\mathcal{H}_p$ .*

*If  $1 < p < +\infty$ , it is a weak solution. Moreover, if  $(S_0, I_0, R_0) \in \mathcal{H}_p$ , then it is a strong solution.*

**Proof.** It follows from Lemma 4.1 that the operator  $A$  is m-accretive on  $\mathcal{H}_p$ . Further, Remark 4.1 together with Lemma 4.2 show that  $F$  is  $\lambda$ -Lipschitz on  $\mathcal{H}_p$  and therefore the operator  $A - F$  is  $\lambda$ -m-accretive on  $\mathcal{H}_p$ . Applying Corollary 4.1 from [6], we conclude that problem (5) has a unique mild solution. Moreover, since the spaces  $X_p$ , for  $1 < p < +\infty$ , are Banach spaces with the Radon-Nikodym property, applying Theorem 3.3, we infer that it is a weak solution on  $\mathcal{H}_p$ . Next, if  $U_0 \in \mathcal{H}_p$ , then applying Theorem 3.1, we infer that this solution is a strong solution.

The next result shows that the solution depends continuously on the initial data. To this end, let us introduce the Banach space  $\mathcal{C}_p := C([0, T]^3; \mathcal{H}_p)$  endowed with the norm

$$\|u\|_\infty := \{\max \|u_i\|_{X_p} : i = 0, 1, 2\}.$$

**Proposition 4.1** *Let  $1 \leq p < \infty$  and  $U_1, U_2 \in \mathcal{C}_p$  be two mild solutions of problem (5). Given  $\epsilon > 0$ , there exists  $\delta > 0$  such that if  $|U_1(0) - U_2(0)| \leq \delta$ , then  $\|U_1 - U_2\|_\infty \leq \epsilon$ .*

**Proof.** Since  $A$  is an  $m$ -accretive operator on  $\mathcal{H}_p$  (see Lemma 4.1) and  $F : \mathcal{H}_p \rightarrow \mathcal{H}_p$  is  $\lambda$ -Lipschitzian, where  $\lambda = \max(c\beta, \alpha + \xi, \alpha + \rho)$  (see Lemma 4.2), we have  $A - F$  is a  $\lambda$ - $m$ -accretive operator on  $\mathcal{H}_p$ . So, for  $i \in 1, 2$ ,  $U_i$  is the unique solution of the problem

$$\begin{cases} U'(t) + AU(t) - FU(t) = 0, \\ U(0) = U_i(0) \in \mathcal{H}_p. \end{cases} \quad (6)$$

Hence, using (3), we have

$$|U_1(t) - U_2(t)| \leq e^{\lambda t} |U_1(0) - U_2(0)|.$$

The above inequality implies that, for every  $t \in [0, T]$ ,

$$|U_1(t) - U_2(t)| \leq e^{\lambda t} |U_1(0) - U_2(0)|,$$

therefore,

$$\|U_1 - U_2\|_\infty \leq e^{\lambda T} |U_1(0) - U_2(0)|.$$

It suffices to take  $\delta = \frac{\epsilon}{e^{\lambda T}}$ , this completes the proof.

**Remark 4.3** We note that we can extend the result obtained above to prove the existence and uniqueness of the solution of the SEIR (Susceptible, Exposed, Infectious and Recovered) model presented in [17].

## 5 Conclusion

In the present work, we have considered a linear SIR model, describing the propagation of an epidemic in given population. The existence and uniqueness results for this problem were obtained in  $L^p$  spaces, for  $1 \leq p < \infty$ , by using the accretive theory. The solution of this model is important because biologists could use it to observe the spread of infectious diseases by introducing natural initial conditions. Therefore they can learn the ways of how to control the propagation of epidemics. In the future works, we will consider the nonlinear SIR model to explain how epidemic diseases can be eradicated by vaccination. Our approach may be extended to the following model:

$$\begin{cases} \frac{\partial S}{\partial t}(t, a) = t \cdot \frac{\partial S}{\partial a}(t, a) + (\alpha - \sigma)N(t, a) - \beta F(I, S), \\ \frac{\partial I}{\partial t}(t, a) = \beta f(I, S) - (\alpha + \xi)I(t, a), \\ \frac{\partial R}{\partial t}(t, a) = \xi G(I, R) + c\beta(1 - \mu)S(t, a), \end{cases}$$

where  $F$  and  $G$  are nonlinear operators. A new parameter  $\sigma$  is introduced in the model and represents the specific vaccination rate of the new infected.

## Acknowledgment

The authors would like to thank the referees for their useful comments and suggestions.

## References

- [1] A. S. Ackleh and L. J. S. Allen. Competitive exclusion and coexistence for pathogens in an epidemic model with variable population size. *Journal of Mathematical Biology* **47** (2) (2003) 153–168.
- [2] I. Al-Darabsah, Y. Yuan. A time-delayed epidemic model for Ebola disease transmission. *Appl. Math. Comput.* **290** (2016) 307–325.
- [3] I. Ameen and P. Novati. The solution of fractional order epidemic model by implicit *Adams Methods. Appl. Math. Model.* **43** (2017) 78–84.
- [4] R. M. Anderson and R. M. May. *Infectious Diseases of Humans: Dynamics and Control*. Oxford University Press, 1992.
- [5] Z. Bai and Y. Zhou. Existence of two periodic solutions for a non-autonomous SIR epidemic model. *Applied Mathematical Modelling* **35** (2011) 382–391.
- [6] V. Barbu. *Nonlinear Differential Equations of Monotone Types in Banach Spaces*. Springer, 2010.
- [7] Ph. Bénéilan, M. G. Crandall and A. Pazy. Evolution Equations Governed by Accretive Operators. Forthcoming.
- [8] D. Bernoulli. Essai d’une nouvelle analyse de la mortalité causée par la petite vérole et des avantages de l’inoculation pour la prévenir. *Mem. Math. Phys. Acad. Roy. Sci.*, Paris, 1, 1760.
- [9] F. E. Browder. Nonlinear mappings of nonexpansive and accretive type in Banach spaces. *Bull Amer. Math. Soc.* **7** (3) (1967) 875–882.
- [10] O. Diekmann, J. A. P. Heesterbeek and J. A. J. Metz. On the definition and the computation of the basic reproduction ratio  $R_0$  in models for infectious diseases in heterogeneous populations. *Journal of Mathematical Biology* **28** (4) (1990) 365–382.
- [11] H. W. Hethcote. The mathematics of infectious. **SIAM Rev.** **42** (2000) 599–653.
- [12] T. Kato. Nonlinear semigroups and evolution equations. *J. Math. Soc. Japan* **19** (1967) 508–520.
- [13] W. O. Kermack and A. G. McKendrick. Contribution to the mathematical theory of epidemics. *Proc. Roy. Soc. Lond. A* **115** (1927) 700–721.
- [14] H. Khan, R.N. Mohapatra, K. Vajravelu and S.J. Liao. The explicit series solution of SIR and SIS epidemic models. *Appl. Math. Comput.* **215**, (2009) 653–669.
- [15] J. D. Murray. *Mathematical Biology*. Springer, Berlin, Germany, 1989.
- [16] H. T. Williams, I. Mazilu and D. A. Mazilu. Stochastic epidemic-type model with enhanced connectivity: exact solution. *Journal of Statistical Mechanics: Theory and Experiment* **2012**, P01017.
- [17] A. Zaghdani. Mathematical study of a modified SEIR model for the novel SARS-Cov-2 coronavirus. *Nonlinear Dynamics and Systems Theory* **21** (3) (2021) 326–336.



# Design of Navigation and Guidance Control System of Mobile Robot with Position Estimation Using Ensemble Kalman Filter (EnKF) and Square Root Ensemble Kalman Filter (SR-EnKF)

T. Herlambang<sup>1\*</sup>, F. A. Susanto<sup>1</sup>, D. Adzkiya<sup>2</sup>, A. Suryowinoto<sup>3</sup>  
and K. Oktafianto<sup>4</sup>

<sup>1</sup> Department of Information Systems, University of Nahdlatul Ulama Surabaya, Indonesia.

<sup>2</sup> Department of Mathematics, Sepuluh Nopember Institute of Technology, Indonesia.

<sup>3</sup> Electrical Engineering Department, Adhi Tama Institute of Technology Surabaya, Indonesia.

<sup>4</sup> Department of Mathematics, University of PGRI Ronggolawe, Indonesia.

Received: October 25, 2021; Revised: September 21, 2022

**Abstract:** A mobile robot is one of the unmanned land vehicles which can be controlled and whose position can be detected when it is equipped with a Global Positioning System (GPS). A mobile robot aims to automate some tasks that were usually done manually by human. To gain an accurate detection of the mobile robot position, the mobile robot must follow the existing trajectory with the right position. Therefore, we need a method to estimate the mobile robot trajectory in order to easily detect its position. In this paper, we propose two trajectory estimation methods, i.e., the Ensemble Kalman Filter (EnKF) and the Square Root Ensemble Kalman Filter (SR-EnKF). Furthermore, we also compare the performance of the two methods on the mobile robot equation. The simulation results showed that the EnKF method has a higher accuracy compared with the SR-EnKF method. The mobile position error of the two methods was less than 2% in the case of 100 and 200 ensembles. The smallest error was obtained when generating 100 ensembles, where the position error w.r.t. the X-axis was 0.02 m, the position error w.r.t. the Y-axis was 0.02 m, and the angle position error was 0.003 rad.

**Keywords:** mobile robot; EnKF; SR-EnKF; trajectory estimation.

**Mathematics Subject Classification (2010):** 93E10, 62F10.

---

\* Corresponding author: <mailto:teguh@unusa.ac.id>

## 1 Introduction

Estimation is made to solve a problem which requires prior information such that the next step of the problem solving can be determined. Estimation is conducted since some problems can be addressed using preceding information or data associated with the problem [1]. In the literature, there are numerous methods that can be used for estimation. The Kalman filter is one of the methods for estimating state variables in a discrete linear dynamic system such that the estimation error covariance is minimized [2]. The Kalman filter was originally proposed by Rudolph E. Kalman in 1960 for the solution of the linear data-discrete filtering problem. However, in many real-world problems, the models are continuous nonlinear dynamic systems. Such systems cannot be estimated accurately by using the Kalman filter. In this case, we can employ some alternative approaches for nonlinear systems, for example the Ensemble Kalman Filter (EnKF) and the Square Root Ensemble Kalman Filter (SR-EnKF). In the literature, there are many approaches for modeling, analysis, estimation and control design of linear and nonlinear systems, see [3–12].

The EnKF method uses a certain number of ensembles to represent the underlying probability distribution of state variables. The mean and covariance of the probability distribution are approximated by the mean and covariance of the generated ensembles [1]. The Square Root Ensemble Kalman Filter method (SR-EnKF) is the development of the EnKF method where there are some decomposition matrix operations in the correction stage. This method was developed to reduce the computational time and to improve the accuracy of the estimation results so that the need for fast and accurate navigation and guidance can be satisfied [13]. The development of the application of trajectory estimation techniques in the the field of robotics will be very beneficial to Indonesia because unmanned vehicles have been widely used for civil and military purposes such as missions of spying, surveillance and exploration of places considered dangerous to humans.

A mobile robot is one of the unmanned vehicles that can be driven and whose position can be tracked or detected when it has a Global Positioning System (GPS). Mobile robots are used to replace human functions in doing dangerous work because they have the advantage of being able to move freely. For that purpose, the mobile robot must follow the existing path with the right position. To do so, a method is required to estimate the mobile robot trajectory.

This paper is a study on the implementation of the EnKF and SR-EnKF methods in mobile robot motion equations applied to estimate the mobile robot path, then both methods are simulated by using Matlab software so that the error between estimated and actual trajectories could be obtained. The focus of this paper is the comparison of two position estimation methods: the EnKF and SR-EnKF for mobile robot motion. The paper provides an analysis of numerical study on the performance of both methods.

## 2 Mathematical Model of Mobile Robot

A mobile robot or car robot is a robot construction that has a wheel actuator to move the whole body of the robot so that the robot can change the position from one point to another. The mobile robot used in the study was a mobile robot operating on land and using the rear wheels to move and transfer position. In other words, the mobile robot system was driven by the rear wheels. Figure 1 shows the position and dimensions of the

mobile robot.

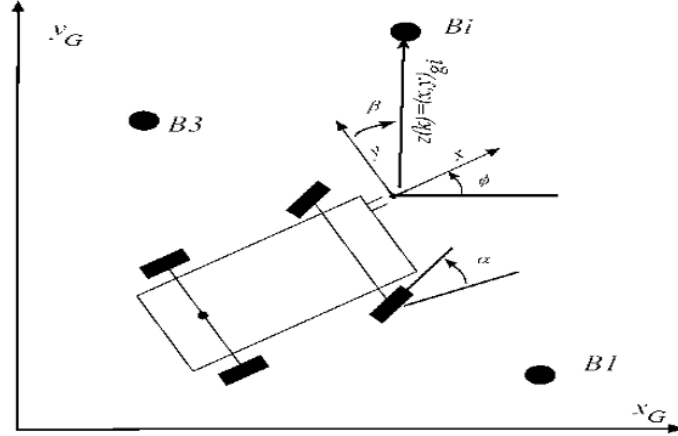


Figure 1: Dynamic model of the mobile robot.

The GPS is mounted right at the midpoint of the car. The steering and front corner systems are shown in Figure 1. In this case, the data are discrete, and the system is nonlinear. The dynamic system equation of a car robot is defined as follows:

$$\begin{bmatrix} \dot{x} \\ \dot{y} \\ \dot{\phi} \end{bmatrix} = \begin{bmatrix} v_c \cos(\phi) - \frac{v_c}{L} (a \sin(\phi) + b \cos(\phi)) \tan(\alpha) \\ v_c \sin(\phi) + \frac{v_c}{L} (a \cos(\phi) - b \sin(\phi)) \tan(\alpha) \\ \frac{v_c}{L} \tan(\alpha) \end{bmatrix}, \quad (1)$$

where

$x, y$  : position of the mobile robot in GPS coordinates;

$\phi$  : position angle of the mobile robot;

$v_c$  : speed of the mobile robot;

$\alpha$  : steering angle of the mobile robot;

$L$  : distance between the front wheel and the rear wheels;

$a$  : distance between the midpoint of the rear car and the GPS position;

$b$  : distance between the center of the car and the GPS position.

### 3 Square Root Ensemble Kalman Filter (SR-EnKF)

The Square Root Ensemble Kalman Filter algorithm (SR-EnKF) is the development of the EnKF algorithm. The correction stage of the SR-EnKF consists of a Singular Value Decomposition (SVD) and a square root matrix. The SVD is a matrix decomposition method which produces a diagonal matrix containing its singular values and another matrix that contains corresponding singular vectors [14]. The singular value decomposition has been widely used in many theoretical and practical applications. The Ensemble Kalman Filter and the Square Root Ensemble Kalman Filter (SR-EnKF) algorithms are summarized in Table 1.

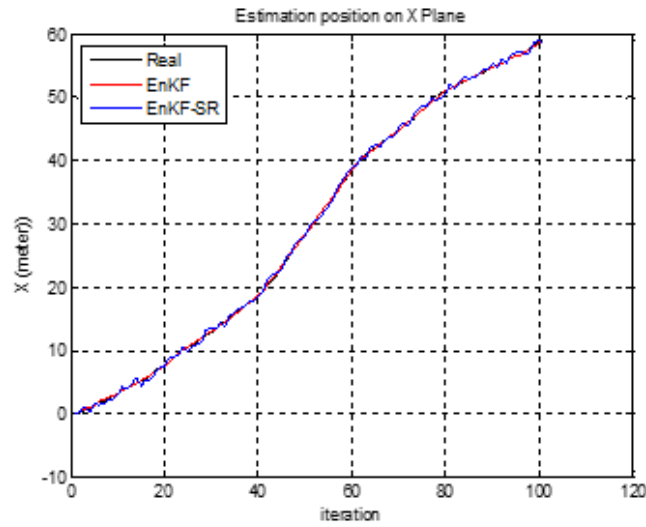
EnKF	EnKF-SR
<b>System Model and Measurement Model</b>	
$x_{k+1} = f(u_k, x_k) + w_k, w_k \sim N(0, Q_k)$ $z_k = Hx_k + v_k, v_k \sim N(0, R_k)$	$x_{k+1} = f(u_k, x_k) + w_k, w_k \sim N(0, Q_k)$ $z_k = Hx_k + v_k, v_k \sim N(0, R_k)$
<b>Initialization</b>	
Generate $N$ ensemble in accordance with initial estimate $\bar{x}_0$ $x_{0,i} = [x_{0,1} \ x_{0,2} \ x_{0,3} \ \dots \ x_{0,N_e}]$ Determine initial value : $\hat{x}_0 = \frac{1}{N_e} \sum_{i=1}^N X_{0,i}$	Generate $N$ ensemble in accordance with initial estimate $\bar{x}_0$ $x_{0,i} = [x_{0,1} \ x_{0,2} \ x_{0,3} \ \dots \ x_{0,N_e}]$ Initial Mean Ensemble : $\bar{x}_{0,i} = x_{0,i} \mathbf{1}_N$ Ensemble initial error : $\tilde{x}_{0,i} = x_{0,i} - \bar{x}_{0,i} = x_{0,i}(\mathbf{I} - \mathbf{1}_N)$
<b>Prediction Stage</b>	
$\hat{x}_{k,i}^- = f(\hat{x}_{k-1,i}, u_{k-1,i}) + w_{k,i}$ with $w_{k,i} \sim N(0, Q_k)$ Estimate : $\hat{x}_k^- = \frac{1}{N_e} \sum_{i=1}^N \hat{x}_{k,i}^-$ Covariance error : $P_k^- = \frac{1}{N_e - 1} \sum_{i=1}^N (\hat{x}_{k,i}^- - \hat{x}_k^-)(\hat{x}_{k,i}^- - \hat{x}_k^-)^T$	$\hat{x}_{k,i}^- = f(\hat{x}_{k-1,i}, u_{k-1,i}) + w_{k,i}$ of which $w_{k,i} \sim N(0, Q_k)$ Ensemble Mean : $\bar{x}_{k,i}^- = \hat{x}_{k,i}^- \mathbf{1}_N$ Ensemble Error : $\tilde{x}_{k,i}^- = \hat{x}_{k,i}^- - \bar{x}_{k,i}^- = \hat{x}_{k,i}^- (\mathbf{I} - \mathbf{1}_N)$
<b>Correction Stage</b>	
$z_{k,i} = z_k + v_{k,i}$ with $v_{k,i} \sim N(0, R_k)$ Kalman gain : $K_k = P_k^- H^T (HP_k^- H^T + R_k)^{-1}$ Estimate : $\hat{x}_{k,i} = \hat{x}_{k,i}^- + K_k(z_{k,i} - H\hat{x}_{k,i}^-)$ $\hat{x}_k = \frac{1}{N_e} \sum_{i=1}^N \hat{x}_{k,i}$	$z_{k,i} = z_k + v_{k,i}$ of which $v_{k,i} \sim N(0, R_k)$ $S_k = H\tilde{x}_{k,i}^-, E_k = (v_1, v_2, \dots, v_N)$ , and $C_k = S_k S_k^T + E_k E_k^T$ Ensemble Mean : $\bar{x}_{k,i} = \hat{x}_{k,i}^- + \tilde{x}_{k,i}^- S_k^T C_k^{-1} (z_{k,i} - H\hat{x}_{k,i}^-)$ Square root schema: <ul style="list-style-type: none"> <li>- decompose eigenvalue of <math>C_k = U_k \Lambda_k U_k^T</math></li> <li>- compute matrices <math>M_k = \Lambda_k^{-1/2} U_k^T S_k^-</math></li> <li>- determine SVD from <math>M_k = Y_k L_k V_k^T</math></li> </ul> Ensemble Error : $\tilde{x}_{k,i} = \tilde{x}_{k,i}^- V_k (\mathbf{I} - L_k^T L_k)^{1/2}$ Ensemble Estimate : $\hat{x}_{k,i} = \tilde{x}_{k,i} + \bar{x}_{k,i}$

Table 1: EnKF and EnKF-SR algorithms [13].

#### 4 Simulation and Analysis Results

In this study, the navigation system and mobile robot guidance used the EnKF and SR-EnKF methods by generating 100 and 200 ensembles on two paths. The comparison of the two methods is either by generating 100 or 200 ensembles. The starting point is given on each path  $x(0) = 0, y(0) = 0$ , and  $z(0) = 0$ . In the first trajectory, we obtained the result of path estimation in the XY field by using the EnKF and SR-EnKF and generating 200 ensembles as in Figure 4. In addition, Table 2 shows the average RMSE

value by generating 100 and 200 ensembles.



**Figure 2:** Estimation of position in the first trajectory on the X plane.

In Figure 2, it appears that the EnKF method is more accurate than the EnKF-SR method, where the EnKF method (red line) is smoother following the specified trajectory. Judging from the first iteration to the 60th iteration, it can be seen that the EnKF method is more accurate than the EnKF-SR method with a difference of 2-5% in accuracy.

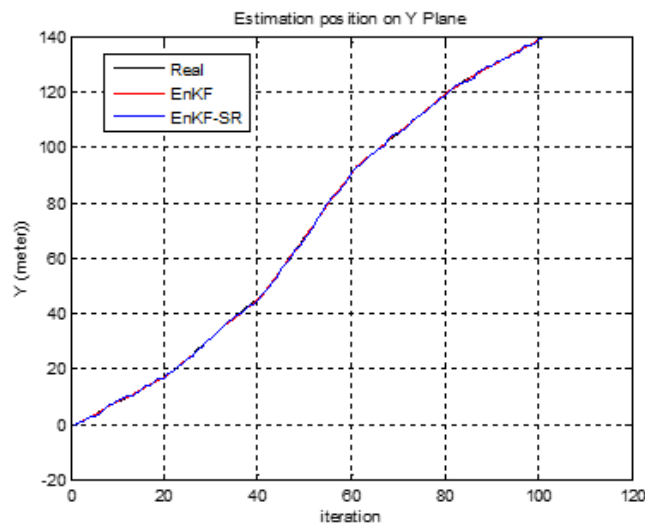


**Figure 3:** Estimation of position in the first trajectory on the Y plane.

In Figure 3, it appears that the EnKF method is more accurate than the EnKF-SR method, where the EnKF method (red line) is smoother following the specified trajectory. Judging from the first iteration to the 40th iteration, it can be seen that the EnKF method is more accurate than the EnKF-SR method with a difference of 2-3% in accuracy. However, after the 40th iteration, the EnKF and EnKF-SR methods have almost the same level of accuracy.

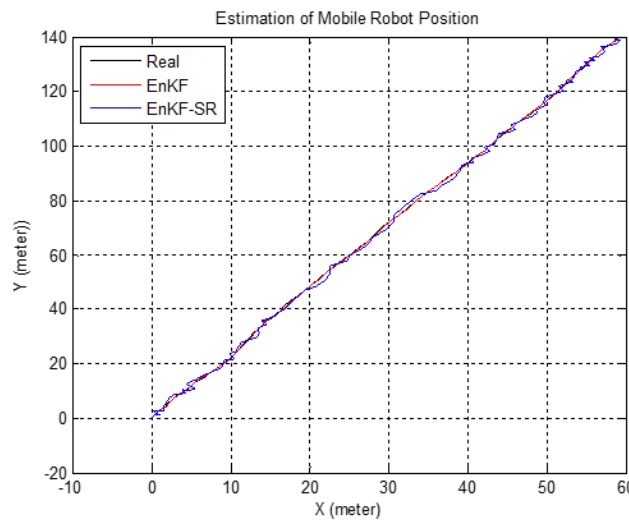


**Figure 4:** Estimation of the trajectory on the first trajectory in the XY plane.

Figure 4 shows that the system is able to follow the desired path in the XY plane, with the trajectory estimation results obtained by using the EnKF and SR-EnKF methods resulted in an accurate estimation with a position error of less than 2%. The error is obtained when the X position is 1.8 m and the Y position is 2 m. The errors obtained in the simulation when generating 100 and 200 ensembles are shown in Table 2.

In Table 2, notice that the EnKF method was more accurate than the SR-EnKF method in the case of 100 and 200 ensembles. The error of the X and Y positions indicated the deviation of the position as it moved along the path, while the angular position error was the error occurring during the turning movement, and this also affected the error of the X and Y position.

	N = 100		N = 200	
	EnKF	SR-EnKF	EnKF	SR-EnKF
X position	<b>0.085328 m</b>	0.45222 m	<b>0.15692 m</b>	0.70455 m
Y position	<b>0.084488 m</b>	0.51156 m	<b>0.096092 m</b>	0.72752 m
Angular position	<b>0.029393 m</b>	0.031061 m	0.072941 m	<b>0.072514 m</b>
Simulation time	1.7031 s	1.8281 s	3.6250 s	3.7813 s

**Table 2:** The comparison of RMSE values with the EnKF and SR-EnKF methods on the first trajectory in the case of 100 and 200 ensembles.

This simulation used  $\Delta t = 0.1$  by generating 100 and 200 ensembles. The third trajectory was the result of the path estimation in the XY plane which was obtained by using the EnKF and SR-EnKF with the starting point given on each path  $x(0) = 0$ ,  $y(0) = 0$  and  $z(0) = 0$  and generating 200 ensembles as shown in Figure 7. In addition, Table 3 shows the average value of RMSE by generating 100 and 200 ensembles.

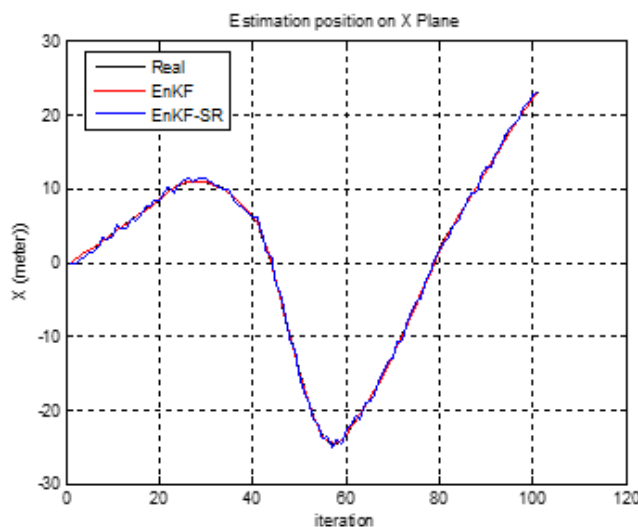


**Figure 5:** Estimation of position in the second trajectory on the X plane.

In Figure 5, it appears that the EnKF method is more accurate than the EnKF-SR method, where the EnKF method (red line) is smoother following what has been determined. Judging from the first iteration to the 40th iteration and the 40th to the 70th iteration, it can be seen that the EnKF method is more accurate than the EnKF-SR method with a difference of about 3-5% in accuracy.

In Figure 6, it appears that the EnKF method is more accurate than the EnKF-SR method, where the EnKF method (red line) is smoother following the specified trajectory. Judging from the first iteration to the 50th iteration, both methods have the same good accuracy, but from the 51st to the 100th iteration, it can be seen that the EnKF method is more accurate than the EnKF-SR method with a difference of about 2-4% accuracy rate.

Based on Figure 7, the mobile robot followed the desired path in the XY plane, where the trajectory estimations using the EnKF and SR-EnKF methods are very accurate with a position error of less than 2%. The error of 2% is obtained when the X position is 0.7 m and the Y position is 0.8 m.

From the analysis of results of the first, second and third trajectory simulation, it was found that the EnKF method has a higher accuracy compared with the SR-EnKF method either by generating 100 or 200 ensembles. However, the EnKF and SR-EnKF methods both had position errors of less than 2%, so the SR-EnKF method could be used as a method of navigation system and mobile robot guidance.

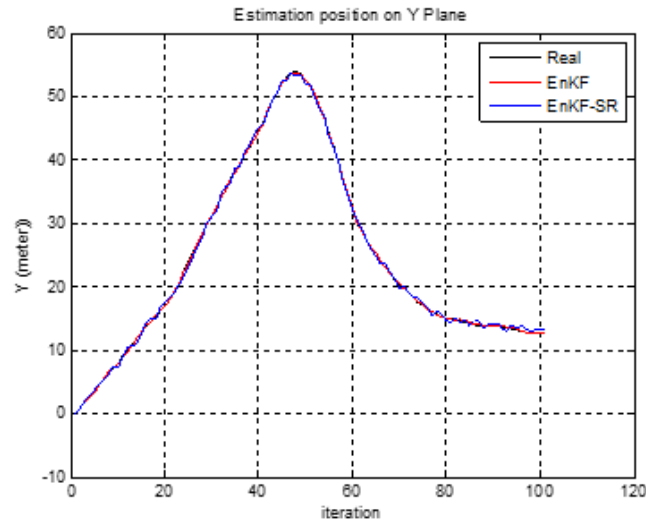


**Figure 6:** Estimation of position in the second trajectory on the Y plane.

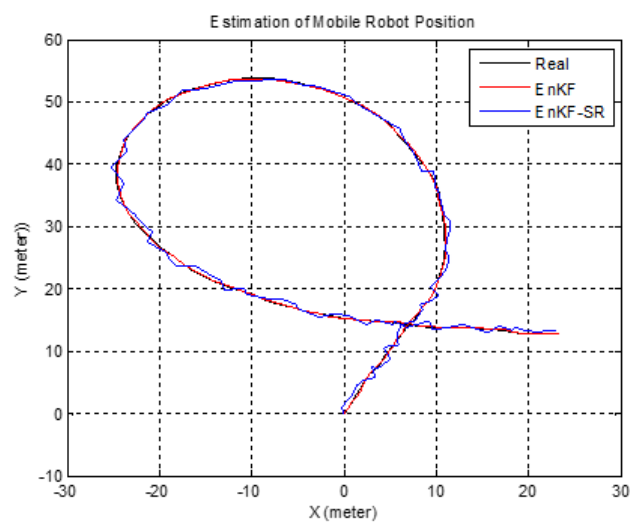


**Figure 7:** Estimation of trajectory on the third trajectory on the XY field.

## 5 Conclusions

According to the results of the study on mobile robot mathematical models as well as navigation systems, both the Ensemble Kalman Filter (EnKF) and the Square Root Ensemble Kalman Filter (SR-EnKF) methods could be effectively used as navigation systems and guidance with trajectory estimates with a position error of less than 2%.

	N = 100		N = 200	
	EnKF	SR-EnKF	EnKF	SR-EnKF
X position	<b>0.071713 m</b>	0.2168 m	<b>0.10462 m</b>	0.31981 m
Y position	<b>0.088223 m</b>	0.22584 m	<b>0.18555 m</b>	0.32489 m
Angular position	<b>0.0082395 m</b>	0.010071 m	<b>0.012895 m</b>	0.014751 m
Simulation time	1.6875 s	1.8281 s	3.0156 s	3.3281 s

**Table 3:** The comparison between the RMSE value of the EnKF method and that of the SR-EnKF method on the third trajectory in the case of 100 and 200 ensembles

Viewed from the generation of ensembles, the generation of 100 ensembles resulted in a more accurate result than that of 200 ensembles.

### Acknowledgment

This research was supported by LPPM - Nahdlatul Ulama Surabaya of University (UN-USA).

### References

- [1] T. Herlambang, E. B. Djatmiko and H. Nurhadi. Navigation and guidance control system of AUV with trajectory estimation of linear modelling. In: *Proc. International Conference on Advanced Mechatronics, Intelligent Manufacture, and Industrial Automation (ICAMIMIA)*. Surabaya, Indonesia, 2015, 184–187.
- [2] R. E. Kalman. A New Approach to Linear Filtering and Prediction Problems. *Journal of Basic Engineering* **82** (1) (1960) 35–45.
- [3] T. Herlambang, S. Subchan, H. Nurhadi and D. Adzkiya. Motion Control Design of UN-USAITS AUV Using Sliding PID. *Nonlinear Dynamics and Systems Theory* **20** (1) (2020) 51–60.
- [4] T. Herlambang, D. Rahmalia, H. Nurhadi, D. Adzkiya and S. Subchan. Optimization of Linear Quadratic Regulator with Tracking Applied to Autonomous Underwater Vehicle (AUV) Using Cuckoo Search. *Nonlinear Dynamics and Systems Theory* **20** (3) (2020) 282–298.
- [5] M. H. DarAssi and M. A. Safi. Analysis of an SIRS Epidemic Model for a Disease Geographic Spread. *Nonlinear Dynamics and Systems Theory* **21** (1) (2021) 56–67.
- [6] Z. Ermayanti, E. Apriliani, H. Nurhadi and T. Herlambang. Estimate and control position autonomous underwater vehicle based on determined trajectory using fuzzy Kalman filter method. In: *Proc. International Conference on Advanced Mechatronics, Intelligent Manufacture, and Industrial Automation (ICAMIMIA)*. Surabaya, Indonesia, 2015, 156–161.
- [7] T. Herlambang, Z. Mufarrikhoh and F. Yudianto. Estimasi Trajectory Mobile Robot Menggunakan Metode Ensemble Kalman Filter Square Root (EnKF-SR). In: *Proc. Seminar Nasional Pascasarjana STTAL Indonesia*, 2016, C-XVI-1–C-XVI-5.
- [8] T. Herlambang and H. Nurhadi. Desain Sistem Kendali Gerak Surge dan Roll pada Sistem Autonomous Underwater Vehicle dengan Metode Sliding Mode Control (SMC). In: *Proc. Seminar Nasional Pascasarjana STTAL Indonesia*, 2016, A-XII.
- [9] T. Herlambang. Desain sistem kendali gerak surge, sway dan yaw pada autonomous underwater vehicle dengan metode sliding mode control (SMC). *Limits: Journal of Mathematics and Its Applications* **14** (1) (2017) 53–60.

- [10] T. Herlambang, H. Nurhadi and E. B. Djatmiko. Optimasi Model Linier 6-DOF pada Sistem Autonomous Underwater Vehicle. *Seminar MASTER PPNS* 1 (1) (2016) 69–74.
- [11] K. Oktafianto, T. Herlambang, Mardlijah and H. Nurhadi. Design of autonomous underwater vehicle motion control using sliding mode control method. In: *Proc. International Conference on Advanced Mechatronics, Intelligent Manufacture, and Industrial Automation (ICAMIMIA)*. Surabaya, Indonesia, 2015, 162–166.
- [12] T. Herlambang, H. Nurhadi and Subchan. Preliminary numerical study on designing navigation and stability control systems for ITS AUV. *Applied Mechanics and Materials* 493 (2014) 420–425.
- [13] T. Herlambang, E. B. Djatmiko and H. Nurhadi. Ensemble kalman filter with a square root scheme (EnKF-SR) for trajectory estimation of AUV SEGOROGENI ITS. *International Review of Mechanical Engineering (I. RE. ME.)* 9 (6) (2015) 553–560.
- [14] E. Apriliani and B. A. Sanjaya. Reduksi Rank pada Matriks-Matriks Tertentu. *Limits: Journal of Mathematics and Its Applications* 4 (2) (2007) 1–8.



# On the Dynamics of a Class of Planar Differential Systems

A. Kina<sup>1,2\*</sup> and A. Bendjeddou<sup>1</sup>

<sup>1</sup> *Laboratory of Applied Mathematics, Department of Mathematics, Faculty of Sciences, University Ferhat Abbas Setif 1, Algeria.*

<sup>2</sup> *Department of Mathematics and Computer Science, University of Ghardaia, 47 000 Algeria.*

Received: May 24, 2021; Revised: October 13, 2022

**Abstract:** In this work, we discuss the existence of the first integral and no-existence of limit cycles for a class of Kolmogorov differential systems. As an application, we give an example to illustrate our results.

**Keywords:** *Kolmogorov systems; periodic orbits; limit cycle; integrability.*

**Mathematics Subject Classification (2010):** 37C07, 34C05, 34C07, 37K10.

## 1 Introduction

By definition, a two-dimensional real planar Kolmogorov system will be a differential system of the form

$$\begin{cases} \dot{x} = xf_1(x, y), \\ \dot{y} = yf_2(x, y), \end{cases} \quad (1)$$

where  $f_1, f_2$  are real functions in the two variables  $x$  and  $y$  and the dot denotes derivative with respect to the time ( $t$ ) variable. There are many natural phenomena which can be modelled by the Kolmogorov systems in mathematical ecology and population dynamics, see for example [5, 10].

Kolmogorov models are widely used in ecology to describe the interaction between two populations, and a limit cycle corresponds to an equilibrium state of the system. In the qualitative theory of dynamical systems, see [2, 4, 5, 11], one of the most important problems is the study of the limit cycles of planar dynamical systems (1). The definition of limit cycles appeared in the works of Poincaré [9], the statement of the 16-th Hilbert's problem, and the discovery by Liénard [8]. A limit cycle of a planar vector field given

---

\* Corresponding author: <mailto:abdelkrimkina@gmail.com>

by (1) is an isolated periodic trajectory (isolated compact leaf of the corresponding foliation), in other words, a periodic trajectory of a vector field is a limit cycles, see for instance [1, 6, 7].

Let  $D$  be a non-empty open and dense subset of  $\mathbb{R}^2$ . We say that a non-locally constant  $C^1$  function  $\varphi : D \rightarrow \mathbb{R}$  is a first integral of the polynomial differential (1) in  $D$  if  $\varphi$  is constant on the trajectories of the polynomial differential system (1) contained in  $D$ , i.e., if

$$\frac{\partial\varphi(x, y)}{\partial x} f_1(x, y) + \frac{\partial\varphi(x, y)}{\partial y} f_2(x, y) = \frac{d\varphi(x, y)}{dt} \equiv 0, \text{ at the points of } D.$$

For a planar vector field, the existence of a first integral totally determines its phase portrait. The simplest planar vector fields having a first integral are the Hamiltonian ones. The integrable planar vector fields which are not Hamiltonian are, in general, very difficult to detect, see [3].

In this paper, we study the existence of first integrals and the non existence of limit cycle of Kolmogorov differential systems of the form

$$\begin{cases} \dot{x} = x \left( F(x, y)^p + k(x, y) \frac{\sum_{i=1}^{m_1} \exp P_i(x, y)}{\sum_{j=1}^{m_2} \exp Q_j(x, y)} \right), \\ \dot{y} = y \left( G(x, y)^p + k(x, y) \frac{\sum_{i=1}^{m_1} \exp P_i(x, y)}{\sum_{j=1}^{m_2} \exp Q_j(x, y)} \right), \end{cases} \tag{2}$$

where  $m_1, m_2$  are positive integers and  $p \in \mathbb{Q}^*$ ,  $F(x, y), G(x, y), k(x, y), P_i(x, y), Q_j(x, y)$  are homogeneous polynomials of degree  $n, n, \delta, m, m$ , respectively.

We define the trigonometric functions

$$\begin{aligned} f(\theta) &= \cos^2 \theta F(\cos \theta, \sin \theta)^p + \sin^2 \theta G(\cos \theta, \sin \theta)^p. \\ g(\theta) &= k(\cos \theta, \sin \theta) \left( \frac{\sum_{i=1}^{m_1} \exp P_i(\cos \theta, \sin \theta)}{\sum_{j=1}^{m_2} \exp Q_j(\cos \theta, \sin \theta)} \right). \\ h(\theta) &= \sin \theta \cos \theta (G(\cos \theta, \sin \theta)^p - F(\cos \theta, \sin \theta)^p). \end{aligned}$$

## 2 Main Result

Our main result on the integrability and the periodic orbits of the Kolmogorov system (2) is the following.

**Theorem 2.1** *Consider a planar Kolmogorov system (2), then the following statements hold:*

(i) *If  $h(\theta) \neq 0, F(\cos \theta, \sin \theta)^p > 0, G(\cos \theta, \sin \theta)^p > 0$ , for  $\theta \in [0, \frac{\pi}{2}]$  and  $\delta - np \neq 0$ , then system (2) has the first integral*

$$\begin{aligned} I(x, y) &= (x^2 + y^2)^{\frac{np+\delta}{2}} \exp \left( -(np + \delta) \int_{\theta_*}^{\arctan \frac{y}{x}} \frac{f(s)}{h(s)} ds \right) - \\ &\quad (np + \delta) \int_{\theta_*}^{\arctan \frac{y}{x}} \exp \left( -(np + \delta) \int_{v_0}^v \frac{f(s)}{h(s)} ds \right) \frac{g(v)}{h(v)} dv, \end{aligned}$$

where  $\theta_* \in [0, \frac{\pi}{2}]$ . Additionally, the system (2) has no limit cycle at the interior of the first quadrant on the plane.

(ii) If  $h(\theta) \neq 0$ ,  $F(\cos \theta, \sin \theta)^p > 0$ ,  $G(\cos \theta, \sin \theta)^p > 0$ , for  $\theta \in [0, \frac{\pi}{2}]$  and  $\delta - np = 0$ , then system (2) has the first integral

$$L(x, y) = (x^2 + y^2)^{\frac{1}{2}} \exp \left( - \int_{\theta_*}^{\arctan \frac{y}{x}} \left( \frac{f(u)}{h(u)} + \frac{g(u)}{h(u)} \right) du \right).$$

where  $\theta_* \in [0, \frac{\pi}{2}]$ . Additionally, the system (2) has no limit cycle at the interior of the first quadrant on the plane.

(iii) If  $h(\theta) = 0$  for all  $\theta \in [0, 2\pi]$ , then system (2) has the first integral  $T(x, y) = \frac{y}{x}$ . Also, the system (2) has no limit cycle.

**Proof.** In order to demonstrate our results, we write the polynomial differential system (2) in polar coordinates  $(r, \theta)$ , defined by  $x = r \cos \theta$  and  $y = r \sin \theta$ , then system (2) becomes

$$\begin{cases} \dot{r} = f(\theta)r^{np+1} + g(\theta)r^{\delta+1}, \\ \dot{\theta} = h(\theta)r^{np}, \end{cases} \quad (3)$$

where  $\dot{r} = \frac{dr}{dt}$ ,  $\dot{\theta} = \frac{d\theta}{dt}$ .

(i) If  $h(\theta) \neq 0$ ,  $F(\cos \theta, \sin \theta)^p > 0$ ,  $G(\cos \theta, \sin \theta)^p > 0$ , for  $\theta \in [0, \frac{\pi}{2}]$  and  $\delta - np \neq 0$ .

Take as an independent variable the coordinate  $\theta$ , then differential system (3) writes

$$\frac{dr}{d\theta} = \frac{f(\theta)}{h(\theta)}r + \frac{g(\theta)}{h(\theta)}r^{\delta-np+1}, \quad (4)$$

which is a Bernoulli equation. We take a new variable  $\rho = r^{np+\delta}$  and we obtain the linear equation

$$\frac{d\rho}{d\theta} = (np + \delta) \left( \frac{f(\theta)}{h(\theta)}\rho + \frac{g(\theta)}{h(\theta)} \right). \quad (5)$$

The general solution of linear equation (5) is

$$\begin{aligned} \rho(\theta) &= \left( k + (np + \delta) \int_{\theta_*}^{\theta} \exp \left( -(np + \delta) \int_{v_0}^v \frac{f(s)}{h(s)} ds \right) \frac{g(v)}{h(v)} dv \right) \times \\ &\quad \exp \left( (np + \delta) \int_{\theta_*}^{\theta} \frac{f(s)}{h(s)} ds \right), \end{aligned}$$

where  $k \in \mathbb{R}$ , which has the first integral

$$\begin{aligned} I(x, y) &= (x^2 + y^2)^{\frac{np+\delta}{2}} \exp \left( -(np + \delta) \int_{\theta_*}^{\arctan \frac{y}{x}} \frac{f(s)}{h(s)} ds \right) - \\ &\quad (np + \delta) \int_{\theta_*}^{\arctan \frac{y}{x}} \exp \left( -(np + \delta) \int_{v_0}^v \frac{f(s)}{h(s)} ds \right) \frac{g(v)}{h(v)} dv. \end{aligned}$$

The curves  $I = l$  with  $l \in \mathbb{R}$ , are created by the trajectories of the differential system (2). These trajectories equations can be written in Cartesian coordinates as follows:

$$x^2 + y^2 = \left( \left( l + (np + \delta) \int_{\theta_*}^{\arctan \frac{y}{x}} \exp \left( -(np + \delta) \int_{v_0}^v \frac{f(s)}{h(s)} ds \right) \frac{g(v)}{h(v)} dv \right) \times \right)^{\frac{2}{np+\delta}} \exp \left( (np + \delta) \int_{\theta_*}^{\arctan \frac{y}{x}} \frac{f(s)}{h(s)} ds \right).$$

So, the periodic orbit  $F$  is contained in the curve equation

$$(\Lambda) : x^2 + y^2 = \left( \left( l_F + (np + \delta) \int_{\theta_*}^{\arctan \frac{y}{x}} \exp \left( -(np + \delta) \int_{v_0}^v \frac{f(s)}{h(s)} ds \right) \frac{g(v)}{h(v)} dv \right) \times \right)^{\frac{2}{(np+\delta)}} \exp \left( (np + \delta) \int_{\theta_*}^{\arctan \frac{y}{x}} \frac{f(s)}{h(s)} ds \right).$$

But the curve  $(\Lambda)$  cannot contain the periodic orbit  $F$  and hence no limit cycle is contained in the first quadrant on the plane because the curve  $(\Lambda)$  in the realistic quadrant contains only a single point or no point on every straight line  $(\Delta_\lambda) : y = \lambda x$  for all  $\lambda > 0$ .

To be persuaded by this verity, let  $(x_0, y_0)$  be a point of intersection of this curve with straight line  $(\Delta_\lambda) : y = \lambda x$  for all  $\lambda > 0$ , then  $x_0$  and  $y_0$  must satisfy

$$\begin{cases} x_0^2 + y_0^2 = \left( \left( l_F + (np + \delta) \int_{\theta_*}^{\arctan \frac{y_0}{x_0}} \exp \left( -(np + \delta) \int_{v_0}^v \frac{f(s)}{h(s)} ds \right) \frac{g(v)}{h(v)} dv \right) \times \right)^{\frac{2}{(np+\delta)}} \\ \times \exp \left( (np + \delta) \int_{\theta_*}^{\arctan \frac{y_0}{x_0}} \frac{f(s)}{h(s)} ds \right) \\ y_0 = \lambda x_0, \end{cases}$$

hence

$$\begin{cases} x_0 = (1 + \lambda^2)^{-\frac{1}{2}} \left( \left( l_F + (np + \delta) \int_{\theta_*}^{\arctan \lambda} \exp \left( -(np + \delta) \int_{v_0}^v \frac{f(s)}{h(s)} ds \right) \frac{g(v)}{h(v)} dv \right) \times \right)^{\frac{1}{(np+\delta)}} \\ \times \exp \left( (np + \delta) \int_{\theta_*}^{\arctan \lambda} \frac{f(s)}{h(s)} ds \right) \\ y_0 = \lambda x_0. \end{cases}$$

There is at most a unique value of  $x_0$  on every half straight  $OX^+$ . Consequently, there is at most a unique point in the first quadrant on the plane. So this curve cannot contain the periodic orbit and hence there is no limit cycle.

(ii) If  $h(\theta) \neq 0, F(\cos \theta, \sin \theta)^p > 0, G(\cos \theta, \sin \theta)^p > 0$ , for  $\theta \in [0, \frac{\pi}{2}]$  and  $\delta - np = 0$ .

Take as an independent variable the coordinate  $\theta$ , then the differential system (3) becomes

$$\frac{dr}{d\theta} = \left( \frac{f(\theta)}{h(\theta)} + \frac{g(\theta)}{h(\theta)} \right) r. \tag{6}$$

The general solution of equation (6) is

$$r(\theta) = k \exp \left( \int_{\theta_*}^{\theta} \left( \frac{f(u)}{h(u)} + \frac{g(u)}{h(u)} \right) du \right),$$

where  $k \in \mathbb{R}$ , which has the first integral

$$L(x, y) = (x^2 + y^2)^{\frac{1}{2}} \exp \left( - \int_{\theta_*}^{\arctan \frac{y}{x}} \left( \frac{f(u)}{h(u)} + \frac{g(u)}{h(u)} \right) du \right).$$

The curves  $L = l$  with  $l \in \mathbb{R}$  are created by the trajectories of the differential system (2). These trajectories can be written in Cartesian coordinates as follows:

$$(x^2 + y^2)^{\frac{1}{2}} = k \exp \left( \int_{\theta_*}^{\arctan \frac{y}{x}} \left( \frac{f(u)}{h(u)} + \frac{g(u)}{h(u)} \right) du \right).$$

Therefore the periodic orbit  $(\Sigma)$  is contained in the curve

$$(C) : x^2 + y^2 = k_{\Sigma}^2 \exp \left( \int_{\theta_*}^{\arctan \frac{y}{x}} \left( \frac{f(u)}{h(u)} + \frac{g(u)}{h(u)} \right) du \right)^2.$$

But the curve  $(C)$  cannot contain the periodic orbit  $(\Sigma)$  and hence no limit cycle contained in the first quadrant on the plane, because the curve  $(C)$  in the realistic quadrant has at most a unique point on every straight line  $y = \lambda x$  for all  $\lambda > 0$ .

To be persuaded by this verity, let  $(x_0, y_0)$  be a point of intersection of this curve with the straight line  $(\Delta_{\lambda}) : y = \lambda x$  for all  $\lambda > 0$ , then  $x_0$  and  $y_0$  must satisfy

$$\begin{cases} (x_0^2 + y_0^2)^{\frac{1}{2}} = k_{\Sigma} \exp \left( \int_{\theta_*}^{\arctan \frac{y_0}{x_0}} \left( \frac{f(u)}{h(u)} + \frac{g(u)}{h(u)} \right) du \right), \\ y_0 = \lambda x_0, \end{cases}$$

hence

$$\begin{cases} x_0 = k_{\Sigma}(1 + \lambda^2)^{-\frac{1}{2}} \exp \left( \int_{\theta_*}^{\arctan \lambda} \left( \frac{f(u)}{h(u)} + \frac{g(u)}{h(u)} \right) du \right), \\ y_0 = \lambda x_0, \end{cases}$$

There is at most a unique value of  $x_0$  on every half straight  $OX^+$ . Consequently, there is at most a unique point in the first quadrant on the plane. So this curve cannot contain the periodic orbit and consequently, there is no limit cycle.

(iii) If  $h(\theta) = 0$  for all  $\theta \in [0, 2\pi]$ , then from (3), it follows that  $\dot{\theta} = 0$ . So the straight lines through the origin of coordinates of the differential system (2) are invariant by the flow of this system. Hence,  $T(x, y) = \frac{y}{x}$  is a first integral of the system. Then all straight lines through the origin are created by the trajectories, which can be written in Cartesian coordinates as  $y = \gamma x$ , where  $\gamma \in \mathbb{R}$ . Hence, there is no limit cycle. This completes the proof of the theorem.

**Example 2.1** If we take  $F(x, y) = \frac{1}{9}x^2y^2(x^2 + y^2)$ ,  $G(x, y) = y^4 + x^2y^2$ ,

$$\sum_{i=1}^2 \exp P_i(x, y) = e^x - e^{-x}, \sum_{j=1}^2 \exp Q_j(x, y) = e^x + e^{-x}, k(x, y) = x^3 + xy^2 + x^2y + y^3,$$

and  $p = -\frac{1}{2}$ , then system (2) becomes

$$\begin{cases} \dot{x} = x \left( \left( \frac{1}{9}x^2y^2(x^2 + y^2) \right)^{-\frac{1}{2}} + (x^3 + xy^2 + x^2y + y^3) \tanh(x) \right), \\ \dot{y} = y \left( (y^4 + x^2y^2)^{-\frac{1}{2}} + (x^3 + xy^2 + x^2y + y^3) \tanh(x) \right), \end{cases} \tag{7}$$

where  $x(t)$  and  $y(t)$  represent the population density of two species at time  $t$ , and

$$\begin{aligned} f_1(x, y) &= \left( \frac{1}{9}x^2y^2(x^2 + y^2) \right)^{-\frac{1}{2}} + (x^3 + xy^2 + x^2y + y^3) \tanh(x), \\ f_2(x, y) &= (y^4 + x^2y^2)^{-\frac{1}{2}} + (x^3 + xy^2 + x^2y + y^3) \tanh(x), \end{aligned}$$

are the capita growth rate of each species.

The Kolmogorov system (7) in polar coordinates  $(r, \theta)$  is written as

$$\begin{cases} \dot{r} = (\cos \theta (\frac{1}{9} \sin^2 \theta)^{-\frac{1}{2}} + \sin \theta) r^{-1} + ((\cos \theta + \sin \theta) \tanh(\theta)) r^4, \\ \dot{\theta} = (\cos \theta - 3) r^{-2}, \end{cases}$$

accordingly,  $f(\theta) = \cos \theta (\frac{1}{9} \sin^2 \theta)^{-\frac{1}{2}} + \sin \theta$ ,  $g(\theta) = (\cos \theta + \sin \theta) \tanh(\theta)$ ,  $h(\theta) = \cos \theta - 3$ . This corresponds to the case (i) of Theorem 2.1. Then the system (7) has the first integral

$$I(x, y) = (x^2 + y^2)^{\frac{1}{2}} \exp \left( \int_{\theta_*}^{\arctan \frac{y}{x}} \frac{\cos s (\frac{1}{9} \sin^2 s)^{-\frac{1}{2}} + \sin s}{3 - \cos s} ds \right) - \int_{\theta_*}^{\arctan \frac{y}{x}} \exp \left( \int_{v_0}^v \frac{\cos s (\frac{1}{9} \sin^2 s)^{-\frac{1}{2}} + \sin s}{3 - \cos s} ds \right) \frac{(\cos v + \sin v) \tanh(v)}{\cos v - 3} dv.$$

The curves  $I = l$  with  $l \in \mathbb{R}$ , which are created by the trajectories of the differential system (7), in Cartesian coordinates are written as

$$x^2 + y^2 = \left( \left( l + \int_{\theta_*}^{\arctan \frac{y}{x}} \exp \left( - \int_{v_0}^v \frac{\cos s (\frac{1}{9} \sin^2 s)^{-\frac{1}{2}} + \sin s}{\cos s - 3} ds \right) \frac{(\cos v + \sin v) \tanh(v)}{\cos v - 3} dv \right) \times \right)^2 \exp \left( \int_{\theta_*}^{\arctan \frac{y}{x}} \frac{\cos s (\frac{1}{9} \sin^2 s)^{-\frac{1}{2}} + \sin s}{\cos s - 3} ds \right).$$

where  $l \in \mathbb{R}$ . Then the system (7) has no periodic orbits, and consequently, no limit cycle.

### 3 Conclusion

In this paper, we proposed a special form of Kolmogorov differential system, where just select the parameters satisfying the conditions of Theorem 2.1, we obtain explicit expression for a first integral and characterize its trajectories, this is one of the classical tools in the classification of all trajectories of dynamical systems.

### References

- [1] A. Bendjeddou, J. Llibre and T. Salhi. Dynamics of the differential systems with homogeneous nonlinearities and a star node. *Journal of Differential Equations* **254** (8) (2013) 3530–3537.
- [2] R. Boukoucha. First Integral of a class of two-dimensional Kolmogorov systems. *Nonlinear Dynamics and Systems Theory* **22** (1) (2022) 13–20.
- [3] F. Dumortier, J. Llibre and J.C. Artés. *Qualitative Theory of Planar Differential Systems*. Springer, New York, 2006.
- [4] X.C. Huang and L. Zhu. Limit cycles in a general Kolmogorov model. *Nonlinear Analysis: Theory, Methods & Applications* **60** (8) (2005) 1393–1414.
- [5] X.C. Huang. Limit cycles in a Kolmogorov-type model and its application in immunology. *Mathematical and Computer Modelling* **14** (1990) 614–617.
- [6] X.C. Huang and L. Zhu. Limit cycles in a general Kolmogorov model. *Nonlinear Analysis: Theory, Methods and Applications* **60** (8) (2005) 1393–1414.
- [7] Yu. Ilyashenko. Centennial history of Hilbert’s 16th problem. *Bulletin of the American Mathematical Society* **39** (3) (2002) 301–354.
- [8] A. Liénard. Etude des oscillations entretenues. *Revue Générale de L’Electricité* **23** (1928) 946–954.

- [9] H. Poincaré. Mémoire sur les courbes définies par une équation différentielle (I). *Journal de mathématiques pures et appliquées* **7** (1881) 375–422.
- [10] K. Sigmund. Kolmogorov and Population Dynamics. *Kolmogorov's Heritage in Mathematics*. Springer, Berlin, Heidelberg (2007) 177–186.
- [11] Y. Yuan, H. Chen, C. Du and Y. Yuan. The limit cycles of a general Kolmogorov system. *Journal of Mathematical Analysis and Applications* **392** (2) (2012) 225–237.



# Chaos Synchronization between Fractional-Order Lesser Date Moth Chaotic System and Integer-Order Chaotic System via Active Control

M. Labid<sup>1</sup> and N. Hamri<sup>2\*</sup>

<sup>1</sup> *Department of Mathematics, University Center of Mila, Mila 43000, Algeria.*

<sup>2</sup> *Laboratory of Mathematics and their interactions, Department of Science and Technology, University Center of Mila, Mila 43000, Algeria.*

Received: January 26, 2022; Revised: September 19, 2022

**Abstract:** This paper investigates the phenomenon of chaos synchronization between the fractional-order lesser date moth and the integer-order chaotic systems. Based on the Lyapunov stability theory and numerical differentiation, an active control is obtained to achieve the synchronization between the fractional-order and the integer-order chaotic systems. Numerical examples are implemented to illustrate and validate the results.

**Keywords:** *chaos; synchronization; active control; fractional-order chaotic system; integer-order chaotic system.*

**Mathematics Subject Classification (2010):** 34H10, 37N35, 93C10, 93C15, 93C95.

## 1 Introduction

Chaos is a very interesting nonlinear phenomenon that has been intensively studied over the past two decades. The chaos theory is found to be useful in many areas such as data encryption [19], financial systems [17,18], biology [22] and biomedical engineering [2], etc. Fractional-order chaotic dynamical systems have begun to attract a lot of attention in recent years and can be seen as a generalization of chaotic dynamic integer-order systems. The synchronization between the fractional-order chaotic system and the integer-order chaotic system is thoroughly a new domain and it began to attract much attention in

---

\* Corresponding author: <mailto:mes.laabid@centre-univ-mila.dz>

recent years [9, 20] because of its potential applications in secure communication and cryptography [11, 12]. Obviously, the synchronization between a fractional-order chaotic system and an integer-order chaotic system is more difficult than the synchronization between fractional-order chaotic systems or integer-order chaotic systems for the different order of their error dynamical system. The synchronization between a fractional-order system and an integer-order system was first studied by Zhou et al. [20]. In the past twenty years, different synchronization types have been proposed, e.g., complete synchronization [24], lag synchronization [4], phase synchronization [10], project synchronization [21], generalized synchronization [6], etc. In this research work, we apply the active control theory to synchronize two chaotic systems when a fractional-order system is chosen as the drive system and an integer-order system serves as the response system, we demonstrate the technique capability by the synchronization between a fractional-order lesser date moth chaotic system and an integer-order chaotic system [15]. The paper is arranged in the following manner. In Section 2, we describe the problem formulation for the fractional-order and the integer-order chaotic systems. In Section 3, we discuss the synchronisation between a fractional-order lesser date moth chaotic system and an integer-order chaotic system by using the active control. Section 4 gives the brief conclusion.

## 2 Problem Formulation for Fractional-Order and Integer-Order Chaotic System

Consider the following fractional-order chaotic system as a drive (master) system

$$D^\alpha x_1 = Ax_1 + g(x_1), \quad (1)$$

where  $x_1 \in \mathbb{R}^n$  is the state vector,  $A \in \mathbb{R}^{n \times n}$  is the linear part,  $g(x_1)$  is a continuous nonlinear function, and  $D^\alpha$  is the Caputo fractional derivative.

Also, the response system (slave) can be described as

$$\dot{x}_2 = Ax_2 + g(x_2) + u(t), \quad (2)$$

where  $x_2 \in \mathbb{R}^n$  is the state vector,  $A \in \mathbb{R}^{n \times n}$  is the linear part, and  $g(x_2)$  is a continuous nonlinear function and  $u(t) \in \mathbb{R}^n$  is the control.

Define the synchronous errors as  $e = x_2 - x_1$ . Our aim is to determine the controller  $u(t) \in \mathbb{R}^n$  such that the drive system and response system are synchronized (i.e.,  $\lim_{t \rightarrow \infty} \|e(t)\| = 0$ ).

The synchronisation error system between the driving system (1) and the response system (2) can be expressed as

$$\dot{e} = \dot{x}_2 - \dot{x}_1,$$

where  $\dot{x}_2$  is obtained from the response system (2), while no exact expressions of  $\dot{x}_1$  can be obtained from the driving system (1). Therefore, the numerical differentiation method is used to obtain  $\dot{x}_1$ . According to the definition of derivative, the derivative is approximately expressed using the difference quotient as

$$g'(a) \approx \frac{g(a+h) - g(a)}{h}, \quad (3)$$

$$g'(a) \approx \frac{g(a) - g(a-h)}{h}, \quad (4)$$

where ( $h > 0$ ) is a small increment. Formulae (3) and (4) are called the pre-difference formula and the post-difference formula, respectively. The post-difference formula is used in this paper.

### 3 Synchronisation of Fractional-Order Lesser Date Moth Chaotic System and Integer-Order Chaotic System by Active Control

In this section, to validate the active control method proposed in [5], we take the fractional-order lesser date moth chaotic system [15] as a drive system and the integer-order chaotic system as a response system.

Thus, the drive and response systems are as follows:

$$\begin{cases} D^\alpha x_1 = x_1(1 - x_1) - \frac{x_1 y_1}{\beta + x_1}, \\ D^\alpha y_1 = -\delta y_1 + \frac{\gamma x_1 y_1}{\beta + x_1} - y_1 z_1, \\ D^\alpha z_1 = -\eta z_1 + \sigma y_1 z_1, \end{cases} \tag{5}$$

and

$$\begin{cases} \dot{x}_2 = x_2(1 - x_2) - \frac{x_2 y_2}{\beta + x_2} + u_1(t), \\ \dot{y}_2 = -\delta y_2 + \frac{\gamma x_2 y_2}{\beta + x_2} - y_2 z_2 + u_2(t), \\ \dot{z}_2 = -\eta z_2 + \sigma y_2 z_2 + u_3(t), \end{cases} \tag{6}$$

where  $u_1(t)$ ,  $u_2(t)$ ,  $u_3(t)$  are the active controls.

It is reported that the fractional-order lesser date moth system (5) with the fractional order of  $\alpha = 0.95$  can behave chaotically [15]. The three-dimensional (3D) phase portraits of the lesser date moth chaotic system with fractional order and integer order, respectively, are shown in Figure 1 and Figure 2.

Subtracting (6) from (5) gives the error system as below:

$$\begin{cases} \dot{e}_1 = e_1 - x_1^2 + x_2^2 - \left(\frac{y_2}{\beta + x_2}\right)e_1 + \frac{x_1 y_2}{(\beta + x_1)(\beta + x_2)}e_1 - \frac{x_1}{\beta + x_1}e_2 + x_1 - x_1^2 \\ \quad - \frac{x_1 y_1}{\beta + x_1} - \dot{x}_1 + u_1(t), \\ \dot{e}_2 = -\delta e_2 + \left[\frac{\gamma y_2}{\beta + x_2} - \frac{\gamma x_1 y_2}{(\beta + x_1)(\beta + x_2)}\right]e_1 - \left(z_2 - \frac{x_1}{\beta + x_1}\right)e_2 - y_1 e_3 - \delta y_1 \\ \quad + \frac{\gamma x_1 y_1}{\beta + x_1} - y_1 z_1 - \dot{y}_1 + u_2(t), \\ \dot{e}_3 = -\eta e_3 + \sigma(y_1 e_3 + z_2 e_2) - \eta z_1 + \sigma y_1 z_1 - \dot{z}_1 + u_3(t), \end{cases} \tag{7}$$

where  $e_1 = x_2 - x_1$ ,  $e_2 = y_2 - y_1$ ,  $e_3 = z_2 - z_1$ .

We introduce a quadratic Lyapunov function

$$V(e) = \frac{1}{2} \sum_{i=1}^3 e_i^2, \tag{8}$$

and calculate the derivative of  $V(e)$  to obtain

$$\dot{V}(e) = e_1[e_1 - (x_2 + x_1)e_1 - \left(\frac{y_2}{\beta + x_2}\right)e_1 + \frac{x_1 y_2}{(\beta + x_2)(\beta + x_1)}e_1 - \frac{x_1}{\beta + x_1}e_2] \tag{9}$$

$$+ x_1 - x_1^2 - \frac{x_1 y_1}{\beta + x_1} - \dot{x}_1] + e_2[-\delta e_2 + \left(\frac{\gamma y_2}{\beta + x_2}e_1 - \frac{\gamma x_1 y_2}{(\beta + x_1)(\beta + x_2)}\right)e_1] \tag{10}$$

$$- \left(z_2 e_2 + \frac{\gamma x_1}{\beta + x_1}\right)e_2 - y_1 e_3 - \delta y_1 + \frac{\gamma x_1 y_1}{\beta + x_1} - y_1 z_1 - \dot{y}_1]$$

$$+ e_3[-\eta e_3 + \sigma z_2 e_2 + \sigma y_1 e_3 - \eta z_1 + \sigma y_1 z_1 - \dot{z}_1] + \sum_{i=1}^3 u_i(t)e_i(t). \tag{11}$$

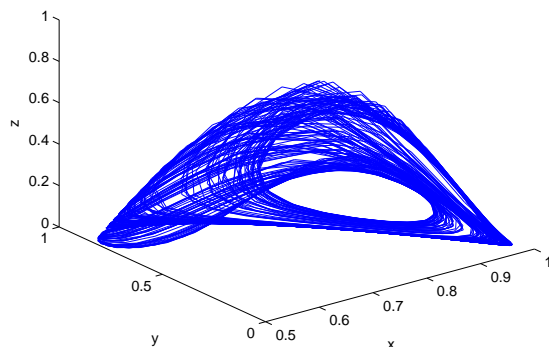


**Figure 1:** The 3D phase portrait of the fractional-order lesser date moth system.

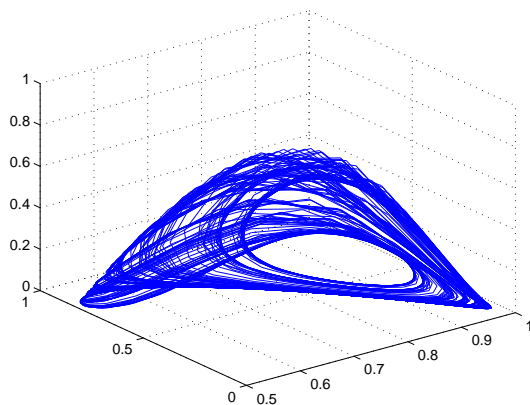


**Figure 2:** The 3D phase portrait of the integer-order lesser date moth system.

From the above equation, we deduce that if the active control functions  $u_i(t)$  are chosen such that

$$\begin{aligned}
 u_1(t) &= -[2e_1 - (x_1 + x_2)e_1 - \left(\frac{y_2}{\beta + x_2}\right)e_1 + \frac{x_1 y_2}{(\beta + x_1)(\beta + x_2)}e_1 - \frac{x_1}{\beta + x_1}e_2 \\
 &\quad + x_1 - x_1^2 - \frac{x_1 y_1}{\beta + x_1} - \dot{x}_1] \\
 u_2(t) &= -\left[\left(\frac{\gamma y_2}{\beta + x_2} - \frac{\gamma x_1 y_2}{(\beta + x_1)(\beta + x_2)}\right)e_1 - \left(z_2 - \frac{\gamma x_1}{\beta + x_1}\right)e_2 - y_1 e_3 - \delta y_1 \right. \\
 &\quad \left. + \frac{\gamma x_1 y_1}{\beta + x_1} - y_1 z_1 - \dot{y}_1\right], \\
 u_3(t) &= -[\sigma z_2 e_2 + \sigma y_1 e_3 - \eta z_1 + \sigma y_1 z_1 - \dot{z}_1],
 \end{aligned}$$

equation (11) becomes

$$\dot{V}(e) = -(e_1^2 + \delta e_2^2 + \eta e_3^2) < 0. \tag{12}$$

According to the inequality (8), the system (7) is asymptotically stable.

For the numerical simulations, we use some documented data for some parameters such as  $\gamma = 3$ ,  $\delta = \eta = 1$ ,  $\sigma = 3$ ,  $\beta = 1.15$ ,  $h = 0.85$ ,  $\alpha = 0.95$ , then we have  $(x_1, y_1, z_1) = (0.7, 0.3, 0.8)$  and  $(x_2, y_2, z_2) = (1.2, 0.12, 2.0)$ . The simulation results are illustrated in Figure 3.

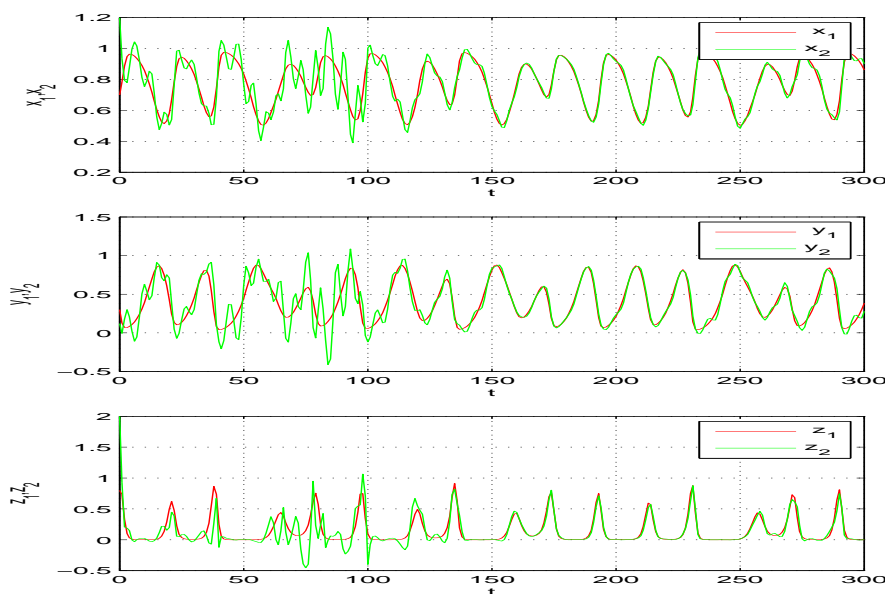


Figure 3: Synchronization between response system (6). and drive system (5)

#### 4 Conclusion

In this paper, we have studied the phenomenon of chaos synchronization between a fractional-order lesser date moth chaotic system and an integer-order chaotic system. Our results demonstrate that if one uses the technique of active control, chaos synchronization can be achieved between a fractional-order chaotic system and an integer-order chaotic system. The numerical results are in good accordance with the theoretical analyses.

#### References

[1] A.E. Matouk. Chaos, feedback control and synchronization of a fractional-order modified autonomous Van der Pol-Duffing circuit. *Commun. Nonlinear Sci. Numer. Simulat.* **16** (2011) 975–986.

[2] B. Zsolt. Chaos theory and power spectrum analysis in computerized cardiocography. *Eur J. Obstet. Gynecol. Reprod. Biol.* **71** (2) (1997) 163–168.

- [3] D. Matignon. Stability result on fractional differential equations with applications to control processing. *Computational Engineering in Systems and Application multi-conference, IMACS, In: IEEE-SMC Proceedings, Lille, France*, **2** (1996) 963–968.
- [4] D. Pazo, M. A. Zaks and J. Kurths. Role of unstable periodic orbit in phase and lag synchronization between coupled chaotic oscillators. *Chaos* **13** (2003) 309–318.
- [5] E. W. Bai and K. E. Lonngren. Synchronization of two Lorenz systems using active control. *Chaos, Solitons and Fractals* **9** (1998) 1555–1561.
- [6] G. Alvarez, S. Li, F. Montoya, G. Pastor and M. Romera. Breaking projective chaos synchronization secure communication using filtering and generalized synchronization. *Chaos, Solitons and Fractals* **24** (2005) 775–783.
- [7] G. M. Mahmoud, T. Bountis, G. M. Abdel-Latif and Emad E. Mahmoud. Chaos synchronization of two different chaotic complex Chen and Lü systems. *Nonlinear Dyn.* **55** (2009) 43–53.
- [8] G. P. Jiang, K. S. Tang and G. Chen. A simple global synchronization criterion for coupled chaotic systems. *Chaos, Solitons and Fractals* **15** (2003) 925–935.
- [9] G. Q. Si, Z. Y. Sun, and Y. B. Zhang. A general method for synchronizing an integer-order chaotic system and a fractional-order chaotic system. *Chinese Physics B* **20** (8) (2011) 080505.
- [10] H. Targhvafard and G. H. Enjace. Phase and anti-phase synchronization of fractional-order chaotic systems via active control. *Commun. Nonlinear Sci. Numer. Simul.* **16** (2011) 4079–4408.
- [11] K. Murali and M. Lakshmanan. Secure communication using a compound signal from generalized synchronizable chaotic system. *Phys. Letters A.* **241** (1998) 303–310.
- [12] L. Kocarev and U. Parlitz. General approach for chaotic synchronization with applications to communication. *Phys. Rev. Lett.* **74** (1995) 5028–5030.
- [13] L. X. Jia, H. Dai, and M. Hui. Nonlinear feedback synchronisation control between fractional-order and integer-order chaotic systems. *Chinese Physics B* **19** (11) (2010) Article ID 110509.
- [14] M. C. Ho, and Y. C. Hung. Synchronization of two different chaotic systems by using generalized active control. *Physics Letters A* **301** (2002) 424–428.
- [15] M. El-Shahed, Juan J. Nieto, A. M. Ahmed and I. M. E. Abdelstar. Fractional-order model for biocontrol of the lesser date moth in palm trees and its discretization. *Advance in Difference Equations* (2017) 2017–2295.
- [16] M. Labid, and N. Hamri. Chaos Synchronization and Anti-Synchronization of two Fractional-Order Systems via Global Synchronization and Active Control. *Nonlinear Dynamics and Systems Theory* **19** (3) (2019) 416–426.
- [17] M. S. Abd-Elouhab, N. Hamri and J. Wang. Chaos Control of a Fractional-Order Financial System. *Mathematical Problems in Engineering* (2010) Article ID270646, 18 pages, doi: 10.1155/2010/270646.
- [18] N. Laskin. Fractional market dynamics. *Physica A* **287** (2000) 482–492.
- [19] N. Zhou, Y. Wang, L. Gong, H. He and J. Wu. Novel single-channel color image encryption algorithm based on chaos and fractional Fourier transform. *Optics Communications* **284** (2011) 2789–2796.
- [20] P. Zhou, Y. M. Cheng and F. Kuang. Synchronization between fractional-order chaotic systems and integer-order chaotic systems (fractional-order chaotic systems). *Chinese Physics B* **19** (9) (2010) 090503.

- [21] R. Mainieri and J. Rehacek. Projective synchronization in three-dimensional chaotic systems. *Phys. Rev. Lett.* **82** (1999) 3042–3045.
- [22] S. Vaidyanathan. Lotka-Volterra two-species mutualistic biology models and their ecological monitoring. *Pharm. Tech. Research* **8** (2015) 199–212.
- [23] W. H. Deng and C. P. Li. Chaos synchronization of the fractional Lü system. *Physica A* **353** (2005) 61–72.
- [24] Y. Zhang and J. Sun. Chaotic synchronization and anti-synchronization based on suitable separation. *Physics Letters A* **330** (2004) 442–447.



# New Design of Stability Study for Linear and Nonlinear Feedback Control of Chaotic Systems

W. Laouira\* and N. Hamri

*Laboratory of Mathematics and their interactions, Department of Science and Technology,  
University Center of Mila, Mila 43000, Algeria.*

Received: May 11, 2022; Revised: September 4, 2022

**Abstract:** This paper presents the control of chaotic dynamical systems by designing linear and nonlinear feedback controllers, the stability of chaotic systems has been studied by three methods, the Lyapunov function, Routh-Hurwitz criteria and finally, a new method which is based on the Jacobian matrix conditions, we proved that we can find stability by the third method and not by the Lyapunov function and Routh-Hurwitz methods, we have also found a good interval or exact value for the parametric control which stabilises the chaotic system at its equilibrium point. Numerical simulations show the effectiveness or non-effectiveness of the results for the three different methods, we apply the feedback control to the Sprott J system, a novel chaotic system and the Genesis system.

**Keywords:** *Lyapunov function; Routh-Hurwitz theorem; Jacobian matrix conditions; feedback control; chaotic systems.*

**Mathematics Subject Classification (2010):** 93B52, 37N35, 93C10, 93D05, 93D15, 65P20, 65P40, 93D20, 93C95.

## 1 Introduction

The term “control of chaos” is used mostly to denote the area of studies lying at the interface between the control theory and the theory of dynamic systems studying the methods of control of deterministic systems with non-regular, chaotic behavior [16]. Several techniques have been devised for chaos control, but most are the developments of two basic approaches: the OGY (Ott, Grebogi and Yorke) method [17], and Pyragas continuous control [18]. Both methods require a previous determination of unstable periodic orbits of the chaotic system before the controlling algorithm can be designed. Different

---

\* Corresponding author: <mailto:w.laouira@centre-univ-mila.dz>

control strategies for stabilizing chaos [11] have been proposed, such as an adaptive control [10, 14], time delay control [3], and fuzzy control [7]. Generally speaking, there are two main approaches for controlling chaos: a feedback control [9, 12] and nonfeedback control. The feedback control approach offers many advantages such as robustness and computational complexity over the non-feedback control method.

We generally study stability for feedback control by two methods: the function of Lyapunov [1] and the criterion of Routh-Hurwitz, but we fail in the cases when we cannot assure the existence of stability for all the control laws. In this work, we show that we can use the third method which is based on the Jacobian matrix conditions, and we can also choose the function of feedback control.

### 2 Stability Condition

Suppose that  $B$  is an  $n \times n$  matrix of real constants, its characteristic polynomial is

$$f(\lambda) = \lambda^n + a\lambda^{n-1} + b\lambda^{n-2} + c\lambda^{n-3} + \dots, \quad n = 1, 2, 3, 4.$$

The Routh-Hurwitz theorem [4–6] is as follows.

**Theorem 2.1** *All the roots of the characteristic polynomial have negative real parts precisely when the given conditions are satisfied:*

$$\lambda^2 + a\lambda + b : a > 0, b > 0.$$

$$\lambda^3 + a\lambda^2 + b\lambda + c : a > 0, c > 0, ab - c > 0.$$

$$\lambda^4 + a\lambda^3 + b\lambda^2 + c\lambda + d : a > 0, ab - c > 0, (ab - c)c - a^2d > 0, d > 0.$$

**Jacobian matrix conditions.** We consider  $A$  is the Jacobian matrix at a fixed point [19],

$$A = \begin{pmatrix} a_{11} & a_{12} & a_{13} \\ a_{21} & a_{22} & a_{23} \\ a_{31} & a_{32} & a_{33} \end{pmatrix}, \tag{1}$$

and  $t = a_{12}a_{23}a_{31} + a_{13}a_{21}a_{32}$ , where

$$A_{11} = \begin{vmatrix} a_{22} & a_{23} \\ a_{32} & a_{33} \end{vmatrix}, \quad A_{22} = \begin{vmatrix} a_{11} & a_{13} \\ a_{31} & a_{33} \end{vmatrix}, \quad A_{33} = \begin{vmatrix} a_{11} & a_{12} \\ a_{21} & a_{22} \end{vmatrix}.$$

**Theorem 2.2** *If  $t \geq 0$ , all the roots of the characteristic polynomial of  $A$  have negative real parts when the given conditions are satisfied:*

$\det(A) < 0, a_{ii} < 0$  and  $A_{ii} > 0$ , for  $i = 1, 2, 3$ .

### 3 Control of Sprott J System

**Theorem 3.1** *The controlled Sprott J system [15] is*

$$\begin{cases} \dot{x} = 2z - u_1, \\ \dot{y} = -2y + z - u_2, \\ \dot{z} = -x + y + y^2 - u_3, \end{cases} \tag{2}$$

where  $u_1 = kx, u_2 = 0, u_3 = y^2 + kz$  and  $k$  is the feedback coefficient, the system (2) will gradually converge to the equilibrium point  $(0; 0; 0)$  when  $k > 1, 5$  for the Lyapunov method and when  $k > 0, 5$  for the Jacobian matrix conditions.

**Proof.** For non linear feedback system (2) consider a quadratic Lyapunov function as  $v = \frac{1}{2}(x^2 + y^2 + z^2)$ , then

$$\begin{aligned}\dot{v} &= -kx^2 - kz^2 - 2y^2 + xz + 2yz \\ &< -kx^2 - kz^2 - 2y^2 + \frac{1}{2}(y^2 + z^2) + y^2 + z^2 \\ &< \left(-k + \frac{1}{2}\right)x^2 - y^2 + \left(-k + \frac{3}{2}\right)z^2.\end{aligned}$$

So, if  $k > 1,5$ , we can obtain  $\dot{v} < 0$ .

For the Jacobian matrix conditions, the Jacobian matrix is as follows:

$$A = \begin{pmatrix} -k & 0 & 2 \\ 0 & -2 & 1 \\ -1 & 1 & -k \end{pmatrix} \Leftrightarrow \det(A) = -2k^2 + k - 4,$$

$$A_{11} = \begin{vmatrix} -2 & 1 \\ 1 & -k \end{vmatrix} = 2k - 1,$$

$$A_{22} = \begin{vmatrix} -k & 2 \\ -1 & -k \end{vmatrix} = k^2 + 2,$$

$$A_{33} = \begin{vmatrix} -k & 0 \\ 0 & -2 \end{vmatrix} = 2k.$$

According to the previous Theorem 2, we have  $t = 0$ , then  $\det(A) < 0$ ,  $a_{ii} < 0$  and  $A_{ii} > 0$  for  $i = 1, 2, 3$  if  $k > 0.5$ .

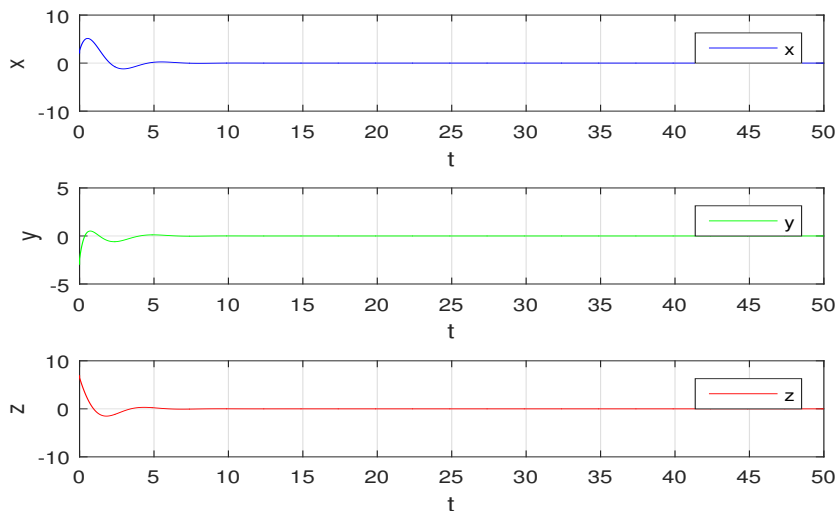


**Figure 1:** Control of the Spratt J system at the equilibrium point  $(0;0;0)$  when  $k = 0,8$ .

**Remark 3.1** For the Routh-Hurwitz method we have not solutions for the same feedback control of the Spratt J system.

#### 4 Control of Novel Chaotic System

**Theorem 4.1** *The controlled novel chaotic system [13] is*

$$\begin{cases} \dot{x} = 0.2x - yz - u_1, \\ \dot{y} = -0.1y + xz - u_2, \\ \dot{z} = -z + xy - u_3, \end{cases} \tag{3}$$

where  $u_1 = k(x - x^*)$ ,  $u_2 = x(z - z^*) + k(y - y^*)$ ,  $u_3 = k(z - z^*)$  and  $k$  is the feedback coefficient, the system (3) will gradually converge to the equilibrium point  $E_2(0.31; 0.44; 0.14)$  when  $k > 0.2$  for the Jacobian matrix conditions.

**Proof.** For non linear feedback system (3) consider a quadratic Lyapunov function as  $v = \frac{1}{2}[(x - x^*)^2 + (y - y^*)^2 + (z - z^*)^2]$ , then

$$\begin{aligned} \dot{v} &= 0.2x^2 - 0.2xx^* + yzx^* - k(x - x^*)^2 - 0.1y(y - y^*) + xz^*(y - y^*) - k(y - y^*)^2 \\ &\quad - z(z - z^*) - (z - z^*)^2 \\ &< (0.7 - k)x^2 + (0.4 - k + \frac{x^*}{2})y^2 + (-0.5 - k + \frac{x^*}{2})z^2 - kx^* - ky^* - kz^* \\ &\quad + \frac{1}{2}(-0.2x^* + 2kx^* - z^*y^*)^2 + \frac{1}{2}(-0.1y^* + 2ky^*)^2 + \frac{1}{2}(z^* + 2kz^*)^2. \end{aligned}$$

So, if  $E_2(0.31; 0.44; 0.14)$ , we can obtain  $\dot{v} < 0$  if

$$\begin{cases} 0.7 - k < 0 \\ 0,555 - k < 0 \\ -0,345 - k < 0 \\ 1.2372k^2 - 0.61602k + 3.6813 \times 10^{-2} < 0 \end{cases} \Leftrightarrow \begin{cases} k > 0.7 \\ k > 0,555 \\ k > -0,345 \\ k \in [6.9445 \times 10^{-2}, 0.42847] \end{cases}.$$

So, we have no solution.

For the Jacobian matrix conditions, the Jacobian matrix is as follows:

$$A = \begin{pmatrix} 0.2 - k & -0.14 & 0 \\ 0.14 & -0.1 - k & 0 \\ 0.44 & 0.31 & -k \end{pmatrix} \Leftrightarrow \det(A) = K((0.2 - k)(0.1 - k) - 0,0434),$$

$$A_{11} = \begin{vmatrix} -0.1 - k & 0 \\ 0.31 & -k \end{vmatrix} = k(0.1 + k),$$

$$A_{22} = \begin{vmatrix} 0.2 - k & 0 \\ 0.44 & -k \end{vmatrix} = k(k - 0.2),$$

$$A_{33} = \begin{vmatrix} 0.2 - k & -0.14 \\ 0.14 & -0.1 - k \end{vmatrix} = k^2 - 0.1k - 0.0004.$$

According to Theorem 2, we have  $t = 0$ , then  $\det(A) < 0$ ,  $a_{ii} < 0$  and  $A_{ii} > 0$  for  $i = 1, 2, 3$  if  $k > 0.2$ .

For the Routh-Hurwitz theorem the characteristic polynomial is:

$$p(\lambda) = \lambda^3 + (3k - 0.1)\lambda^2 + (3k^2 - 0.2k - 0.0004)\lambda + k^3 - 0.1k^2 - 0.0004k,$$

then

$$\begin{cases} a = 3k - 0.1, \\ b = 3k^2 - 0.2k - 0.0004, \\ c = k^3 - 0.1k^2 - 0.0004k, \\ ab - c = 8.0k^3 - 0.8k^2 + 0.0192k + 0.00004, \end{cases}$$

then  $a > 0, c > 0$  and  $ab - c > 0$  if  $k \in ]0.10385, +\infty[$ .

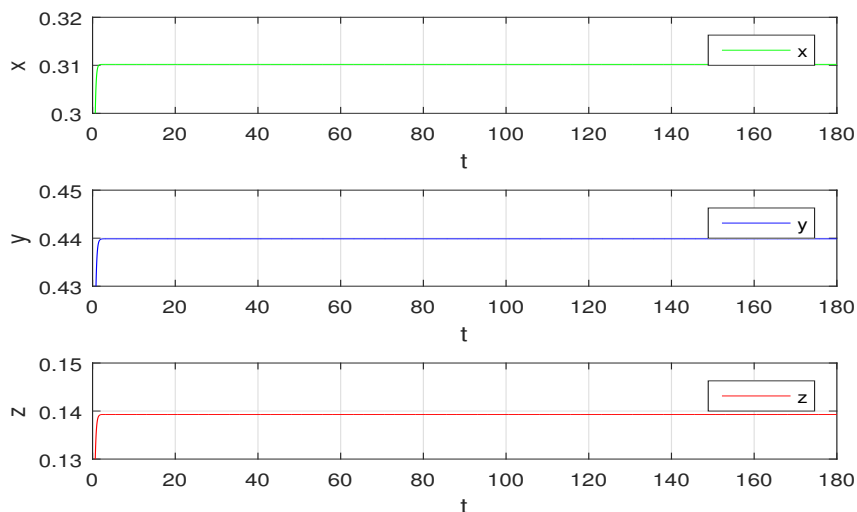


**Figure 2:** Control of a novel chaotic system at the equilibrium point  $E_2(0.31; 0.44; 0.14)$  and  $k = 4$ .

## 5 Control of Modified Genesio System

**Theorem 5.1** *The controlled modified Genesio system [8] is*

$$\begin{cases} \dot{x} = y - u_1, \\ \dot{y} = -0.5y + z - u_2, \\ \dot{z} = 3x^2 - 6x - 2.85y - 0.5z - u_3, \end{cases} \quad (4)$$

where  $u_1 = k(x - x^*)$ ,  $u_2 = ky + z$ ,  $u_3 = kz + 3(x - x^*)$  and  $k$  is the feedback coefficient, the system (2) will gradually converge to the equilibrium point  $(x^*; 0; 0)$  when  $k \in ]-0.25, 0[ \cup ]0.5, +\infty[$  for the Routh-Hurwitz method and when  $k \in ]0.5, +\infty[$  for the Jacobian matrix conditions.

**Proof.** For non linear feedback system (4) consider a quadratic Lyapunov function as  $v = \frac{1}{2}[(x - x^*)^2 + y^2 + z^2]$ , then

$$\dot{v} = -kx^2 + (0.5 - k)y^2 + (-0.5 - k)z^2 + xy + 6(x^* - 1)xz - 2.85yz - yx^* - 3x^*z + 2kxx^* - kx^*$$

for  $x^* = 2$ ,

$$\dot{v} < (k + 3.5)x^2 + \left(\frac{2.85}{2} - k\right)y^2 + \left(\frac{1.85}{2} - k\right)z^2 - 2k - 4.$$

So, we can obtain  $\dot{v} < 0$ , if

$$\begin{cases} k + 3.5 < 0 \\ \frac{2.85}{2} - k < 0 \\ \frac{1.85}{2} - k < 0 \\ -2k - 4 < 0 \end{cases} \Leftrightarrow \begin{cases} k < -3.5 \\ k > \frac{2.85}{2} \\ k > \frac{1.85}{2}, \\ k > -2 \end{cases}$$

so we have no solution.

For  $x^* = 0$ ,

$$\dot{v} < (k + 3)x^2 + \left(\frac{4.85}{2} - k\right)y^2 + \left(\frac{8.85}{2} - k\right)z^2,$$

then  $\dot{v} < 0$

$$\begin{cases} k + 3 \leq 0 \\ \frac{4.85}{2} - k < 0 \\ \frac{8.85}{2} - k < 0 \end{cases} \Leftrightarrow \begin{cases} k < -3 \\ k < \frac{4.85}{2} \\ k > \frac{8.85}{2} \end{cases},$$

so we have no solution.

For the Routh-Hurwitz method, the Jacobian matrix is as follows:

$$J_{(0;0;0)} = \begin{pmatrix} -K & 1 & 0 \\ 0 & -0.5 - K & 0 \\ -6 & -2.85 & 0.5 - K \end{pmatrix}, \text{ so } \det J_{(0;0;0)} = 0.25K - K^3,$$

$$A_{11} = \begin{vmatrix} -0.5 - K & 0 \\ -2.85 & 0.5 - K \end{vmatrix} = K^2 - 0.25,$$

$$A_{22} = \begin{vmatrix} -k & 0 \\ -6 & 0.5 - k \end{vmatrix} = k^2 - 0.5k,$$

$$A_{33} = \begin{vmatrix} -K & 1 \\ 0 & -0.5 - K \end{vmatrix} = K^2 + 0.5K,$$

we have  $t = 0$ , then  $\det(j) < 0$ ,  $a_{ii} < 0$  and  $A_{ii} > 0$  for  $i = 1, 2, 3$  if  $k \geq 0.5$ .

For the second equilibrium point,

$$J_{(2;0;0)} = \begin{pmatrix} -K & 1 & 0 \\ 0 & -0.5 - K & 0 \\ 6 & -2.85 & 0.5 - K \end{pmatrix},$$

so,  $\det J_{(2;0;0)}$ ,  $A_{11}$ ,  $A_{22}$  and  $A_{33}$  have the same value of the first point, then, if  $k > 0.5$  the system (2) will gradually converge to the equilibrium point  $(2; 0; 0)$ . For the Routh-Hurwitz method the characteristic polynomial for  $E_1(0; 0; 0)$  and  $E_2(2; 0; 0)$  equilibrium points is:

$$p(\lambda) = \lambda^3 + 3K\lambda^2 + ((K - 0.5)(2K + 0.5) + K(K + 0.5))\lambda + K(K - 0.5)(K + 0.5),$$

$$a = 3K,$$

$$b = 3.0K^2 - 0.25,$$

$$ab - c = K(8.0K^2 - 0.5),$$

then, if  $k \in ] - 0.25, 0[ \cup ] 0.5, +\infty[$ , we have  $a > 0, b > 0$  and  $ab - c > 0$ .

**Remark 5.1** For  $k$  with a negative value of the Routh-Hurwitz method, we have not a good result for the same feedback control of the Genesio system as we see in the figures.

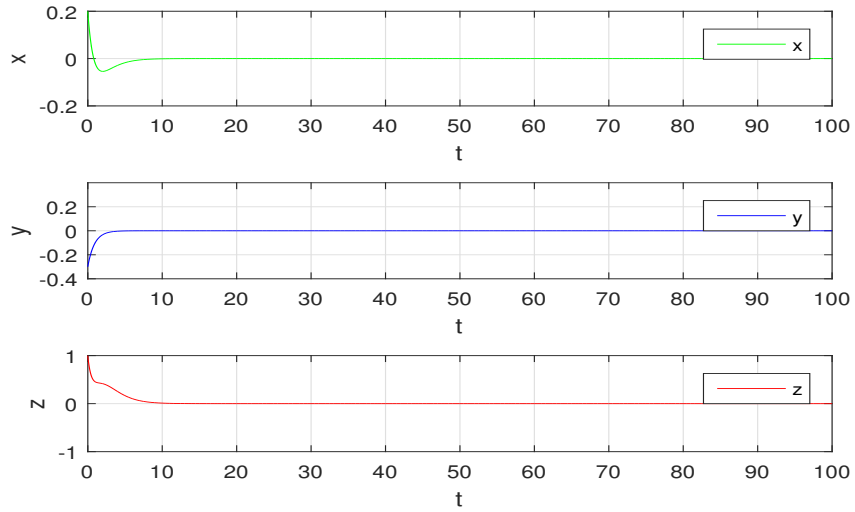


**Figure 3:** Control of the Genesio system at the equilibrium point  $E_1(0;0;0)$ .

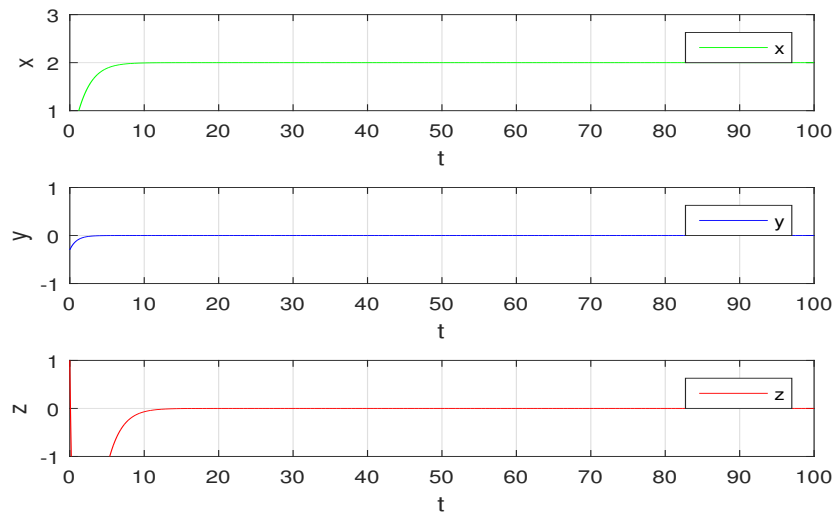


**Figure 4:** Control of the Genesio system at the equilibrium point  $E_2(2;0;0)$ .

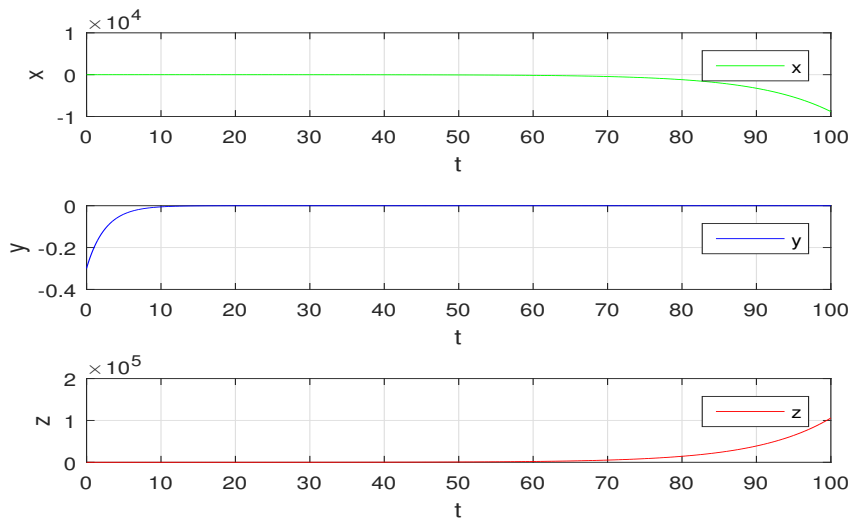


**Figure 5:** Control of the Genesis system at the equilibrium point  $E_1(0;0;0)$  when  $k = -0.1$  .

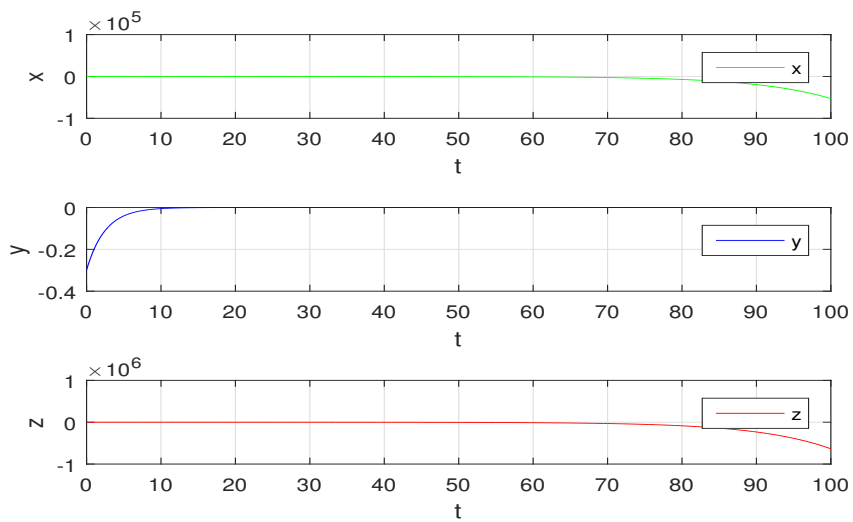


**Figure 6:** Control of the Genesis system at the equilibrium point  $E_2(2;0;0)$  when  $k = -0.1$  .

## 6 Conclusion

This work presents linear and nonlinear feedback control for the Sprott J system, a novel chaotic system and the Genesio system, we use for stabilizing the systems at equilibrium points three different methods: the Lyapunov function, the Routh-Hurwitz criterion and a new method based on the Jacobian matrix, which is a modification of Routh-Hurwitz conditions. We proved that the stability by new method is satisfied where we do not have it for the others, and we can get a good interval or exact value for gain matrix where the stability is satisfied.

## References

- [1] A. Ayadi, K. Dchich, B. Sfaihi and M. Benrejeb. Unified Continuous and Discrete Lur'e Systems Stability Analysis Based on Augmented Model Description. *Nonlinear Dynamics and Systems Theory* **20** (3) (2020) 242–252.
- [2] B. R. Andrievskii and A. L. Fradkov. Control of Chaos: Methods and Applications. I. Methods 1. *Automation and Remote Control* **64** (5) (2003) 673–713.
- [3] M. E. Brandt, H. T. Shih and G. Chen. Linear Time-delay Feedback Control of a Pathological Rhythm in a Cardiac Conduction Model. *Phys. Rev. E* **56** (1997) 1334–1337.
- [4] S. Barnett and R. G. Cameron. *Introduction to Mathematical Control Theory*. Clarendon Press. OXFORD, Second Edition (1985).
- [5] R. L. Borrelli and C. S. Coleman. *Differential Equations* (fourth ed.). John Wiley and Sons, Inc. New York, (1998).
- [6] W. E. Boyce and R. C. DiPrima. *Elementary Differential Equations and Boundary Value Problems* (eighth ed.). John Wiley and Sons, Inc. United States of America, (2010).
- [7] W. Chang, J. B. Park, Y. H. Joo and G. R. Chen. Output feedback control of Chen chaotic attractor using fuzzy logic. In: *Proceedings of IECON 2000*, Japan, 2159–2164.
- [8] K. Deng, J. Li and S. Yu. Dynamics analysis and synchronization of a new chaotic attractor. *Opt Int J. Light Electron Opt.* **125** (13) (2014) 3071–3075.
- [9] W. Q. Feng Gao, V. Liu and K. L. Teo. Sreeram. Nonlinear Feedback Control for the Lorenz System. *Dynamics and Control* **11** (2001) 57–69.
- [10] W. He and J. Cao. Adaptive synchronization of a class of chaotic neural networks with known or unknown parameters. *Phys. Lett. A* **372** (2008) 408–416.
- [11] H. Norouzi and D. Younesian. Chaos control for the plates subjected to subsonic flow. *Regular and Chaotic Dynamics* **21** (2016) 437–454.
- [12] J. Zhang and W. Tang. Control and synchronization for a class of new chaotic systems via linear feedback. *Nonlinear Dyn.* **58** (2009) 675.
- [13] K. Rajagopal, A. Akgul, I. M. Moroz, Z. Wei, S. Jafari and I. Hussain. A Simple Chaotic System With Topologically Different Attractors. *IEEE Access* 10.1109/ACCESS.2019.2922164.
- [14] J. A. Lu, X. P. Han, Y. T. Li and M. H. Yu. Adaptive coupled synchronization among multi-Lorenz systems family. *Chaos Solitons Fractals* **31** (2007) 866–878.
- [15] M. Islam, N. Islam and S. Nikolov. Adaptive Control and Synchronization of Sprott J System With Estimation Of Fully Unknown Parameters. *Journal of Theoretical and Applied Mechanics* **45** (2) (2015) 45–58.
- [16] L. Meddour and K. Belakroum. On the Equivalence of Lorenz System and Li System. *Nonlinear Dynamics and Systems Theory* **22** (1) (2022) 58–65.

- [17] E. Ott, C. Grebogi and J. A. Yorke. Controlling chaos. *Phys. Rev. Lett.* **64** (11) (1990) 1196–1199.
- [18] K. Pyragas. Continuous control of chaos by self-controlling feedback. *Phys. Lett. A* **170** (6) (1992) 421–428.
- [19] W. Laouira, and N. Hamri. Feedback Control of Chaotic Systems by Using Jacobian Matrix Conditions. *Nonlinear Dynamics and Systems Theory* **18** (3) (2018) 285–296.



# Control of a Shunt Active Power Filter by the Synchronous Referential Method Connected with a Photovoltaic Solar Energy

A. Morsli<sup>1</sup>, A. Tlemcani<sup>1\*</sup> and H. Nouri<sup>2</sup>

<sup>1</sup> *Electrical Engineering and Automation Research Laboratory (LREA), University of Medea, 26000, Medea, Algeria.*

<sup>2</sup> *Power Systems, Electronics and Control Research Group, Department of Engineering Design and Mathematics, University of West of England, Bristol, BS16 1QY, U.K.*

Received: February 14, 2022; Revised: August 30, 2022

**Abstract:** This paper presents a depollution technique for low voltage electrical networks. This technique is based on the control of the shunt active power filter (SAPF) at two levels by the instantaneous power method (Synchronous Reference Frame - SRF) which has allowed us to obtain reference currents by eliminating the harmonic currents generated by the non-linear load (three-phase rectifier). We have thus proposed a DC voltage source from the SAPF by a photovoltaic solar generator while ensuring energy maximization by the MPPT controller. The simulation results under the MATLAB/Simulink environment obtained from the shunt active filtering system clearly indicate the efficiency of the chosen control (SRF) and follow the international standard recommendations IEEE519-92 which require that the Total Harmonic Distortion of the source current less than 5 %.

**Keywords:** *maximum power point tracking (MPPT), photovoltaic generator (PVG), perturb and observe (PandO), synchronous reference frame (SRF), total harmonic distortion (THD).*

**Mathematics Subject Classification (2010):** 93C42, 03B52, 93E11, 93Cxx.

---

\* Corresponding author: [mailto:h\\_tlemcani@yahoo.fr](mailto:h_tlemcani@yahoo.fr)

### 1 Introduction

The increase in pollution of power supply networks is caused by the appearance of devices based on power electronics components as a non-linear load. For this, the best solution to improve the quality of electrical energy is the Active Power Filter [1–3]. In this paper, the shunt active power filter is the main responsible for eliminating the harmonics in the power supply lines caused by the non-linear load (Three-phase rectifier). For the shunt Active Filter to work within the standards and give good results of Total Harmonic Distortion of the supply currents, it suffices to choose its best control in terms of precision and speed [4]. The authors of [5,6] propose a resonant control scheme in the SRF method to reduce the calculation rate. This proposal is essential for non-linear loads such as DC-DC converters where there are electric currents composed by the fundamentals and harmonics of order  $6h \pm 1$ ,  $h = 1, 2, \dots$  [7].

### 2 Principle of the Shunt Active Power Filtering System

The global diagram of the proposed shunt active power filtering system is shown in Figure 1. It consists of a non-linear load (three-phase rectifier) which is the source of the harmonics injected into the supply network which becomes polluted [8].

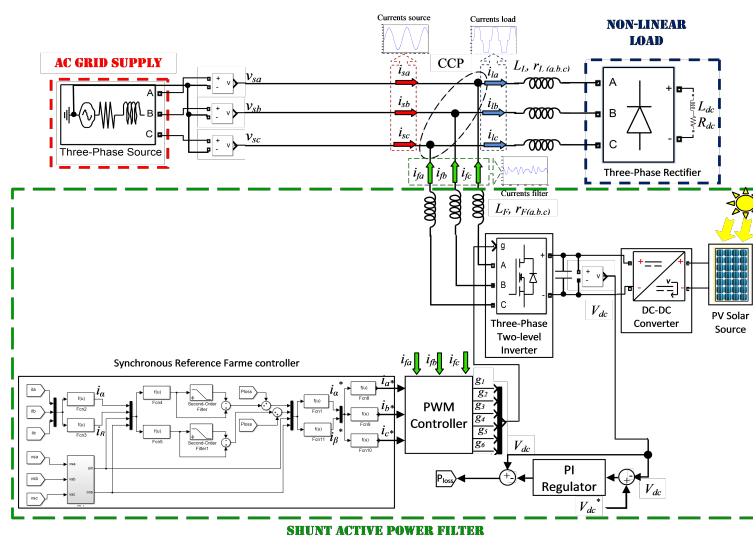
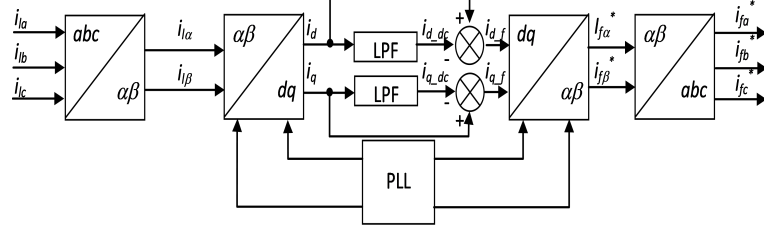


Figure 1: Structure of the SAPF controlled by the SRF method and powered by the PV system.

### 3 Synchronous Reference Frame (SRF) Method

Figure 2 shows the block diagram of the SRF method [1,9]. This method is based on the transformation of three-phase load currents ( $i_{la}, i_{lb}, i_{lc}$ ) into a two-phase stationary



**Figure 2:** Block diagram of the SRF method.

frame  $(\alpha - \beta)$  as shown in equation (1):

$$\begin{bmatrix} i_{L\alpha} \\ i_{L\beta} \end{bmatrix} = \sqrt{\frac{2}{3}} \begin{bmatrix} 1 & -1/2 & -1/2 \\ 0 & \sqrt{3}/2 & -\sqrt{3}/2 \end{bmatrix} \begin{bmatrix} i_{La} \\ i_{Lb} \\ i_{Lc} \end{bmatrix}. \quad (1)$$

The two-phase currents  $i_{L\alpha}$  and  $i_{L\beta}$  of stationary  $(\alpha - \beta)$  axes are transformed in  $i_d$  and  $i_q$  into two-phase synchronous frame (d-q axes) employing equation (2), where  $\cos\theta$  and  $\sin\theta$  represent the synchronous unit vectors which can be generated using the Phase Locked Loop system (PLL):

$$\begin{bmatrix} i_d \\ i_q \end{bmatrix} = \begin{bmatrix} \cos\theta & \sin\theta \\ -\sin\theta & \cos\theta \end{bmatrix} \begin{bmatrix} i_{L\alpha} \\ i_{L\beta} \end{bmatrix}. \quad (2)$$

So, we see the alternative components  $i_{dq-f}$  can be obtained by subtracting the  $i_{dq-dc}$  part from the total d-axis current ( $i_d$  and  $i_q$ ), which leaves behind the harmonic component present in the load current. The inverse Park transformation allowed us to obtain the reference currents of the two-phase stationary frame  $i_{f,\alpha\beta}^*$  from the currents of the two-phase stationary frame  $i_{dq-dc}$  as shown in equation (3):

$$\begin{bmatrix} i_{f\alpha}^* \\ i_{f\beta}^* \end{bmatrix} = \begin{bmatrix} \cos\theta & -\sin\theta \\ \sin\theta & \cos\theta \end{bmatrix} \begin{bmatrix} i_{d-dc} \\ i_{q-dc} \end{bmatrix}. \quad (3)$$

Finally, the currents of the two-phase stationary frame  $i_{f,\alpha\beta}^*$  are transformed back into a three-phase stationary frame and the reference filter currents  $i_{fa}^*$ ,  $i_{fb}^*$  and  $i_{fc}^*$  are obtained according to equation (4):

$$\begin{bmatrix} i_{fa}^* \\ i_{fb}^* \\ i_{fc}^* \end{bmatrix} = \sqrt{\frac{2}{3}} \begin{bmatrix} 1 & 0 \\ -\frac{1}{2} & \frac{\sqrt{3}}{2} \\ -\frac{1}{2} & -\frac{\sqrt{3}}{2} \end{bmatrix} \begin{bmatrix} i_{f\alpha}^* \\ i_{f\beta}^* \end{bmatrix}. \quad (4)$$

#### 4 The Photovoltaic Solar Source Description and Modeling

In PV systems, they achieve great performance, fast responses and less fluctuations in steady state for rapid irradiance and/or temperature variation improving the amount of energy effectively extracted from the PV generator [10]. The datasheet of the monocrystalline photovoltaic module of BP SOLAR MSX120 type is given in Table 1.

Technical characteristics	Values
Maximum power : $P_{max}$	120 W
Open-circuit voltage : $V_{OC}$	42.1 V
Short-circuit current : $I_{SC}$	3.87 A
Maximum power voltage : $V_{max}$	33.7 V
Maximum power current : $I_{max}$	3.56 A
Number of cells	72
Température coefficient of $I_{SC}$ : $k_i$	$(0.065 \pm 0.015) \% / ^\circ C$
Température coefficient of $V_{OC}$ : $k_v$	$-(80 \pm 10) mV / ^\circ C$

**Table 1:** Technical characteristics of the PV module of BP SOLAR MSX120 type.

The model used to simulate the performance of the PV module (group of cells in series) is deduced from the model of the characteristic of a solar cell by the following equation, with  $z$  photovoltaic cells connected in series [11,12]:

$$I_{pv} = I_{ph} - I_0 \left[ e^{\frac{q(V_{pv} + z.R_s.I_{pv})}{z.a.k.T_{ck}}} - 1 \right] - \frac{V_{pv} + z.R_s.I_{pv}}{z.R_{sh}}. \tag{5}$$

Figure 3 shows the block diagram of the PV system containing the boost chopper with its MPPT controller by the Perturb and Observe algorithm (PandO).

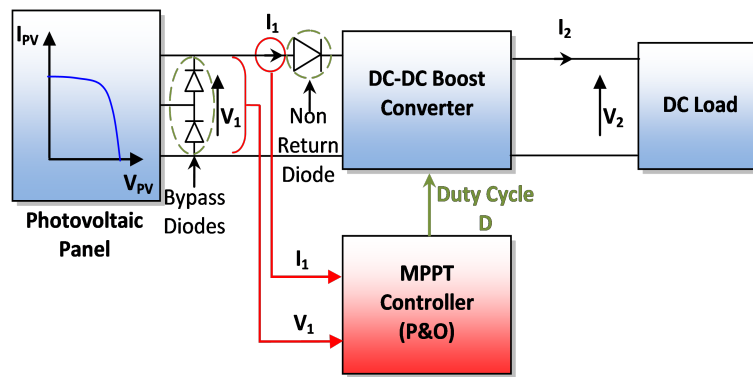


**Figure 3:** Block diagram of the PV system used.

### 5 Simulation Results and Discussion

Table 2 shows the parameters of the two-level shunt active filtering system controlled by the Synchronous Reference Frame (SRF) method.

Figure 4 illustrates the two forms of line currents. The first, the load current  $i_{la}$  (before filtering up to 0.05 s), and the second, the source current  $i_{sa}$  (after filtering up to 0.1 s). We observe in the first part that the non-linear load influences the supply line and distorts the  $i_{la}$  wave, which indicates that this line is full of harmonics. We also note in the second part that the electric current began to take its sinusoidal curve  $i_{sa}$  after

Parameters	Values
Supply voltage $v_S(rms)$ and frequency $f$	220V, 50 Hz
Line's inductance $L_s$ and resistance $r_s$	19.4 $\mu H$ , 0.25m $\Omega$
DC link's inductance $L_{dc}$ , and resistance $r_{dc}$	15 mH, 4 $\Omega$
Load inductance $L_l$ and resistance $r_l$	0.3 mH, 0.3 $\Omega$
DC link voltage $V_{dc}$	620V
Coupling inductance $L_{fa}$ and resistance $r_{fa}$	1.22 mH, 0.2 $\Omega$

**Table 2:** Parameters of the shunt active filtering system controlled by the Synchronous Reference Frame (SRF) method.

it had passed the transient phase in the time of 0.07 seconds. This indicates that the SAPF has almost completely eliminated impurities.

The THD of the load current  $i_{la}$  shown in Figure 5 is high (23.56 %) and that would be rejected by the energy supplier. It is also affects the non-linear load (devices malfunction). We also see that the harmonics of order  $(6h \pm 1)$  appeared because of the use of the non-linear load (the rectifier).

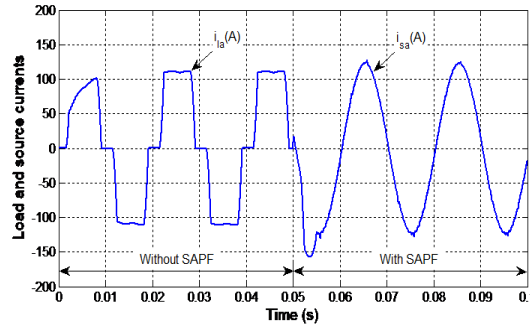


**Figure 4:** Load and source currents of the SAPF system supplied by a PV source.

In Figure 6, we can clearly see the harmonics decrease by the THD ratio of the source current  $i_{sa}$  equal to 1.16 %, which is very acceptable.

Figure 7 shows the three currents of the shunt active filtering system. Before the insertion of the SAPF, the line current is deformed, it is the load current  $i_{la}$  only. After closing the breaker at the time of 0.05 s, the filter current intervenes and compensates for the line current and becomes almost sinusoidal source current  $i_{sa}$ .

The two stages of the filter current  $i_{fa}$  and its reference  $i_{fa}^*$  are shown in Figure 8. At the breaker closing time (at 0.05 s), the filter current follows the trajectory of its reference produced by the SRF block, especially in the permanent state. This means that the error is almost zero.

The DC link voltage  $V_{dc}$  which supplies the inverter is shown in Figure 9. Its value increases from 351.2 V without the SAPF to 620 V with the SAPF. Note that the value stabilizes just after the transient regime in each part.

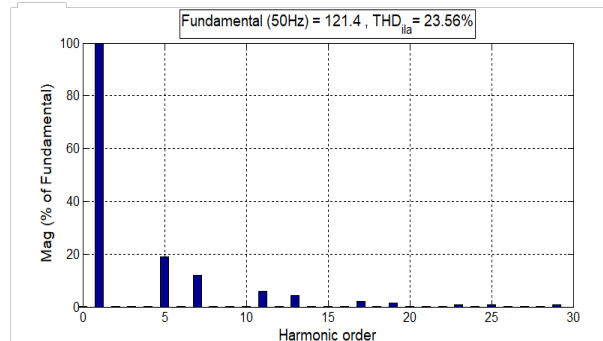


Figure 5: Total Harmonic Distortion of the load current before applying the SAPF.

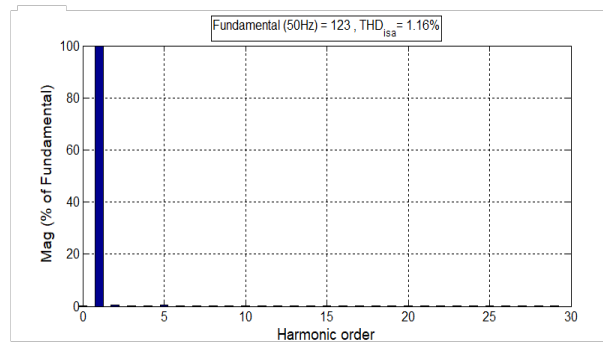


Figure 6: Total Harmonic Distortion of the source current after applying the SAPF.

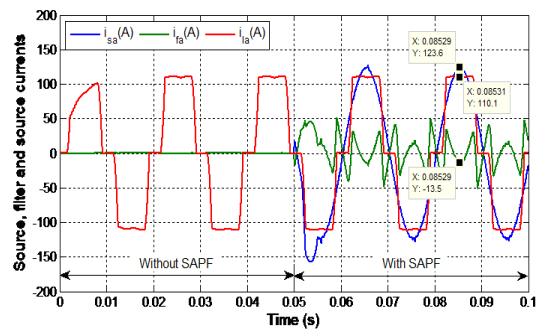


Figure 7: Different currents before and after the insertion of the SAPF.

## 6 Conclusion

In this paper, we studied the identification by the Synchronous Referential Frame method (SRF) on the one hand and the optimization of the energy which feeds the inverter by

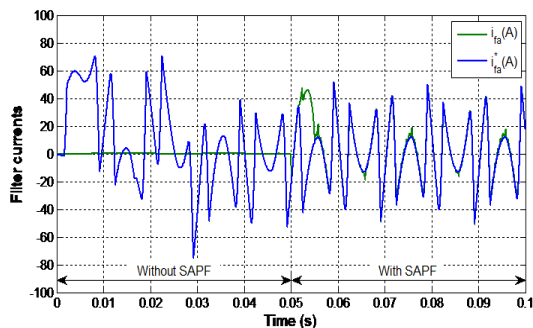


Figure 8: Filter current and its reference before and after the insertion of the SAPF.

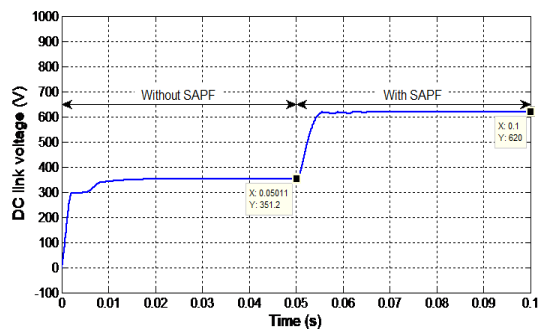


Figure 9: DC link voltage before and after the insertion of the SAPF.

the MPPT controller on the other hand, we can say that the quality of the compensation of current harmonics depends on the performance of the chosen identification method. The simulation results have shown the efficiency of the SAPF powered by a photovoltaic generator and controlled by the SRF technique and offering good results from the THD of the current on the source side, so the power factor is close to unity. This implies that the conditions of the international recommendation IEEE519-92 are well verified.

## References

- [1] L. Xiangshun, H. Hongliang, L. Jianghua and L. Zhiwei. Modified Synchronous Reference Frame Method for Active Power Filter Under Asymmetric and Distorted Supply Voltages Condition. In: *International Conference on Industrial Informatics-Computing Technology, Intelligent Technology, Industrial Information Integration*. Wuhan, China, 2016, 1–5.
- [2] A. Morsli, A. Tlemçani and M. S. Boucherit. Shunt Active Power Filter Based Harmonics Compensation of a Low-Voltage Network Using Fuzzy Logic System. *Nonlinear Dynamics and Systems Theory* **17** (1) (2017) 70–85.
- [3] A. Morsli, A. Tlemçani, A. Krama, A. Abbadi, L. Zellouma and H. Nouri. Application of the Direct Power Control Strategy in a Shunt Active Filter by Exploiting the Solar

- Photovoltaic Energy as a Continuous Source. *Nonlinear Dynamics and Systems Theory* **20** (4) (2020) 410–424.
- [4] Y. Hoon, M. A. M. Radzi, M. K. Hassan and N. F. Mailah. Three-phase Three-level Shunt Active Power Filter with Simplified Synchronous Reference Frame. In: *IEEE Industrial Electronics and Applications Conference (IEACon)*. Kota Kinabalu, Malaysia, 2017, 1–6.
- [5] R.I. Bojoi, G. Griva, V. Bostan, M. Guerriero, F. Farina and F. Profumo. Current control strategy for power conditioners using sinusoidal signal integrators in synchronous reference frame. *IEEE Transactions on Power Electronics* **6** (20) (2005) 1402–1412.
- [6] M. Liserre, R. Teodorescu and F. Blaabjerg. Multiple harmonics control for three-phase grid converter systems with the use of PI-RES current controller in a rotating frame. *IEEE Transactions on Power Electronics* **3** (21) (2006) 836–841.
- [7] T. Zou, H. Geng and K. Wang. Optimized harmonic detecting and repetitive control scheme for shunt active power filter in synchronous reference frame. *IEEE 8th International Power Electronics and Motion Control Conference (IPEMC-ECCE Asia)*. Hefei, China, 2016, 22–26.
- [8] A. Benzahia, R. Boualaga, A. Moussi, L. Zellouma, M. Meriem and C. Bouziane. A PV powered shunt active power filter for power quality improvement. *Global Energy Interconnection Development and Cooperation Organization* **2** (2) (2019) 143–149.
- [9] M.J. Diaz, E. Bueno, H.E.P. Souza, F.A.S. Neves and M.C. Cavalcanti. FPGA implementation of a sequence separation algorithm based on a generalized delayed signal cancellation method. *Energy Conversion Congress and Exposition (ECCE2009)*. IEEE, 2009, 562–567.
- [10] F. Hamidia, A. Abbadi, A. Tlemçani and M.S. Boucherit. Dual Star Induction Motor Supplied with Double Photovoltaic Panels Based on Fuzzy Logic Type-2. *Nonlinear Dynamics and Systems Theory* **18** (4) (2018) 359–371.
- [11] A. Loukriz, M. Haddadi and S. Messalti. Simulation and experimental design of a new advanced variable step size Incremental Conductance MPPT algorithm for PV systems. *ISA Transactions, Elsevier* **62** (2016) 30–38.
- [12] S. Bentouati, A. Tlemçani, N. Henini and H. Nouri. Adaptive Sliding Mode Control Based on Fuzzy Systems Applied to the Permanent Magnet Synchronous Machine. *Nonlinear Dynamics and Systems Theory* **21** (5) (2021) 457–470.



# A Neural Network Approximation for a Model of Micromagnetism

M. Moumni\* and M. Tilioua

*MAIS Laboratory, MAMCS Group, FST Errachidia, Moulay Ismail University of Meknès,  
P.O. Box: 509 Boutalamine, 52000 Errachidia, Morocco.*

Received: January 24, 2022; Revised: September 13, 2022

**Abstract:** Micromagnetics is a continuum theory describing magnetization patterns inside ferromagnetic media. The dynamics of a ferromagnetic material are governed by the Landau-Lifshitz equation (LL). This equation is highly nonlinear and has a non-convex constraint. In this work, we propose two new algorithms for solving this equation in high dimension, by using deep neural networks. Numerical and comparative tests using TensorFlow illustrate the performance of our algorithms.

**Keywords:** *data-driven scientific computing; machine learning; numerical analysis; micromagnetism; Landau-Lifshitz equation.*

**Mathematics Subject Classification (2010):** 78A25, 35Q60, 35B40, 93-10, 70K75.

## 1 Introduction

Differential equations, including ordinary differential equations (ODEs) and partial differential equations (PDEs), formalize the description of the dynamical nature of the world around us. However, solving these equations is a challenge due to extreme computational cost and because most PDEs do not have an analytical solution, their solution can be approximated using classical numerical methods (which are based on a discretization of the domain) [17], [18], [11]. These methods are particularly efficient for low-dimensional problems on regular geometries; however, finding an appropriate discretization for a complex geometry can be as difficult as solving the partial differential equation itself. This problem is particularly severe if the space dimension is large as there is no straightforward way to discretize irregular domains in space dimensions larger than three. Solving equations is a high-level human intelligence work and a crucial step towards general

---

\* Corresponding author: <mailto:md.moumni@gmail.com>

artificial intelligence (AI). Therefore, the obstacle of extreme computational cost in numerical solution may be bypassed by using general AI techniques such as deep learning and reinforcement learning, which were rapidly developed during the last decades. Data used to train the network is randomly sampled within the entire solution domain in each training batch, including initial conditions and boundary conditions.

Recently, deep learning has revolutionized many scientific fields [4], [7], [5]. Including the solution of the differential equation PDEs, Raissi [14] propose a deep learning approach for discovering nonlinear partial differential equations from scattered and potentially noisy observations in space and time. Beck and *et al.* [6] propose a new method for solving high-dimensional fully nonlinear second-order PDEs. The Deep Galerkin Method uses a deep neural network instead of a linear combination of basis functions. The deep neural network is trained to satisfy the differential operator, initial condition, and boundary conditions using stochastic gradient descent at randomly sampled spatial points. In the stochastic framework, Weinan *et al.* [23] propose a new algorithm for solving PDEs and backward stochastic differential equations in high dimension. There are many other works on solving differential equations using the neural network [22], [9], [16]. The ODEs and PDEs are equations which impose relationships between the different partial derivatives of a multivariable function. We ask the following question: if there exists a neural network capable of simultaneously and uniformly approximating a function and its partial derivatives. The answer to this question and the mathematical theory of physics-informed neural networks is already treated by Allan Pinkus in [20]. In this work, we will solve the LL equation in high dimension, using the artificial neural network by two different methods as will be described below. One of the major difficulties that exists for solving this equation by the classical methods is the non-convex constraint, see [2, 3, 17]. We will see that this constraint is not a problem for the neural network approach because we add this constraint in the loss function.

The rest of the paper is structured as follows. In the next section, we present the LL equation arising in micromagnetism and which will be the subject of our investigation. In Section 3, we explore the use of deep learning for solving the PDEs under consideration in micromagnetism in high dimension. To this end, it is necessary to formulate the PDEs as a learning problem. We put forth two distinct classes of algorithms of deep learning, and highlight their performance through the lens of different benchmark problems. In fact, we use a deep neural network to approximate the PDE solution with this parameterization, a loss function is set up, and then we train so that the *Loss* function becomes very small. For the training data, the network uses points randomly sampled from the region where the function is defined, and the optimization is performed using gradient descent. We conclude the paper in Section 4 by giving some comments and a direction for future work.

## 2 The Model Statement

In this paper, we consider the simplified LL equation in which we neglect magnetostatic, anisotropy, and a Zeeman field. To describe the model equations, we consider  $\Omega \subset \mathbb{R}^d$ ,  $d \in \mathbb{N}^*$ , a bounded and regular open set. We assume that a ferromagnetic material occupies the domain  $\Omega$ . The magnetization field of the ferromagnetic material is denoted by  $M(x, t)$ , where  $x$  and  $t$  mean the position and time, respectively. Then, the LL model in  $Q = \Omega \times (0, T)$  is described by

$$\partial_t M(x, t) = -M(x, t) \times \Delta M(x, t) - \mu M(x, t) \times M(x, t) \times \Delta M(x, t) \text{ in } Q \quad (1)$$

subject to the initial conditions

$$M(x, 0) = M_0(x), \quad |M_0(x)| = 1 \text{ in } \Omega \quad (2)$$

and a periodic boundary condition. Here,  $\times$  denotes the exterior product,  $M(x, t) = (m_1(x, t), m_2(x, t), m_3(x, t)) \in \mathbb{R}^3$ , and  $\mu \geq 0$  is the damping parameter. Next, we consider the energy-structure

$$E(M(t)) = \|\nabla M(t)\|_{L^2(\Omega)}.$$

By integration on the equation (1), we obtain the following energy equation:

$$E(M(t)) = E(M(0)) - 2\mu \int_0^t \int_{\Omega} \|M(x, s) \times \Delta M(x, s)\|^2 dx ds. \quad (3)$$

For any  $t \geq 0$ , equation (3) implies that the problem has the energy dissipation property for the case  $\mu > 0$  and the energy conservation property for the case  $\mu = 0$ .

If we multiply the LL equation (1) by  $M(x, t)$ , we obtain the important hypothesis of micromagnetism is that the local magnetization vector must be constant in magnitude

$$|M(x, t)| = |M_0(x)| = 1 \quad \text{for any } t > 0. \quad (4)$$

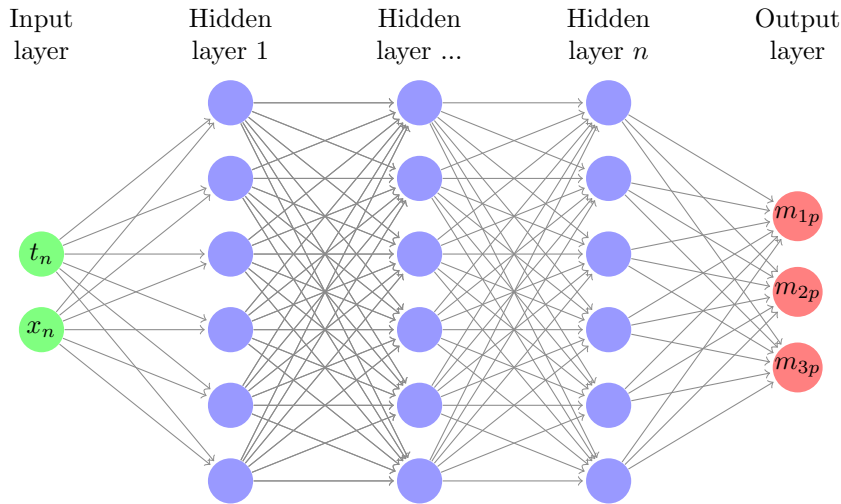
Ferromagnetic materials are very important in industry and modern technology and have been used for fundamental studies and in many everyday applications such as sensors, electric motors, generators, hard disk media, and most recently spintronic memories.

### 3 Deep Learning Algorithm

The goal is to approximate the solution  $M = (m_1, m_2, m_3)$  for the equation (1) by a deep neural network with parameter set {weights, biases}. For this, we will work on two different cases. In the first case, suppose we know the solution at some random points in  $Q$ . In the second case, assume we only know the solution at some random points in  $\partial Q$  and some random points in  $\Omega \times \{0\}$ .

#### 3.1 First case

We consider a neuron network composed by several layers such that the first layer represents the inputs (the random points  $(t^i, x^i)$  of  $Q$ ), while the last layer represents the output solution  $M_p = (m_{1p}, m_{2p}, m_{3p})$  at the random points  $(t^i, x^i)$  linked by the parameters weights and biases, the other layers are hidden layers.



The first step in approximating the solution  $M$  at all points of  $Q$  is to calculate the objective function  $Loss$ .

Let  $N$  be the number of the random points  $(x^i, t^i) \in Q$  at which we know the exact solution. We define

$$(f_{m_1}, f_{m_2}, f_{m_3}) = \frac{\partial M_p(x, t)}{\partial t} + M_p(x, t) \times \Delta M_p(x, t) + \mu M_p(x, t) \times M_p(x, t) \times \Delta M_p(x, t),$$

$$MSE_f = MSE_{f_{m_1}} + MSE_{f_{m_2}} + MSE_{f_{m_3}},$$

$$MSE_M = MSE_{m_1} + MSE_{m_2} + MSE_{m_3}$$

and

$$MSE_{Constraint} = \frac{1}{N} \sum_{i=1}^N |(m_1(x^i, t^i))^2 + (m_2(x^i, t^i))^2 + (m_3(x^i, t^i))^2 - 1|^2$$

with

$$MSE_{f_{m_r}} = \frac{1}{N} \sum_{i=1}^N |f_{m_r}(x^i, t^i)|^2,$$

$$MSE_{m_r} = \frac{1}{N} \sum_{i=1}^N |m_r(x^i, t^i) - m_{rp}(x^i, t^i)|^2.$$

for  $r = 1, 2, 3$ . The objective function  $Loss$  is given by

$$Loss = MSE_f + MSE_M + MSE_{Constraint}.$$

In the next step, we will deduce an iterative gradient algorithms designed to minimize  $Loss$ . This minimization is achieved by an adequate weight configuration. For this, we will use the limited-memory quasi-Newton code for unconstrained optimization L-BFGS, developed at the Optimization Center, a joint venture of Argonne National Laboratory and Northwestern University by Liu and Nocedal [13]. Numerical and comparative tests using TensorFlow [1] illustrate the performance of our algorithm. More specifically, we

- 
1. Initialize the parameter set {weights,biases}.
  2. Generate random samples  $(t^i, x^i)$  from  $Q$ .
  3. Calculate the *Loss* functional for the current mini-batch  $s^i = \{(t^i, x^i)\}$ .
  4. We choose {weights,biases} randomly such that *Loss* becomes minimal.
  5. Repeat steps (3)-(4) until *Loss* is very small.
- 

apply the following algorithm.

When the *Loss* function becomes small enough, we say that the neuron network has become trained and in this case, we can determine the solution of the equation (1) at any point of  $Q$ .

**Numerical simulation.** For our purpose we consider non-trivial exact solutions [10] for LL equation (1) on  $\Omega$ . Here, let  $\alpha \in \mathbb{R}$ ,  $l \in \mathbb{Z}$  and  $k = l\pi$ . The exact solution in one-dimensional space is given by

$$M(t, x) = (m_1(t, x), m_2(t, x), m_3(t, x)),$$

where

$$\begin{aligned} m_1(t, x) &= \frac{\sin \alpha \cos(kx - \phi(x, t, \alpha, k, \mu))}{d(t, \alpha, k, \mu)}, \\ m_2(t, x) &= \frac{\sin \alpha \sin(kx - \phi(x, t, \alpha, k, \mu))}{d(t, \alpha, k, \mu)}, \\ m_3(t, x) &= \frac{\exp(k^2 \mu t) \cos \alpha}{d(t, \alpha, k, \mu)}, \end{aligned}$$

with

$$d(t, \alpha, k, \mu) = \sqrt{\sin^2 \alpha + \exp(2k^2 \mu t) \cos^2 \alpha}$$

and

$$\phi(x, t, \alpha, k, \mu) = \frac{1}{\mu} \log \left( \frac{d(t, \alpha, k, \mu) + \exp(k^2 \mu t) \cos \alpha}{1 + \cos \alpha} \right).$$

The exact solution in two-dimensional space is given by

$$M(t, x) = (m_1(t, x, y), m_2(t, x, y), m_3(t, x, y)),$$

where

$$\begin{aligned} m_1(t, x, y) &= \frac{\sin \alpha \cos(k(x+y) - \phi(x, t, \alpha, k, \mu))}{d(t, \alpha, k, \mu)}, \\ m_2(t, x, y) &= \frac{\sin \alpha \sin(k(x+y) - \phi(x, t, \alpha, k, \mu))}{d(t, \alpha, k, \mu)}, \\ m_3(t, x, y) &= \frac{\exp(2k^2 \mu t) \cos \alpha}{d(t, \alpha, k, \mu)}, \end{aligned}$$

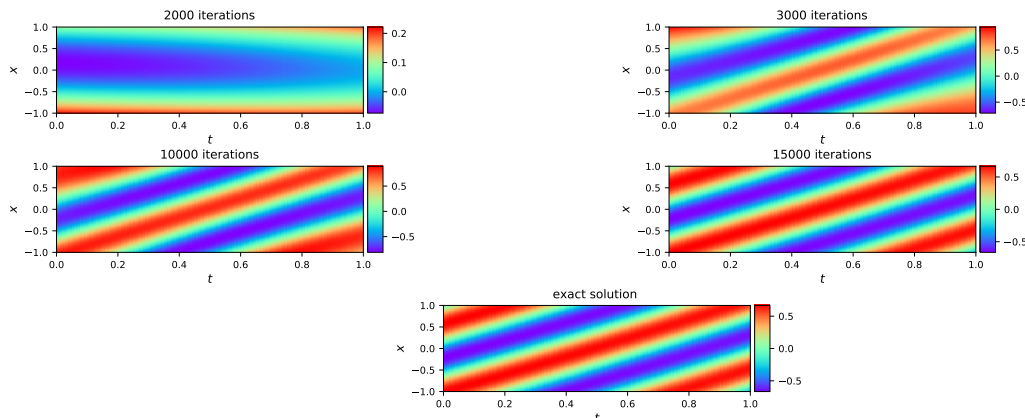


**Figure 1:** A comparison between the exact solution  $m_1$  and the calculated solution  $m_{1p}$ , for different number of iterations and  $d = 1$ .

with

$$d(t, \alpha, k, \mu) = \sqrt{\sin^2 \alpha + \exp(4k^2\mu t) \cos^2 \alpha}$$

and

$$\phi(x, t, \alpha, k, \mu) = \frac{1}{\mu} \log \left( \frac{d(t, \alpha, k, \mu) + \exp(2k^2\mu t) \cos \alpha}{1 + \cos \alpha} \right).$$

We trained the neural network on 2000 random points; which took approximately 5000 and 25000 iterations for the one-dimensional space and two-dimensional space, respectively. After the training we gave to neural network  $100 \times 100$  for  $d = 1$ , and  $100 \times 100 \times 100$  for  $d = 2$  and after that we compared the outputs  $m_{1p}$ ,  $m_{2p}$  and  $m_{3p}$  with the exact solutions  $m_1$ ,  $m_2$  and  $m_3$ . We observed that they were almost equal, indicating that the neural network has become well trained to find the value of  $m_1$ ,  $m_2$  and  $m_3$  at each point of the domain  $Q$ . The following figures illustrate everything we have said. Figures 1, 2 and 3 propose a comparison between the exact solutions  $m_1$ ,  $m_2$  and  $m_3$  and the calculated solutions  $m_{1p}$ ,  $m_{2p}$  and  $m_{3p}$ , respectively, for different number of iterations and  $d = 1$ . Figure 4 proposes a comparison between the exact solution  $m_1$  and the calculated solution  $m_{1p}$ , for different number of iterations,  $t = 0.5$  and  $d = 1$ . Figures 5 and 6 propose a comparison between the exact solutions  $m_1$  and  $m_2$  and the calculated solutions  $m_{1p}$  and  $m_{2p}$ , respectively, for different number of iterations,  $t = 0.5$  and  $d = 2$ . We use the parameters  $\mu = 0.01$ ,  $\alpha = \pi/3$  and  $k = 4$ . This data-set is then used to train a 5-layer deep neural network with 200 neurons per a hidden layer by minimizing the mean square error loss of using the L-BFGS optimizer.

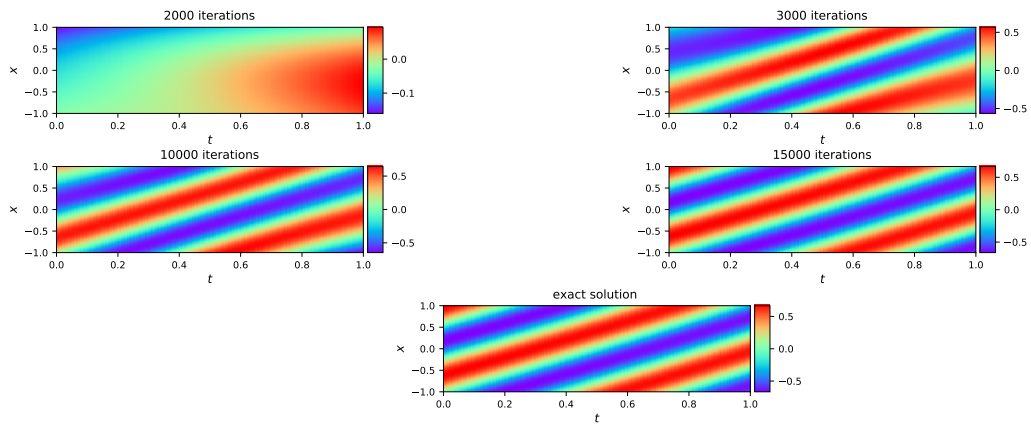


**Figure 2:** A comparison between the exact solution  $m_2$  and the calculated solution  $m_{2p}$ , for different number of iterations and  $d = 1$ .

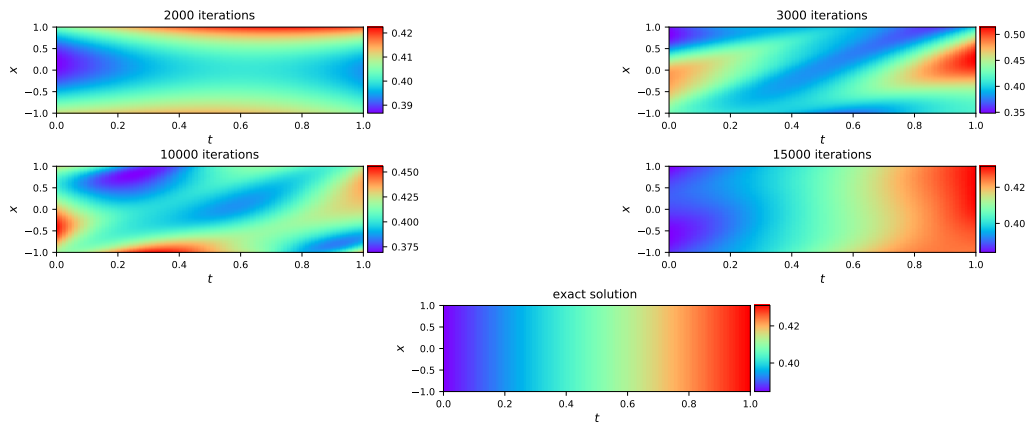


**Figure 3:** A comparison between the exact solution  $m_3$  and the calculated solution  $m_{3p}$ , for different number of iterations and  $d = 1$ .

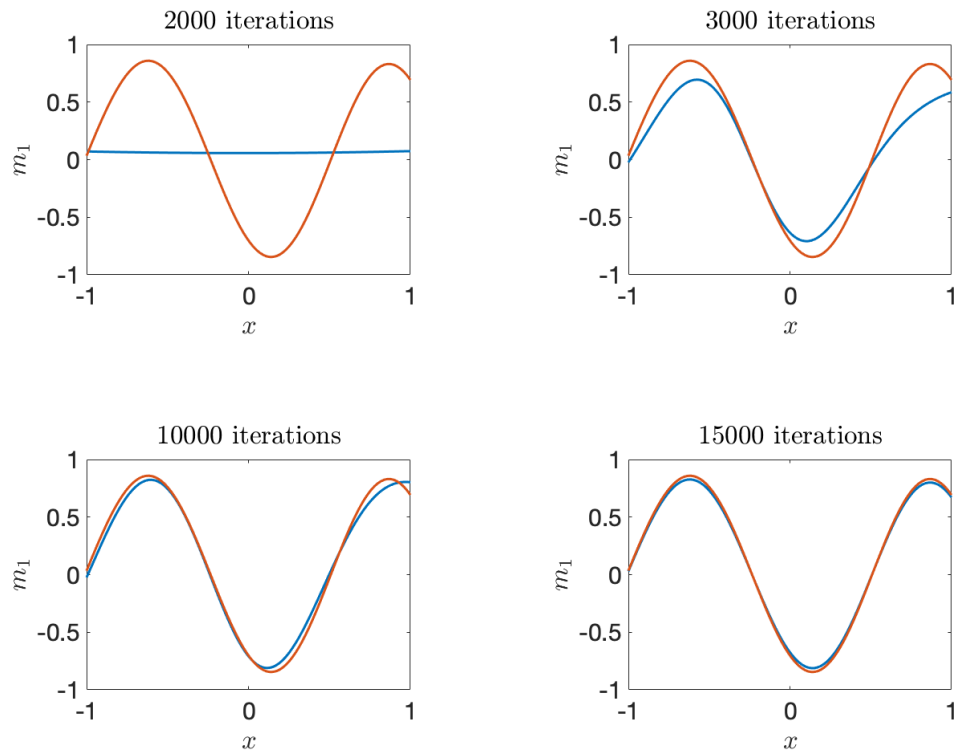


**Figure 4:** A comparison between the exact solution represented by the red color and the approximate solution represented by the blue color for  $t = 0.50$ ,  $d = 1$  and for different iterations.

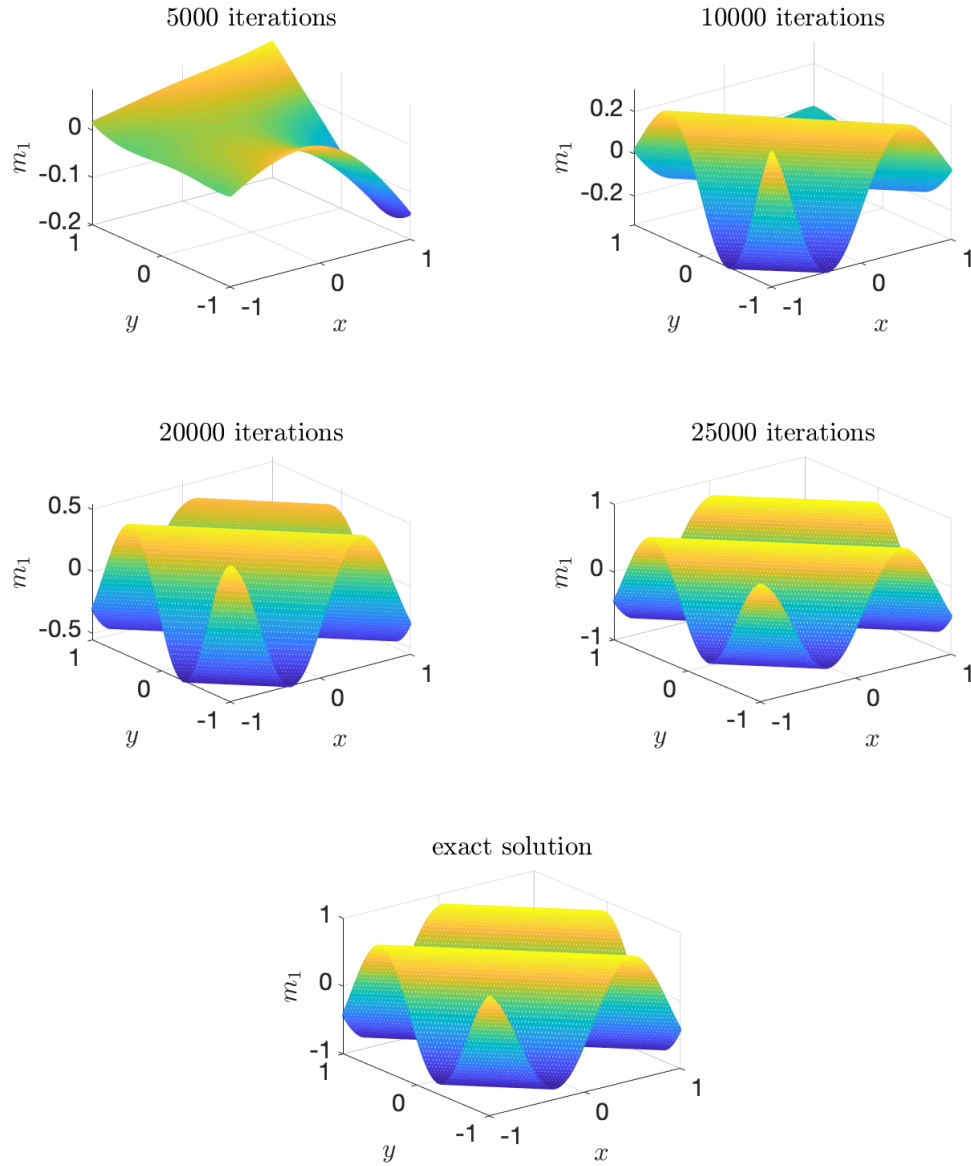


**Figure 5:** A comparison between the exact solution  $m_1$  and the approximate solution  $m_{1p}$  for  $t = 0.50$ ,  $d = 2$  and for different iterations.

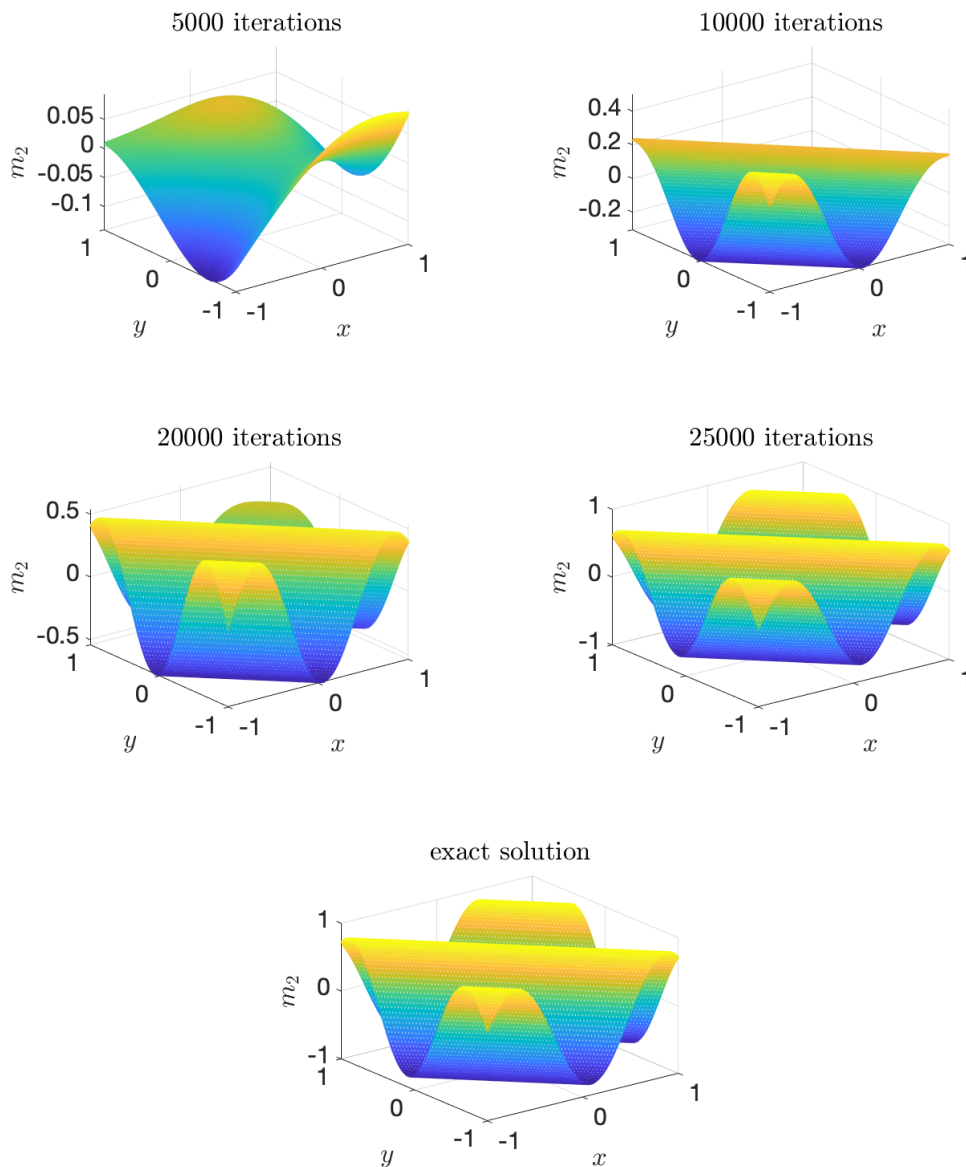
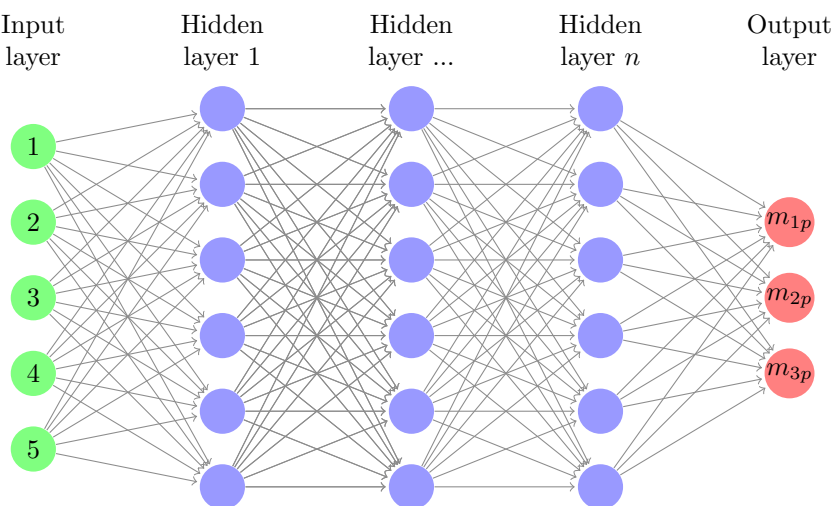


**Figure 6:** A comparison between the exact solution  $m_2$  and the approximate solution  $m_{2p}$  for  $t = 0.50$ ,  $d = 2$  and for different iterations.

### 3.2 Second case

This situation differs from the first case in the input layer, but it is very similar in terms of the method and steps used in determining the solution of the equation at all points. Here we will consider a neuron network composed by several layers such that the first layer represents the inputs (the random points  $s_n = \{(x_n, t_n), (\delta_n, v_n), w_n\}$  on  $Q$ ,  $\partial Q$  and  $\Omega$ ), it is composed of five neurons, the first for  $x_n$ , the second for  $t_n$ , the

third for  $\delta_n$ , the fourth for  $v_n$  and the last for  $w_n$ , the last layer represents the output solution  $M_p = (m_{1p}, m_{2p}, m_{3p})$  at the random points  $\{(t_n, x_n), \delta_n, v_n, (w_n, 0)\}$  linked by the weights and biases parameters, while the other layers are hidden layers.



The objective function  $Loss$  in this case is given by

$$Loss = MSE_f + MSE_{init} + MSE_{bound} + MSE_{Constraint}$$

with

$$MSE_{init} = MSE_{m_{1init}} + MSE_{m_{2init}} + MSE_{m_{3init}},$$

and

$$MSE_{bound} = MSE_{m_{1bound}} + MSE_{m_{2bound}} + MSE_{m_{3bound}},$$

with

$$MSE_{m_{rinit}} = \frac{1}{N_{init}} \sum_{i=1}^{N_{init}} |m_r(\delta^i, v^i) - m_{rp}(\delta^i, v^i)|^2,$$

$$MSE_{m_{rbound}} = \frac{1}{N_{bound}} \sum_{i=1}^{N_{bound}} |m_r(w^i, 0) - m_{rp}((w^i, 0))|^2,$$

for  $r = 1, 2, 3$ , the numbers  $N_{init}$  and  $N_{bound}$  are, respectively, the numbers of the random points  $(\delta^i, v^i) \in \partial Q$  and  $(w^i, 0) \in \Omega \times \{0\}$  for which we know the solution of the equation (1). In the next step, we will deduce an iterative gradient algorithm designed to minimize  $Loss$ . We apply the following algorithm.

- 
1. Initialize the parameter set {weights,biases}.
  2. Generate random samples from the domain's and time spatial boundaries, *i.e.*,
    - Generate  $(t_n, x_n)$  from  $Q$ .
    - Generate  $(\delta_n, v_n)$  from  $\partial Q$ .
    - Generate  $w_n$  from  $\Omega$ .

3. Calculate the *Loss* functional for the current mini-batch

$$s_n = \{(x_n, t_n), (\delta_n, v_n), w_n\}.$$

4. We choose {weights,biases} randomly such that *Loss* becomes minimal.
  5. Repeat steps (3)-(4) until *Loss* is very small
- 

**Numerical simulation.** At this stage, we solve the equation in the two -dimensional space only, for the numerical test, we apply an initial condition

$$M_0(x, y) = \begin{cases} \sin(\alpha) \cos(k(x + y)), \\ \sin(\alpha) \sin(k(x + y)), \\ \cos(\alpha). \end{cases} \quad (5)$$

We trained the neural network on  $N = 2000$  random points in  $Q$ ,  $N_{init} = 100$  in  $\Omega \times \{0\}$  and  $N_{bound} = 200$  in  $\partial Q$ . We use the parameters  $\mu = 3$ ,  $\alpha = \pi/3$  and  $k = 4$ . This data-set is then used to train a 5-layer deep neural network with 50 neurons per a hidden layer. Figure 7 represent Magnetization component averages  $\langle m_1 \rangle$ ,  $\langle m_2 \rangle$ ,  $\langle m_3 \rangle$ ,  $\langle norm \rangle$  and the *Energy* versus time. Through this figure, we find that the solution obtained realizes all the properties of the equation, the decreasing energy, the conservation of the norm. Thus, we conclude that this method is effective in solving differential equation (1).

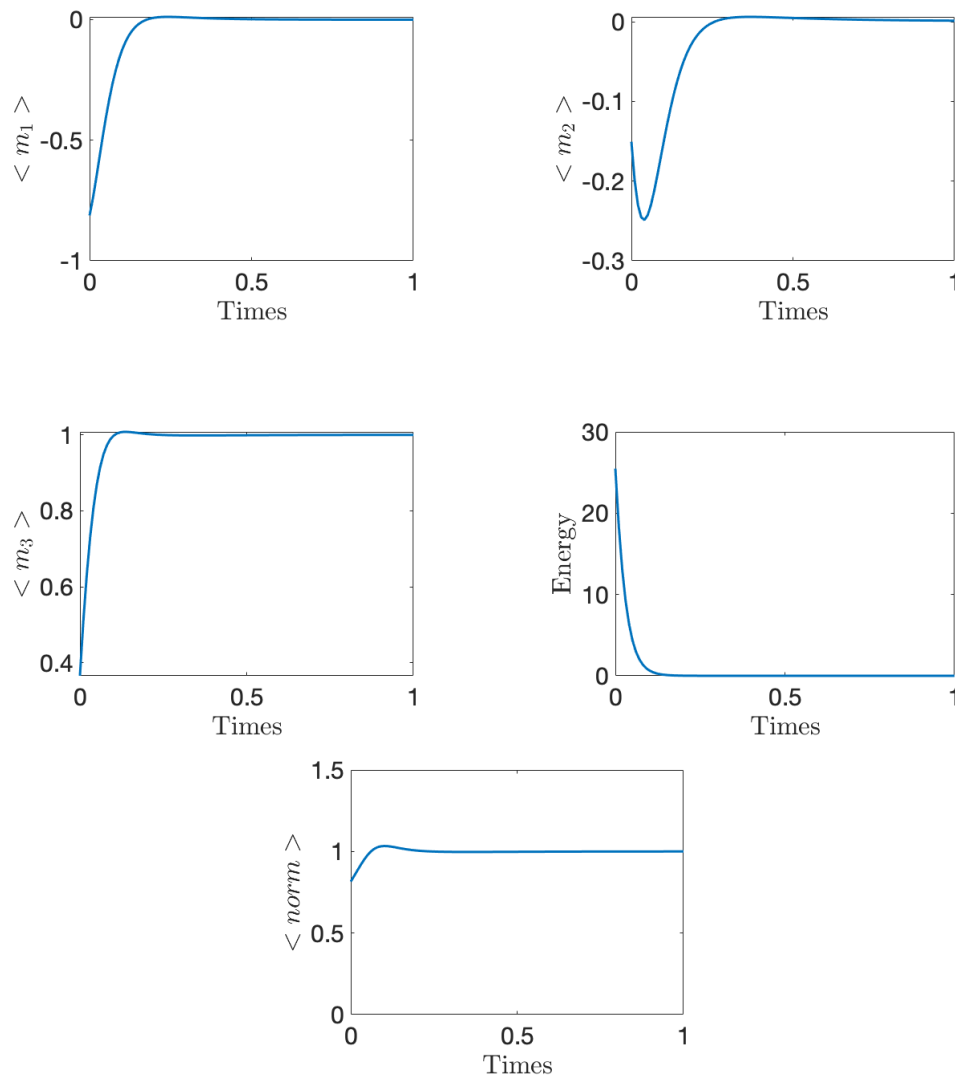


**Figure 7:** Magnetization component averages  $\langle m_1 \rangle$ ,  $\langle m_2 \rangle$ ,  $\langle m_3 \rangle$ ,  $\langle norm \rangle$  and Energy versus time for  $\mu = 3$ ,  $\alpha = \pi/3$  and  $k = 4$ .

#### 4 Concluding Remarks

In this work, we proposed two essentially different approaches, but they are similar in steps for solving differential equation (1). The first method is based on knowledge of equation solutions at some random points of the field  $Q$ . The second depends on the knowledge of the solution at some random points of the fields  $\Omega \times \{0\}$  and  $\partial Q$ . We obtain good results because we can find a solution for the equation using the two methods at each point of  $Q$ . Through these results, we conclude the following. The first method is ineffective because we often do not know the solution at some random points

of  $Q$ , but they are good at identifying some variables in the differential equation, for example, looking for the correct PDEs, see [15], as we think, it will give good results in an inverse source problem. For the PDEs to be well posed, it is necessary to give the initial conditions and the conditions at the edge, which implies that it is possible to find the solutions of PDEs at random points of  $\Omega \times \{0\}$  and  $\partial Q$ , this makes the second method more effective and more realistic in solving differential equations. In the next works, we will apply a deep learning approach to solve the model of magnetization dynamics with inertial effects [8] and compare the results we will get with the results obtained in [17]. Also, we will try to propose a new algorithm for solving PDE (1) in high dimension, by making an analogy between the backward stochastic differential equations and reinforcement learning with the gradient of the solution playing the role of the policy function.

## References

- [1] M. Abadi, A. Agarwal, P. Barham, E. Brevdo, Z. Chen, C. Citro, G.S. Corrado, A. Davis, J. Dean and M. Devin. Tensorflow: Large-scale machine learning on heterogeneous distributed systems. arXiv preprint arXiv: 1603.04467. 2016.
- [2] F. Alouges. A new finite element scheme for Landau-Lifshitz equations. *Discrete Contin. Dyn. Syst. Ser. S* **1** (2) (2008) 187–196.
- [3] F. Alouges, and P. Jaisson. Convergence of a finite element discretization for the Landau-Lifshitz equations in micromagnetism. *Math. Models Methods Appl. Sci.* **16** (2006) 299–316.
- [4] C. Angermueller, T. Pärnamaa, L. Parts and O. Stegle. *Deep learning for computational biology Molecular systems biology* **12** (7) 2016.
- [5] A. Bachouch, C. Huré, N. Langrené and H. Pham. Deep neural networks algorithms for stochastic control problems on finite horizon, Part 2. arXiv preprint arXiv:1812.05916. 2018.
- [6] C. Beck, E. Weinan, and A. Jentzen. Machine learning approximation algorithms for high-dimensional fully nonlinear partial differential equations and second-order backward stochastic differential equations. *Journal of Nonlinear Science* **29** (4) (2019) 1563–1619.
- [7] F. Cabitza, R. Rasoini and G. F. Gensini. Unintended consequences of machine learning in medicine. *Jama* **318** (6) (2017) 517–518.
- [8] M. Ciornei, J. Rubí and J. Wegrowe. Magnetization dynamics in the inertial regime: Nutation predicted at short time scales. *Physical Review B* **83** (2) (2011).
- [9] T. Dockhorn. *A Discussion on Solving Partial Differential Equations using Neural Networks*. arXiv preprint arXiv:1904.07200. 2019.
- [10] D. Jeong and J. Kim. An accurate and robust numerical method for micromagnetics simulations. *Current Applied Physics* **14** (3) (2014) 476–483.
- [11] M. Khumalo and A. Dlamini. The Finite Element Method for Nonlinear Nonstandard Volterra Integral Equations. *Nonlinear Dynamics and Systems Theory* **20** (2) (2020) 191–202.
- [12] L. Landau and E. Lifshitz. On the theory of magnetic permeability in ferromagnetic bodies. *Phys', Zeitsch* **8** (1935) 153–169.
- [13] D. C. Liu and J. Nocedal. On the limited memory BFGS method for large scale optimization. *Mathematical programming* **45** (3)(1989) 503–528.
- [14] R. Maziar. Deep hidden physics models: Deep learning of nonlinear partial differential equations. *The Journal of Machine Learning Research* **19** (1) (2018) 932–955.

- [15] R. Maziar, P. Perdikaris and G. E. Karniadakis. Physics informed deep learning (part ii): Data-driven discovery of nonlinear partial differential equations. arXiv preprint arXiv:1711.10566. 2017.
- [16] M. Mellah, A. Ouannas, A. A. Khennaoui and G. Grassi. Fractional Discrete Neural Networks with Different Dimensions: Coexistence of Complete Synchronization, Antiphase Synchronization and Full State Hybrid Projective Synchronization. *Nonlinear Dynamics and Systems Theory* **21** (4) (2021) 410–419.
- [17] M. Moumni and M. Tilioua. A finite-difference scheme for a model of magnetization dynamics with inertial effects. *Journal of Engineering Mathematics* **100** (1) (2016) 95–106.
- [18] M. Moumni and M. Tilioua. A finite element approximation of a current-induced magnetization dynamics model. *Journal of Mathematical Modeling* **10** (1) (2022) 53–69.
- [19] H. T. Nembach, J. M. Shaw, C., T. Boone and T. J. Silva. Mode-and size-dependent Landau-Lifshitz damping in magnetic nanostructures: evidence for nonlocal damping. *Physical review letters* **110** (11) (2013) 117201.
- [20] A. Pinkus. Approximation theory of the MLP model in neural networks. *Acta numerica* **8** (1999) 143–195.
- [21] W. M. Saslow. Landau–Lifshitz or Gilbert damping? That is the question. *Journal of Applied Physics* **105** (7) (2009).
- [22] J. Sirignano and K. Spiliopoulos. DGM: A deep learning algorithm for solving partial differential equations. *Journal of Computational Physics* **375** (2018) 1339–1364.
- [23] E. Weinan, J. Han and A. Jentzen. Deep learning-based numerical methods for high-dimensional parabolic partial differential equations and backward stochastic differential equations. *Communications in Mathematics and Statistics* **5** (4) (2017) 349–380.



# A New Fractional-Order Three-Dimensional Chaotic Flows with Identical Eigenvalues

S. Rouar\* and O. Zehrour

*Laboratory LSDC, Department of Mathematics and Informatics, University of Oum El Bouaghi, Oum El Bouaghi, Algeria.*

Received: January 2, 2022; Revised: September 16, 2022

**Abstract:** This paper deals with certain new fractional-order three-dimensional chaotic systems. These autonomous systems are the fractional version of dynamical systems introduced recently by Faghani et al. [6]. The feature property of these systems is the presence of fractional order derivatives as well as equality of their eigenvalues. Numerical investigations on the dynamics of these systems have been carried out using a systematic computer search. Some simple fractional chaotic systems with identical eigenvalues were obtained, and their dynamical properties have been analyzed by means of the Lyapunov exponents.

**Keywords:** *fractional order derivative; chaotic system; Lyapunov exponents.*

**Mathematics Subject Classification (2010):** 34C28, 37D45, 37M22, 70K42, 93D05.

## 1 Introduction

Chaos systems have been receiving much attention from scientific community in the study of dynamical systems due to their applications in ecology, engineering and secure communications [3, 20]. Since the publication of Lorenz's seminal paper in 1963, there is no theory that allows us to predict chaotic solutions. The relationship between chaotic systems and their strange attractors is still unknown. Thanks to numerical simulations, we have been studying chaos, it was the essential tool by which many works have been done to study chaos in dynamical systems. Chaotic systems can be categorized as systems with self-excited attractors and systems with hidden attractors. The basin of attraction for the chaotic system with self-excited attractor intersects with an unstable equilibrium, while the chaotic system with hidden attractors has a basin of attraction which does not

---

\* Corresponding author: <mailto:salim.rouar@univ-oeb.dz>

intersect with the neighborhoods of the equilibrium. It is well known that if real parts of all eigenvalues at the equilibrium point are negative, then there exist stable manifolds in a small neighborhood of an equilibrium point, whereas the existence of a positive real part in at least one eigenvalue of them shows the unstable manifolds.

Recently, fractional calculus, which is a mathematical topic whose history goes back more than 300 years, has received a considerable attention. It has been found that many systems can be described by fractional differential equations. For instance, fractional derivatives have been widely used in viscoelasticity, anomalous diffusion phenomena, electromagnetism, digital cryptography and many other phenomena [13, 15]. Some fractional-order dynamical systems have been investigated since the seminal paper of Grigorenko and Grigorenko [7], which demonstrated the existence of chaotic solutions in the fractional-order Lorenz dynamical system, see [2, 4, 5, 8, 9, 11, 18, 19].

In 2011, Sprott presented criteria for proposing new systems with strange attractors. To date, many new chaotic systems which satisfy Sprott's criteria are proposed, among which we cite chaotic systems without any equilibria, with a line, curve, and surface equilibria [1, 10, 12, 14].

Recently, Faghani et al. [6] defined a new category of chaotic systems with identical eigenvalues, proposed three general structures with special conditions and described their chaotic attractors.

In this paper, we propose the fractional version of systems studied by Faghani et al. [6]. These systems have the features of the presence of fractional derivatives and the equality of eigenvalues. The paper is organized as follows. In Section 2, the fractional systems are defined with their conditions. From defined systems, 14 simple chaotic flows are proposed according to the initial conditions, parameters, and fractional orders. The paper is concluded in Section 3.

## 2 Proposed Fractional Systems

First of all, we define the Caputo fractional derivative. The reader can refer to [13], for more details.

**Definition 2.1** The  $\alpha$ th-order Caputo fractional derivative of function  $f(t)$  with respect to  $t$  and the terminal 0 is given by

$${}_0D_t^\alpha f = \frac{d^\alpha f(t)}{dt^\alpha} = \frac{1}{\Gamma(m-\alpha)} \int_0^t \frac{f^{(m)}(\tau)}{(t-\tau)^{\alpha+1-m}} d\tau,$$

where  $m$  is an integer such that  $m-1 \leq \alpha < m$ , and  $\Gamma$  is the well-known Gamma function.

We consider now the fractional version of systems proposed in [6] with the Caputo fractional derivatives as follows:

$$D^{\alpha_1} x = y, \tag{1}$$

$$D^{\alpha_2} y = z,$$

$$D^{\alpha_3} z = a_1x + a_2y + a_3z + a_4x^2 + a_5y^2 + a_6z^2 + a_7xy + a_8xz + a_9yz + a_{10},$$

$$D^{\alpha_1} x = -z, \tag{2}$$

$$D^{\alpha_2} y = b_1x + b_2z,$$

$$D^{\alpha_3} z = a_1x + a_2y + a_3z + a_4x^2 + a_5y^2 + a_6z^2 + a_7xy + a_8xz + a_9yz + a_{10},$$

$$\begin{aligned} D^{\alpha_1}x &= z, \\ D^{\alpha_2}y &= z - y \\ D^{\alpha_3}z &= a_1x + a_2y + a_3z + a_4x^2 + a_5y^2 + a_6z^2 + a_7xy + a_8xz + a_9yz + a_{10}, \end{aligned} \tag{3}$$

where  $D^{\alpha_i}$  denotes the derivatives of order  $\alpha_i$  ( $0 < \alpha_i < 1, i = \overline{1,3}$ ) in the sense of Caputo,  $a_i, i = \overline{1,10}$ , are the real parameters of the systems, and  $(b_1, b_2) = (-1, 1)$  or  $(b_1, b_2) = (1, -1)$ .

Our next step is to make the three eigenvalues equal, we do this by putting some suitable conditions on systems parameters. The equilibrium points of the above systems are calculated as follows:

$$\begin{aligned} D^{\alpha_1}x &= 0, \\ D^{\alpha_2}y &= 0, \\ D^{\alpha_3}z &= 0. \end{aligned}$$

For the system (1) and system (3), the equilibrium point is

$$(x^*, y^*, z^*) = (m, 0, 0), m = \frac{-a_1 \pm \sqrt{a_1^2 - 4a_4 a_{10}}}{2a_4},$$

if  $a_4 \neq 0$  and  $a_1^2 - 4a_4 a_{10} \geq 0$ .

For the system (2), the equilibrium point is

$$(x^*, y^*, z^*) = \left( 0, \frac{-a_2 \pm \sqrt{a_2^2 - 4a_5 a_{10}}}{2a_5}, 0 \right),$$

for  $a_5 \neq 0$  and  $a_2^2 - 4a_5 a_{10} \geq 0$ .

The eigenvalues of the equilibrium points for the systems are determined by setting the determinant of the matrix  $\lambda I - J$  to zero, where  $J$  is the Jacobien matrix defined as

$$J = \begin{pmatrix} \delta_x f_1(q) & \delta_y f_1(q) & \delta_z f_1(q) \\ \delta_x f_2(q) & \delta_y f_2(q) & \delta_z f_2(q) \\ \delta_x f_3(q) & \delta_y f_3(q) & \delta_z f_3(q) \end{pmatrix},$$

where  $D^{\alpha_i}x_i = f_i(x, y, z), 1 \leq i \leq 3, (x_1, x_2, x_3) = (x, y, z)$  and  $q = (x^*, y^*, z^*)$  is the equilibrium point.

We obtain the characteristic equation for each equilibrium point. For example, the characteristic equation for the equilibrium point  $\left( \frac{-a_1 + \sqrt{a_1^2 - 4a_4 a_{10}}}{2a_4}, 0, 0 \right)$  is

$$\lambda^3 - (a_3 + a_8m)\lambda^2 - (a_2 + a_7m)\lambda - (a_1 + 2a_4m) = 0,$$

where

$$m = \frac{-a_1 + \sqrt{a_1^2 - 4a_4 a_{10}}}{2a_4}.$$

Eigenvalues are solutions of the characteristic equation, if they are equal, we have identical eigenvalues. Under the following conditions, the eigenvalues are equal

$$a_2 = \frac{-1}{3} \left( a_3 + a_8 \frac{-a_1 + \sqrt{a_1^2 - 4a_4 a_{10}}}{2a_4} \right)^2 - a_7 \frac{-a_1 + \sqrt{a_1^2 - 4a_4 a_{10}}}{2a_4}, \tag{4}$$

and

$$a_3 = 3 \left( \sqrt{a_1^2 - 4a_4a_{10}} \right)^{\frac{1}{3}} - a_8 \frac{-a_1 + \sqrt{a_1^2 - 4a_4a_{10}}}{2a_4}. \quad (5)$$

In a similar manner, we found conditions for the second equilibrium point of Eq. (1) and for the equilibrium points in the other structures in Eqs. (2) and (3).

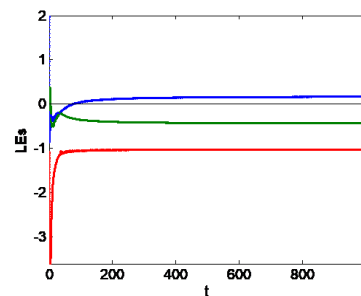
Under these conditions, we search for systems according to the fractional-order, parameters, and initial conditions which show chaotic dynamics.

So, using a systematic computer search, fourteen systems with chaotic dynamics were found by combining the parameters  $a_1$  through  $a_{10}$ , which satisfy the constraints in Eq. (4)-(5) (and similar constraints for systems (2) and (3)) on the fractional-orders and initial conditions. The found simple chaotic systems are listed in Table 1 as  $FE_1 - FE_{14}$ . The equilibriums of all these systems are at the origin. The systems  $FE_1 - FE_9$  have three zero eigenvalues, then the stability of the equilibrium point is not determined, while the systems  $FE_{10} - FE_{14}$  have positive identical eigenvalues, thus the equilibrium point is unstable. The Lyapunov exponents of the systems are calculated by Wolf's method [17]. The chaotic solutions are determined by the positivity of at least one Lyapunov exponent, which is the case in all systems  $FE_1 - FE_{14}$ . Also, the Lyapunov exponents with respect to time of some proposed systems are presented in Fig.1. Attractors projected onto the  $xy$ -plane for all proposed systems are shown in Fig. 2.

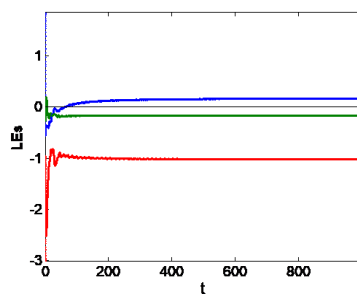
Case	Equations	F.O ( $\alpha$ )	Parameters	Equilibrium	Eigenvalues	LEs	$(x_0, y_0, z_0)$
$FE_1$	$D^{\alpha_1}x = y$	0.99	$a = 0.78$	0	0	0.0103	-48.73
	$D^{\alpha_1}y = z$			0	0	0.0007	-30.86
	$D^{\alpha_1}z = x^2 - y^2 + axz$			0	0	-16.6512	63.52
$FE_2$	$D^{\alpha_1}x = y$	0.98	$a = 0.78$	0	0	0.0085	-48.73
	$D^{\alpha_1}y = x - z$			0	0	-0.0011	-30.86
	$D^{\alpha_1}z = -x^2 + ay^2 + byz$			0	0	-16.9313	63.52
$FE_3$	$D^{\alpha_1}x = -z$	0.95	$a = 6$	0	0	0.0207	-2.64
	$D^{\alpha_1}y = x - z$		$b = 9$	0	0	-0.0006	0.91
	$D^{\alpha_1}z = x^2 - y^2 + axz$		0	0	-0.8690	-4.14	
$FE_4$	$D^{\alpha_1}x = -z$	0.9	$a = 6$	0	0	0.0212	-2.64
	$D^{\alpha_1}y = x - z$		$b = 9$	0	0	-0.0003	0.91
	$D^{\alpha_1}z = x^2 - y^2 + axz$		0	0	-1.0683	-4.14	
$FE_5$	$D^{\alpha_1}x = z$	0.9	$a = 0.3$	0	0	0.1450	-39.56
	$D^{\alpha_1}y = z - y$		$b = -1.5$	0	0	0.0002	-2.85
	$D^{\alpha_1}z = -y + z + ax^2 + bxy + cxz$		$c = 0.6$	0	0	-37.5602	-41.22
$FE_6$	$D^{\alpha_1}x = z$	0.8	$a = 0.3$	0	0	0.1914	-39.56
	$D^{\alpha_1}y = z - y$		$b = -1.5$	0	0	-0.0008	-2.85
	$D^{\alpha_1}z = -y + z + ax^2 + bxy + cxz$		$c = 0.6$	0	0	-44.2027	-41.22

$FE_7$	$D^{\alpha_1}x = z$	0.9	$a = -0.4364$	0	0	0.1812	-3.87
	$D^{\alpha_1}y = z - y$		$b = 2$	0	0	0.0010	-0.7
	$D^{\alpha_1}z = -y + z + ax^2 + bxy + cxz$		$c = -0.7229$	0	0	-36.7658	2.31
$FE_8$	$D^{\alpha_1}x = z$	0.85	$a = -0.4364$	0	0	0.1743	-3.87
	$D^{\alpha_1}y = z - y$		$b = 2$	0	0	0.0009	-0.7
	$D^{\alpha_1}z = -y + z + ax^2 + bxy + cxz$		$c = -0.7229$	0	0	-41.3095	2.31
$FE_9$	$D^{\alpha_1}x = -z$	0.99	$a = 0.128$	0	0.2	0.0323	-21.36
	$D^{\alpha_1}y = -x + z$		$b = 0.008$	0	0.2	0.0001	-18.43
	$D^{\alpha_1}z = ax + by + cz$		$c = 0.6$	0	0.2	-1.7123	-11.03
	$+dx^2 + ey^2 + fzy$		$d = -0.16$ $e = 0.01$ $f = 0.1$				
$FE_{10}$	$D^{\alpha_1}x = -z$	0.88	$a = 0.128$	0	0.2	0.0538	-21.36
	$D^{\alpha_1}y = -x + z$		$b = 0.008$	0	0.2	0.0002	-18.43
	$D^{\alpha_1}z = ax + by + cz$		$c = 0.6$	0	0.2	-2.5653	-11.03
	$+dx^2 + ey^2 + fzy$		$d = -0.16$ $e = 0.01$ $f = 0.1$				
$FE_{11}$	$D^{\alpha_1}x = -z$	0.99	$a = 0.544$	0	0.4	0.1754	-21.36
	$D^{\alpha_1}y = -x + z$		$b = 0.64$	0	0.4	-0.1676	-18.43
	$D^{\alpha_1}z = ax + by + cz$		$c = 1.2$	0	0.4	-1.0270	-11.03
	$+dx^2 + ey^2 + fzy$		$d = -0.16$ $e = 0.01$ $f = 0.1$				
$FE_{12}$	$D^{\alpha_1}x = -z$	0.89	$a = 0.544$	0	0.4	0.2714	-21.36
	$D^{\alpha_1}y = -x + z$		$b = 0.64$	0	0.4	-0.2575	-18.43
	$D^{\alpha_1}z = ax + by + cz$		$c = 1.2$	0	0.4	-1.5700	-11.03
	$+dx^2 + ey^2 + fzy$		$d = -0.16$ $e = 0.01$ $f = 0.1$				
$FE_{13}$	$D^{\alpha_1}x = -z$	0.97	$a = 0.875$	0	0.5	0.17.86	-21.36
	$D^{\alpha_1}y = -x + z$		$b = 0.125$	0	0.5	-0.4383	-18.43
	$D^{\alpha_1}z = ax + by + cz$		$c = 1.5$	0	0.5	-1.0196	-11.03
	$+dx^2 + ey^2 + fzy$		$d = -0.16$ $e = 0.01$ $f = 0.1$				
$FE_{14}$	$D^{\alpha_1}x = -z$	0.99	$a = 0.875$	0	0.5	0.1636	-21.36
	$D^{\alpha_1}y = -x + z$		$b = 0.125$	0	0.5	-0.4013	-18.43
	$D^{\alpha_1}z = ax + by + cz$		$c = 1.5$	0	0.5	-0.9368	-11.03
	$+dx^2 + ey^2 + fzy$		$d = -0.16$ $e = 0.01$ $f = 0.1$				

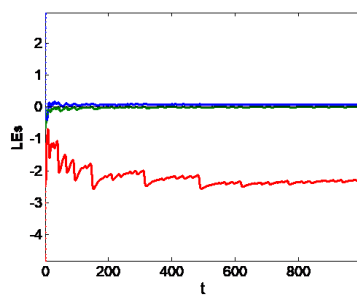
**Table 1:** Fourteen fractional-order three-dimensional chaotic systems with identical eigenvalues.



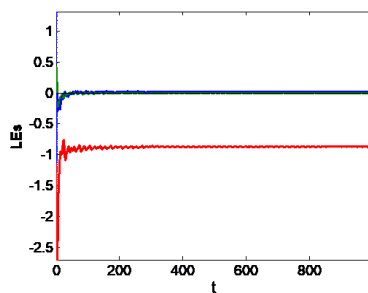
FE13



FE11



FE10



FE3

Figure 1: Lyapunov Exponents of some systems in Table 1 with respect to time.

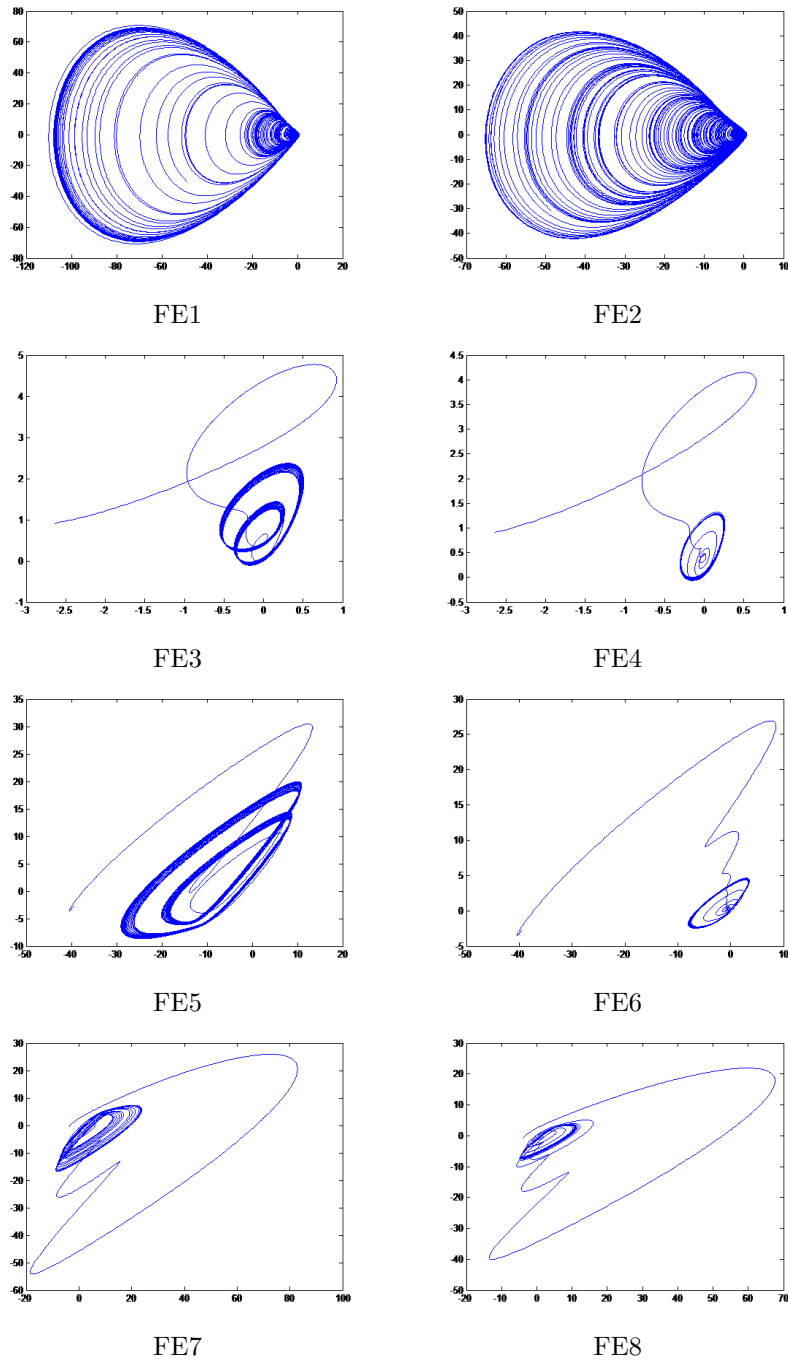


**Figure 2:** Attractors for 14 fractional-order systems in the xy-plane with initial conditions given in Table 1.

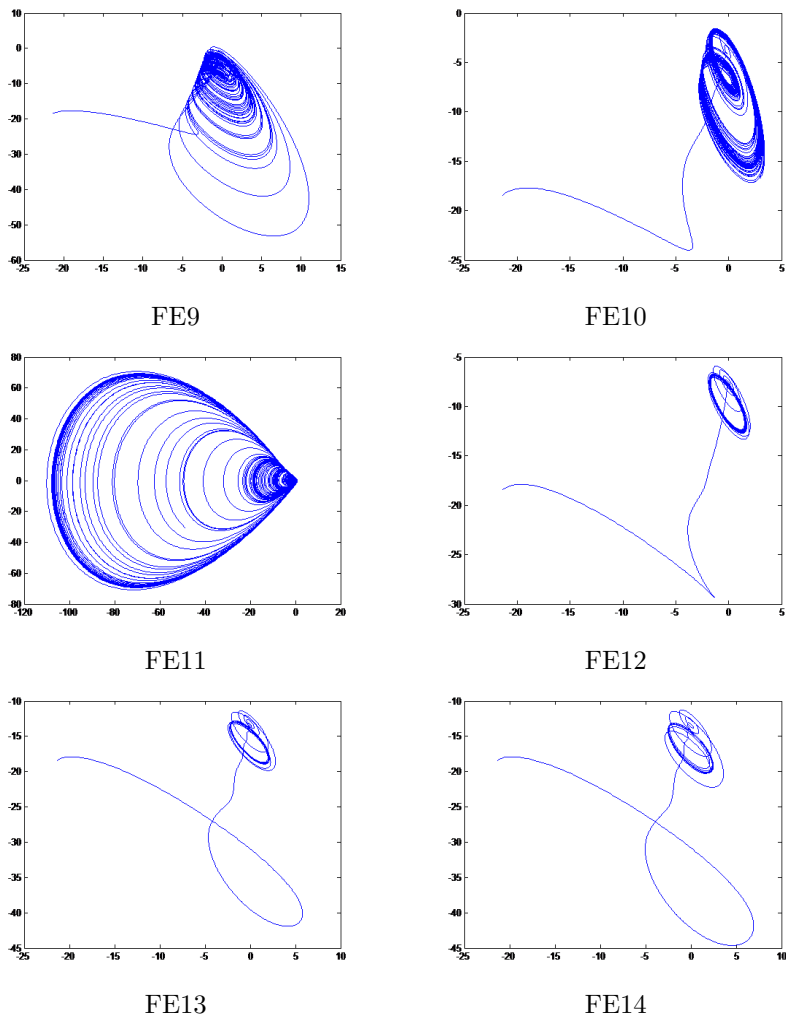


**Figure 3:** Attractors for 14 fractional-order systems in the  $xy$ -plane with initial conditions given in Table 1 (continued).

### 3 Conclusion

This paper introduces new fractional-order three-dimensional chaotic systems which have identical eigenvalues as a particular property. Using an exhaustive computer search, we proposed 14 fractional-order systems which show chaotic dynamics, where the origin was the equilibrium of these systems. Eight of the proposed systems have zero identical eigenvalues, while six of the other systems have three positive and equal eigenvalues. For all fractional-order chaotic systems proposed, the attractors were projected onto the  $xy$ -plane, and the Lyapunov exponents were calculated.

**References**

- [1] K. Barati, S. Jafari, J.C. Sprott and V.-T. Pham. Simple chaotic flows with a curve of equilibria. *Int. J. Bifurc. Chaos* **26** 1630034 (2016) 1–6.
- [2] R.R. Barkat and T. Menacer. Dynamical analysis, stabilization and discretization of a chaotic financial model with fractional order. *Nonlinear Dynamics and Systems Theory* **20** (3) (2020) 253–266.
- [3] C. Cao, K. Sun and W. Liu. A novel bit-level image encryption algorithm based on 2d-licm hyperchaotic map. *Sign. Proc.* **143** (2018) 122–133.
- [4] W.C. Chen. Nonlinear dynamics and chaos in a fractional order financial system. *Chaos Solitons Fractals* (2006) 1305–1314.
- [5] A. Diar and O. Zehrou. The new fractional order hyperchaotic system derived from a Kind of Hyper-Chaotic Systems. *Nonlinear Studies* **25** (2018) 359–365.
- [6] Z. Faghani, F. Nazarimehr, S. Jafari and J. C. Sprott. A new category of three-dimensional chaotic flows with identical eigenvalues. *Int. J. Bifurc. Chaos* **30** 2050026 (2020) 1–9.
- [7] I. Grigorenko and E. Grigorenko. Chaotic dynamics of the fractional Lorenz system. *Phys. Rev. Lett.* **91** 034101 (2003) 1–4.
- [8] D. Hamri and F. Hannachi. A New fractional-order 3D chaotic system analysis and synchronization. *Nonlinear Dynamics and Systems Theory* **21** (4) (2021) 381–392.
- [9] T. Houmor, H. Zerimeche and A. Berkane. Dynamical behaviors of fractional-order Selkov model and its discretization. *Nonlinear Dynamics and Systems Theory* **21** (3) (2021) 246–261.
- [10] S. Jafari, J.C. Sprott and M. Molaie. A simple chaotic flow with a plane of equilibria. *Int. J. Bifurc. Chaos* **26** 1650098 (2016) 1–6.
- [11] A.Ouannas, O. Zehrou and Z. Laadjal. Nonlinear methods to control synchronization between fractional-order and integer-order chaotic systems. *Nonlinear Studies* **25** (2018) 91–106.
- [12] V.T. Pham, S. Jafari, C. Volos and L. Fortuna. Simulation and experimental implementation of a line–equilibrium system without linear term. *Chaos Solitons Fractals* **120** (2019) 213–221.
- [13] I. Podlubny. *Fractional Differential Equations*. Academic Press, San Diego, 1999.
- [14] S. Ren, S. Panahi, K. Rajagopal, A. Akgul, V.-T. Pham and S. Jafari. A new chaotic flow with hidden attractor: The first hyperjerk system with no equilibrium. *Z. Naturforsch. A.* **73** (2018) 239–249.
- [15] S.G. Samko, A.A. Kilbas and O.I. Marichev. *Fractional Integrals and Derivatives: Theory and Applications*. Gordon and Breach, Yverdon, 1993.
- [16] J.C. Sprott. A proposed standard for the publication of new chaotic systems. *Int. J. Bifurc. Chaos* **21** (2011) 2391–2394.

- [17] A.Wolf, J. B. Swift and H. L. Swinney & J. A.Vastano. Determining Lyapunov exponents from a time series. *Physica D* **16** (1985) 285–317.
- [18] O.Zehrou, A.Sihem and A. Diar. A new fractional order modified hyperchaotic Pan system. *Journal | MESA* **9** (2018) 339–346.
- [19] O.Zehrou, D .Nadjette and Z Sihem. Dynamics of fractional-order chaotic and hyper-chaotic systems. *Nonlinear Studies* **26** (2019) 98–103.
- [20] C. Zhu & K. Sun. Cryptanalyzing and improving a novel color image encryption algorithm using RT-enhanced chaotic tent maps. *IEEE Access* **6** (2018) 18759–18770.



# Estimation of Closed Hotels and Restaurants in Jakarta as Impact of Corona Virus Disease (Covid-19) Spread Using Backpropagation Neural Network

F. A. Susanto<sup>1</sup>, M. Y. Anshori<sup>2</sup>, D. Rahmalia<sup>3</sup>, K. Oktafianto<sup>4</sup>,  
D. Adzkiya<sup>5</sup>, P. Katias<sup>2</sup> and T. Herlambang<sup>1\*</sup>

<sup>1</sup> *Department of Information Systems, University of Nahdlatul Ulama Surabaya, Indonesia.*

<sup>2</sup> *Department of Management, University of Nahdlatul Ulama Surabaya, Indonesia.*

<sup>3</sup> *Department of Mathematics, University of Islam Darul Ulum Lamongan, Indonesia.*

<sup>4</sup> *Department of Mathematics, University of PGRI Ronggolawe, Tuban, Indonesia.*

<sup>5</sup> *Department of Mathematics, Sepuluh Nopember Institute of Technology, Surabaya, Indonesia.*

Received: October 11, 2021; Revised: September 10, 2022

**Abstract:** Corona Virus Disease (Covid-19) has become the focus of world attention because it attacked many people in the world and many people died. The effect of Covid-19 is not only on the health of people, it is negatively affecting all aspects of life including the social area, economy, sport, and tourism. Hotels and restaurants that are an important part of the tourism industry have got a big negative impact from Covid-19. Since this disease has spreaded in many countries including Indonesia, the Indonesian government adopted regulations to close the hotels and restaurants to prevent the spread of Covid-19. This research comes from the need to find out the estimated number of hotels and restaurants to be closed due to Covid-19. The estimation method will involve the Backpropagation Neural Network. The backpropagation Neural Network can make estimation of the number of closed hotels and restaurants approaching the target. Simulations are applied by splitting the dataset into training data (80%) and testing data (20%). From Backpropagation Neural Network simulations, the Backpropagation Neural Network can make estimation of the number of closed hotels and restaurants in training data with optimal RMSE being 9.2422 and testing data with optimal RMSE being 8.9419.

**Keywords:** *backpropagation; neural network; estimation; Covid-19.*

**Mathematics Subject Classification (2010):** 68T07, 92B20.

---

\* Corresponding author: <mailto:teguh@unusa.ac.id>

## 1 Introduction

In early 2020, Corona Virus Disease (Covid-19) has become the focus of world attention because it attacked many people in the world and many people died. This disease was firstly found in China and then it spreaded worldwide, including Indonesia. Covid-19 is the disease caused by the Corona virus resembling SARS so that it is named SARS-CoV2. The symptoms of this disease are fever, tiredness, dry cough, sore throat, difficulty in breathing or shortness of breath.

Because this disease has spreaded in many countries including Indonesia, the Indonesia governments adopted regulations to close the hotels and restaurants to prevent the spread of Covid-19. The tourism industry is the industry that has multiplier effect in a country or region. This industry is strongly affected by Covid-19 and it will need a long time to recover. Hotels are one of the biggest players in the tourism industry. Many new hotels are built in tourism cities and metropolitan cities such as Jakarta and Surabaya [1,2]. Jakarta is the city in Indonesia where the first victim came and the city with the most Covid-19 positive victims. Because of that, the estimation of the number of closed hotels and restaurants in Jakarta is important to be done. In this research, the estimation method will involve the Backpropagation Neural Network [3].

A neural network (NN) was introduced by McCulloch and Pitts in 1943. The NN work resembles that of the human neuron system. The type of a Neural Network used in the estimation process is Backpropagation. Backpropagation consists of forward propagation, backward propagation, and updating weight matrices. In forward propagation, some computations using an activation function start from the input, hidden layer, and output, respectively. In backward propagation, error factor computations are applied from the output, hidden layer, and input, respectively. After that, we update weight matrices [4,5].

In the previous research, forecasting methods for estimation have been applied by exponential smooting [1], Kalman Filter on mobile robot trajectory [6], Kalman Filter Estimation [7], Autonomous Underwater Vehicle Optimization [8–10] steam temperature and water level estimation [11], stock price estimation [12,13], crude oil and profitability estimation [14–16], Blood Stock Estimation [17,18], arm robot motion estimation [19], and fuzzy logic by Adaptive Neuro Fuzzy Inference System [20]. Backpropagation has been applied in weather prediction [2,21] with various types of data [22]. This algorithm is applied in training data and testing data in a certain proportion. In this research, the Backpropagation Neural Network will be used for estimating the number of closed hotels and restaurants in Jakarta. In making estimation of the number of closed hotels and restaurants using the Backpropagation Neural Network, some inputs are required such as the number of positive victims in Jakarta, the number of recovered victims in Jakarta, the number of dead victims in Jakarta, the number of positive victims in Indonesia, the number of recovered victims in Indonesia, the number of dead victims in Indonesia, the number of positive victims in the world, the number of recovered victims in the world, and the number of dead victims in the world.

From Backpropagation Neural Network simulations, the Backpropagation Neural Network can make estimation of the number of closed hotels and restaurants in training data with optimal RMSE being 9.2422 and testing data with optimal RMSE being 8.9419. We also repeat these simulations five times.

**2 Literature Review**

A Neural Network was introduced by Mc Culloch and Pitts in 1943. The behavior of a Neural Network is as follows [23]: (a) the signal is traveling between neurons through a connector; (b) connectors have weight which will either increase or decrease the signal; (c) To determine the output, a neuron uses an activation function applied in the sum of inputs received.

In a Neural Network, an activation function is used for determining the output of a neuron. The argument of an activation function is a linear combination of the input and weight as in equation (1):

$$net = \sum_i x_i w_i, \quad f(net) = f\left(\sum_i x_i w_i\right). \tag{1}$$

The activation function used is continuous, differentiable, and not descending function [4]. In this research, the activation function applied is binary sigmoid with the range (0-1) as in equation (2):

$$f(net) = \frac{1}{1 + e^{-net}},$$

$$f'(net) = f(net)(1 - f(net)). \tag{2}$$

Backpropagation is a type of the Neural Network used in the estimation process. Backpropagation consists of some inputs  $x_1, x_2, \dots, x_n$ , some hidden layer  $z_1, z_2, \dots, z_p$ , and some output  $y_1, y_2, \dots, y_m$ . In the input and hidden layer, there is bias with value 1. Weight  $v_{ij}$  connects input  $x_i$  to hidden layer  $z_j$ . Weight  $w_{jk}$  connects hidden layer  $z_j$  to output  $y_k$ . In Backpropagation, there are three phases of calculation such as forward propagation, backward propagation, and update weight matrices [4]. A backpropagation model can be seen in Figure 1.

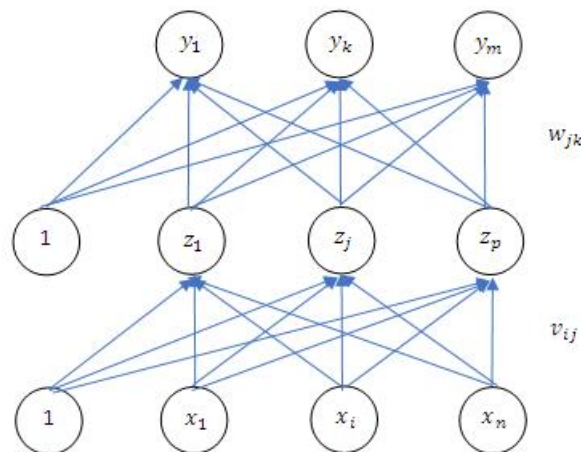


**Figure 1:** Backpropagation Neural Network Model.

The algorithm of a Backpropagation Neural Network is as follows:

Initialization weight matrices  $V$  and  $W$  with random number between  $-0.5$  to  $0.5$ .

$e = 1$

*while*( $e \leq \text{max\_epoch}$  &&  $MSE \geq \text{min\_MSE}$ )

*for*( $d = 1 : \text{datasize}$ )

1. Each input receives a signal which continues to each hidden layer through forward propagation in equation (3) until equation (6) and backward propagation in equation (7) until equation (11).

Forward Propagation

2. All outputs  $z_j, j = 1, 2, \dots, p$  are calculated in the hidden layer in equation (4).

$$z_{net_j} = v_{oj} + \sum_{i=1}^n x_i v_{ij}, \quad (3)$$

$$z_j = f(z_{net_j}) = \frac{1}{1 + e^{-z_{net_j}}}. \quad (4)$$

3. Calculate all outputs  $y_k, k = 1, 2, \dots, m$ , in equation (6).

$$y_{net_k} = w_{ok} + \sum_{j=1}^p z_j w_{jk}, \quad (5)$$

$$y_k = f(y_{net_k}) = \frac{1}{1 + e^{-y_{net_k}}}. \quad (6)$$

Backward Propagation

4. Calculate the factor  $\delta$  output based on the error in each output  $y_k, k = 1, 2, \dots, m$ ,

$$\delta_k = (t_k - y_k) f'(y_{net_k}). \quad (7)$$

5. Calculate the weight update

$$\Delta w_{jk} = \alpha \delta_k z_j, \quad k = 1, 2, \dots, m, \quad j = 0, 1, 2, \dots, p. \quad (8)$$

6. Calculate the factor  $\delta$  hidden layer in equation (10) based on the error in each hidden layer  $z_j, j = 1, 2, \dots, p$ ,

$$\delta_{net_j} = \sum_{k=1}^m \delta_k w_{jk}, \quad (9)$$

$$\delta_j = \delta_{net_j} f'(z_{net_j}). \quad (10)$$

7. Calculate the weight update

$$\Delta v_{ij} = \alpha \delta_j x_i, \quad j = 1, 2, \dots, p, \quad i = 0, 1, 2, \dots, n. \quad (11)$$

Update Weight Matrices

8. Update the new weight matrices

$$w_{jk} = w_{jk} + \Delta w_{jk}, \quad (12)$$

$$v_{ij} = v_{ij} + \Delta v_{ij}. \quad (13)$$

*end*

Compute the root of mean square error (RMSE)

$$RMSE = \sqrt{\frac{1}{datasize} \sum_{d=1}^{datasize} \frac{1}{m} \sum_{k=1}^m (T_{dk} - Y_{dk})^2}, \quad (14)$$

where  $T_{dk}$  is the target value and  $Y_{dk}$  is outputs.

$e = e + 1$

*end*

### 3 Result and Discussion

Datasets are taken from the report of closed hotels and restaurants from March 1, 2020 until April 30, 2020 (61 days), issued by the Indonesian Hotels and Restaurants Association, with the observed area of Jakarta as the first city where Covid-19 was first discovered. These data will be estimated by the Backpropagation Neural Network.

In addition, there are the data of the number of Covid-19 victims (positive, recovered, dead) in Jakarta from March 1, 2020 until April 30, 2020, obtained from the official Covid-19 Jakarta website, the data of the number of Covid-19 victims (positive, recovered, dead) in Indonesia from March 1, 2020 until April 30, 2020, obtained from the Ministry of Health, Republic of Indonesia, and the data of the number of Covid-19 victims (positive, recovered, dead) in world from March 1, 2020 until April 30, 2020, obtained from the Worldometer website. They will be used as inputs in the Backpropagation Neural Network, where the output is the number of closed hotels and restaurants in Jakarta from March 1, 2020 until April 30, 2020, as estimations.

#### 3.1 Data Used

The graph of the number of closed hotels and restaurant from March 1, 2020 until April 30, 2020, in Jakarta can be seen in Figure 2.

For estimating the number of closed hotels and restaurants by the Backpropagation Neural Network, we need some inputs such as the number of positive victims in Jakarta, the number of recovered victims in Jakarta, the number of dead victims in Jakarta, the number of positive victims in Indonesia, the number of recovered victims in Indonesia, the number of dead victims in Indonesia, the number of positive victims in the world, the number of recovered victims in the world, and the number of dead victims in the world.

The graph of the number of Covid-19 victims in Jakarta from March 1, 2020 until April 30, 2020, can be seen in Figure 3. There are three parts of the graph with different colors that are the number of positive victims, the number of recovered victims, and the number of dead victims.

The graph of the number of Covid-19 victims in Indonesia from March 1, 2020 until April 30, 2020, can be seen in Figure 4. There are three parts of the graph with different

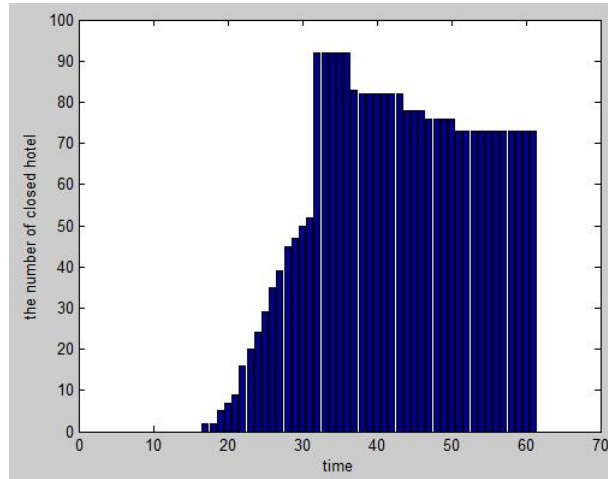


**Figure 2:** The number of closed hotels and restaurants.

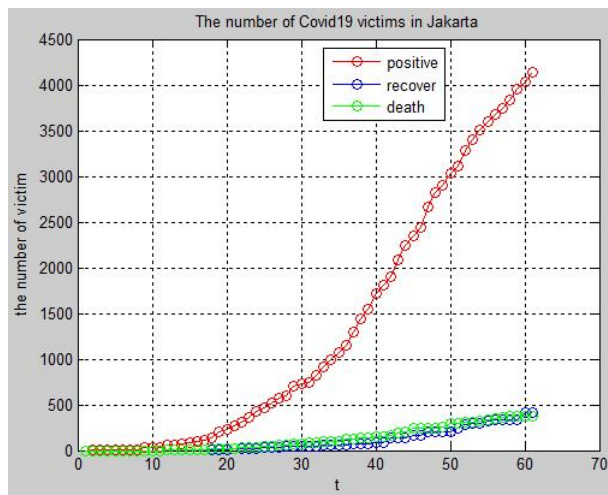


**Figure 3:** The number of Covid-19 victims in Jakarta.

colors that are the number of positive victims, the number of recovered victims, and the number of dead victims.

The graph of the number of Covid-19 victims in the world from March 1, 2020 until April 30, 2020, can be seen in Figure 5. There are three parts of the graph with different colors that are the number of positive victims, the number of recovered victims, and the number of dead victims.

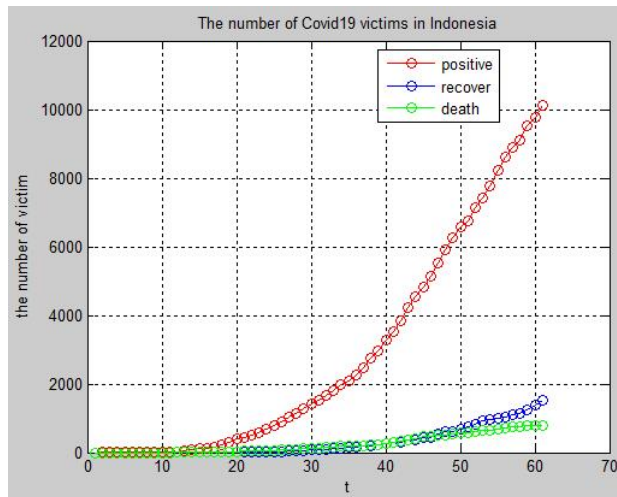


Figure 4: The number of Covid-19 victims in Indonesia.

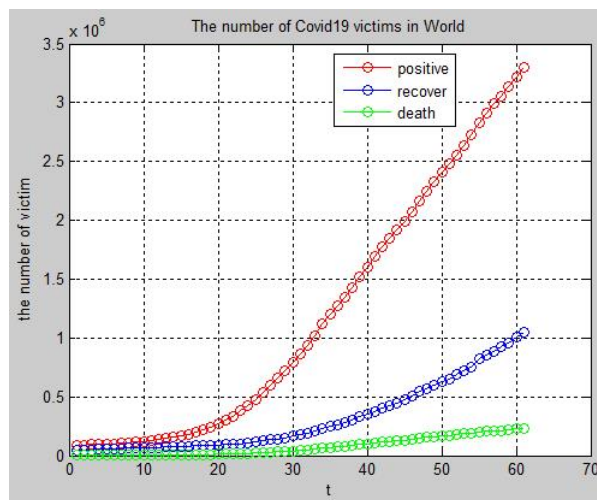
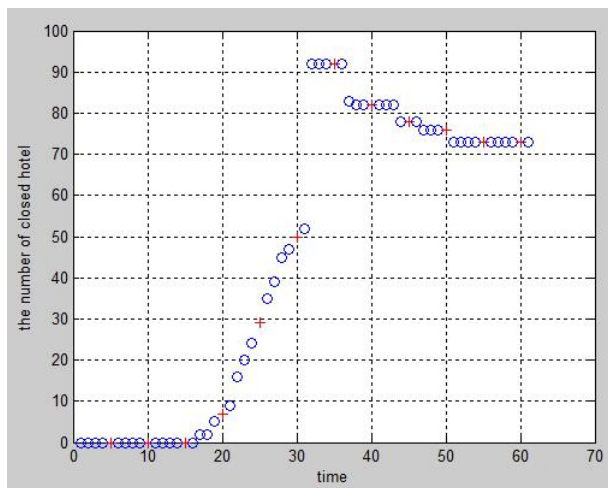


Figure 5: The number of Covid-19 victims in the world.

### 3.2 Estimation Results

Before applying the estimation process, we need to split the data into training data and testing data. The data partition used is as follows: for training data, the data used have the proportion of 80% of all data, while for testing data, the data used have the remaining proportion (20% of all data). Figure 6 shows the data partition, where the red plus marks represent the distribution of testing data, and the blue ones represent training data.

The parameters used in the Backpropagation Neural Network simulation are:



**Figure 6:** Data partition into training data (blue) and testing data (red).

Learning rate : 0.2.

The number of hidden layer : 2.

Maximum epoch : 1000.

The model of backpropagation : 9 (input) – 10 (hidden layer 1) – 10 (hidden layer 2) – 1 (output).

The simulation of the Backpropagation Neural Network can be seen in Figures 7, 8 and 9 below. First, initialize the weight matrices and apply to training data using the Backpropagation Neural Network until the maximum epoch, the convergence process can be seen in Figure 7. It can be seen in the early epoch, the RMSE resulted is quite large. In the optimization, the RMSE is decreased and converged. Figure 8 shows the comparison and error between the target and output. From the training process until 1000 epochs, optimal weight matrices are obtained. Then, the optimal weight matrices are applied to testing data. Figure 9 shows simulation for testing data.

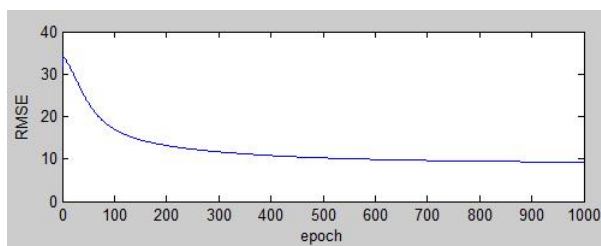


**Figure 7:** Convergence Process of the Backpropagation Neural Network.

From the simulation, we obtain the estimation with the root of mean square error (RMSE) in equation (14) as follows:

Training data : 9.2422.

Testing data : 8.9419.

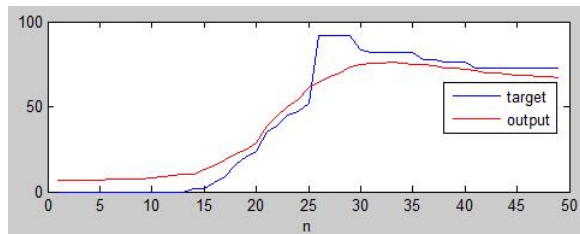


Figure 8: Estimation result for training data.

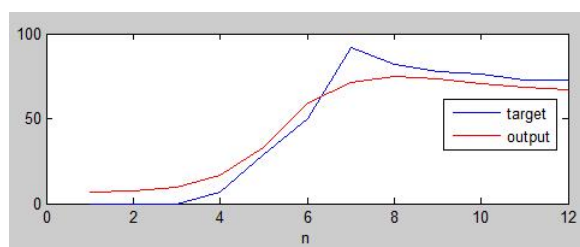


Figure 9: Estimation result for testing data.

We repeat the simulations five times using different initial weights and the results are given in Table 1.

Number	Max epoch	RMSE for training data	RMSE for testing data
1	1000	9.5604	9.3628
2	1000	9.0513	8.7649
3	1000	9.0156	8.8002
4	1000	9.1428	8.9463
5	1000	8.9626	8.6265

Table 1: The root of mean square error (RMSE) in the Backpropagation Neural Network with five times trials.

#### 4 Conclusion

The corona Virus (Covid-19) has been negatively affecting the hotels and restaurants businesses. Hotels and restaurants have become a primary need of the business people, especially in a big city like Jakarta. The closed hotels and restaurants due to Covid-19 are also affecting the tax income of the government as well as the income of the suppliers. In making estimation of the number of closed hotels and restaurants using the Backpropagation Neural Network, some inputs are required, such as the number of positive victims in Jakarta, the number of recovered victims in Jakarta, the number of dead victims in Jakarta, the number of positive victims in Indonesia, the number of recovered victims in Indonesia, the number of dead victims in Indonesia, the number

of positive victims in the world, the number of recovered victims in the world, and the number of dead victims in the world.

The Backpropagation Neural Network can make estimation of the number of closed hotels and restaurants approaching the target. Simulations are applied by splitting the dataset into training data (80%) and testing data (20%). From Backpropagation Neural Network simulations, the Backpropagation Neural Network can make estimation of the number of closed hotels and restaurants in training data with optimal RMSE being 9.2422 and testing data with optimal RMSE being 8.9419.

The developments of this research are making estimation and classification of the results by data mining and machine learning techniques.

### Acknowledgment

This research was supported by LPPM – Nahdlatul Ulama Surabaya of University (UNUSA).

### References

- [1] D. Rahmalia. Estimation of Exponential Smoothing Parameter on Pesticide Characteristic Forecast using Ant Colony Optimization (ACO). *Eksakta: Jurnal Ilmu-ilmu MIPA* **18** (1) (2018) 56–63.
- [2] D. Rahmalia and N. Aini. Pengaruh Korelasi Data pada Peramalan Suhu Udara Menggunakan Backpropagation Neural Network. *Zeta-Math. Journal* **4** (1) (2018) 1–6.
- [3] H. A. Abbas, A. Seghieur, M. Belkheiri and M. Rahmani. Robust Output Feedback Stabilization and Boundedness of Highly Nonlinear Induction Motors Systems Using Single-Hidden-Layer Neural-Networks. *Nonlinear Dynamics and Systems Theory* **19** (3) (2019) 331–347.
- [4] L. Fausett. *Fundamental of Neural Networks*. Prentice Hall, USA, 1994.
- [5] B. Benaid, H. Bouzahir, C. Imzegouan and F. E. Guezar. Stability Analysis for Stochastic Neural Networks with Markovian Switching and Infinite Delay in a Phase Space. *Nonlinear Dynamics and Systems Theory* **19** (3) (2019) 372–385.
- [6] T. Herlambang, R. A. Rasyid, S. Hartatik and D. Rahmalia. Estimasi Posisi Mobile Robot Menggunakan Akar Kuadrat Unscented Kalman Filter (AK-UKF). *Technology Science and Engineering Journal* **1** (2) (2017).
- [7] D. K. Arif, D. Adzkiya and H. N. Fadhilah. Kalman Filter Estimation of Identified Reduced Model Using Balanced Truncation: a Case Study of the Bengawan Solo River. *Nonlinear Dynamics and Systems Theory* **19** (4) (2019) 455–463.
- [8] T. Herlambang, D. Rahmalia, and T. Yulianto. Particle Swarm Optimization (PSO) and Ant Colony Optimization (ACO) for Optimizing PID Parameters on Autonomous Underwater Vehicle (AUV) Control System. In: *The Second International Conference on Combinatorics, Graph Theory and Network Topology, University of Jember-Indonesia, 24-25 Nov 2018. Journal of Physics: Conference Series* 1211 (2019), 012039.
- [9] T. Herlambang, S. Subchan, H. Nurhadi and D. Adzkiya. Motion Control Design of UN-USAITS AUV Using Sliding PID. *Nonlinear Dynamics and Systems Theory* **20** (1) (2020) 51–60.
- [10] T. Herlambang, D. Rahmalia, H. Nurhadi, D. Adzkiya and S. Subchan. Optimization of Linear Quadratic Regulator with Tracking Applied to Autonomous Underwater Vehicle (AUV) Using Cuckoo Search. *Nonlinear Dynamics and Systems Theory* **20** (3) (2021) 282–298.

- [11] T. Herlambang, Z. Mufarrikoh, D. F. Karya, and D. Rahmalia. Estimation of Water Level and Stem Temperature Using Ensemble Kalman Filter Square Root (EnKF-SR). *Journal of Physics: Conference Series*. Jember, Indonesia, 2018.
- [12] D. F. Karya, K. Puspandam, and T. Herlambang. Stock Price Estimation Using Ensemble Kalman Filter Square Root Methods. *The First International Conference on Combinatorics, Graph Theory and Network Topology, University of Jember-Indonesia, 25-26 Nov 2017*. *Journal of Physics: Conf. Series* 1008 (2018), 012026.
- [13] D. F. Karya, P. Katias, T. Herlambang, and D. Rahmalia. Development of Unscented Kalman Filter Algorithm for Stock Price Estimation. *Journal of Physics: Conference Series*. Jember, Indonesia, 2019.
- [14] D. F. Karya, M. Y. Anshori, R. R. Mardhotillah, K. Puspandam, A. Muhith and T. Herlambang. Estimation of Crude Oil Price Using Unscented Kalman Filter. In: *The Third International Conference on Combinatorics, Graph Theory and Network Topology, University of Jember-Indonesia, 26-27 Oct 2019*. *Journal of Physics: Conference Series* 1538 (2020), 012035.
- [15] M. Y. Anshori, T. Herlambang, D. F. Karya, A. Muhith, and R. A. Rasyid. Profitability Estimation of A Company In PT.ABCD Using Extended Kalman Filter. In: *The Third International Conference on Combinatorics, Graph Theory and Network Topology, University of Jember-Indonesia, 26-27 Oct 2019*. *Journal of Physics: Conference Series* 1538 (2020), 012035.
- [16] M. Y. Anshori, D. F. Karya, N. Muslinah, and T. Herlambang. Analysis of Transformational Leadership Style for Employee Performance with Job Satisfaction as Intervening Variable. *International Journal of Advanced Science and Technology*. **29** (9s) (2020) 3967–3973.
- [17] A. Muhith, T. Herlambang, Irhamah and D. Rahmalia. Estimation of Thrombocyte Concentrate (TC) and Whole Blood (WB) using Unscented Kalman Filter. *International Journal of Advanced Science and Technology* **29** (8s) (2020) 25–32.
- [18] A. Muhith, T. Herlambang, M. Y. Anshori, R. R. Mardhotillah and D. Rahmalia. Estimation of Whole Blood (WB) and Anti-Hemophiliate Factor using Extended Kalman Filter in PMI Surabaya. In: *The Third International Conference on Combinatorics, Graph Theory and Network Topology, University of Jember-Indonesia, 26-27 Oct 2019*. *Journal of Physics: Conference Series* 1538 (2020), 012035.
- [19] T. Herlambang, A. Muhith, D. Rahmalia, and H. Nurhadi. Motion Optimization using Modified Kalman Filter for Invers-Kinematics based Multi DOF Arm Robot. *International Journal of Control and Automation* **13** (2s) (2020) 6–71.
- [20] D. Rahmalia and A. Rohmatullah. Pengaruh Korelasi Data pada Peramalan Kelembaban Udara Menggunakan Adaptive Neuro Fuzzy Inference System (ANFIS). *Applied Technology and Computing Science* **2** (1) (2019) 10–24.
- [21] D. Rahmalia and T. Herlambang. Prediksi Cuaca Menggunakan Algoritma Particle Swarm Optimization-Neural Network (PSO-NN). *Prosiding Seminar Nasional Matematika dan Aplikasinya*. Surabaya, Indonesia, (2017).
- [22] D. Rahmalia and M. S. Pradana. Backpropagation Neural Network pada Data yang tak Stasioner (Studi Kasus: Jumlah Penderita Penyakit Ebola). *Jurnal Riset dan Aplikasi Matematika (JRAM)* **3** (1) (2019) 32–42.
- [23] J. Han, M. Kamber and J. Pei. *Data Mining Concepts and Techniques*. Elsevier, USA, 2012.



# Stabilization of Chaotic $h$ -Difference Systems with Fractional Order

Hasna Yousfi<sup>1</sup>, Ahlem Gasri<sup>1</sup> and Adel Ouannas<sup>2\*</sup>

<sup>1</sup> *Laboratory of Mathematics, Informatics and Systems (LAMIS), Department of Mathematics and Computer Science, University of Larbi Tebessi, Tebessa 12002 Algeria.*

<sup>2</sup> *Department of Mathematics and Computer Science, University of Larbi Ben M'hidi, Oum El Bouaghi, Algeria.*

Received: January 26, 2022; Revised: September 1, 2022

**Abstract:** Based on the Lyapunov approach as well as on the properties of the Caputo  $h$ -difference operator, a one-dimensional linear control law is introduced to stabilize the chaotic fractional discrete-time Ushio system. Numerical results are presented throughout the paper to illustrate the findings.

**Keywords:** *discrete fractional calculus; fractional discrete Ushio system; linear stabilization; Lyapunov approach.*

**Mathematics Subject Classification (2010):** 44A55, 37N35, 65P40, 65P20.

## 1 Introduction

Fractional discrete calculus is a very interesting topic in mathematics with several potential applications in many fields [1]. Namely, since fractional discrete operators are non local, they are suitable for constructing models characterized by memory effect [2]. This is the reason why fractional-order difference systems, when describing engineering phenomena over large periods of time, perform better with respect to integer-order discrete-time systems [3]. Recently, attention has been focused on the presence of chaotic phenomena in fractional-order systems, described by difference equations [4, 5].

One of the important aspects in the study of chaotic systems is the development of control strategies to achieve stabilization. The aim of stabilizing chaotic systems is to derive one-dimensional control law such that both of the map trajectories are controlled to zero asymptotically. Recently, the topic of stabilization of fractional discrete chaotic systems started to attract increasing attention [6–10].

This study presents a novel contribution to the topic of stabilization of chaos in Caputo  $h$ -difference chaotic systems. After investigating the existence of chaotic behaviors in the fractional Ushio system, a linear scheme is introduced to control the fractional Ushio system.

---

\* Corresponding author: <mailto:adel.ouannas@yahoo.com>

## 2 The Fractional Chaotic Ushio System

Referring to the discrete-time Ushio system, it was introduced in [11]. Herein, by exploiting the Caputo  $h$ -difference operator, the following fractional Ushio system is proposed:

$$\begin{cases} {}^C_h\Delta_a^\nu x(t) = (d - 1)x(t + h\nu) - x^3(t + h\nu) + y(t + h\nu), \\ {}^C_h\Delta_a^\nu y(t) = 0.5x(t + h\nu) - y(t + h\nu), \end{cases} \quad (1)$$

where  ${}^C_h\Delta_a^\nu$  denotes the Caputo  $h$ -difference operator,  $0 \leq \nu \leq 1$ ,  $t \in (h\mathbb{N})_{a+(1-\nu)h}$ ,  $(h\mathbb{N})_{a+(1-\nu)h} = \{a + (1 - \nu)h, a + (2 - \nu)h, \dots\}$ ,  $a$  is the starting point and  $d$  is a system parameter.

The Caputo  $h$ -difference operator  ${}^C_h\Delta_a^\nu X(t)$  of a function  $X(t)$  [12] is defined as

$${}^C_h\Delta_a^\nu X(t) = \Delta_a^{-(n-\nu)}\Delta^n X(t), \quad t \in (h\mathbb{N})_{a+(n-\nu)h}, \quad (2)$$

where  $\Delta X(t) = \frac{X(t+h)-X(t)}{h}$ ,  $n = \lceil \nu \rceil + 1$ , and the  $\nu$ -th order  $h$ -sum [13] is given by

$${}_h\Delta_a^{-\nu} X(t) = \frac{h}{\Gamma(\nu)} \sum_{s=\frac{a}{h}}^{\frac{t}{h}-\nu} (t - \sigma(sh))^{\nu-1} x(sh), \sigma(sh) = (s + 1)h, a \in \mathbb{R}, t \in (h\mathbb{N})_{a+\nu h}, \quad (3)$$

where the  $h$ -falling factorial function is defined as

$$t_h^{(\nu)} = h^\nu \frac{\Gamma\left(\frac{t}{h} + 1\right)}{\Gamma\left(\frac{t}{h} + 1 - \nu\right)}, \quad t, \nu \in \mathbb{R}. \quad (4)$$

Now, according to [14], the equivalent implicit discrete formula can be written in the form

$$\begin{cases} x(n + 1) = x(0) + \frac{h^\nu}{\Gamma(\nu)} \sum_{j=0}^n \frac{\Gamma(n-j+\nu)}{\Gamma(n-j+1)} ((d - 1)x(j + 1) - x^3(j + 1) + y(j + 1)), \\ y(n + 1) = y(0) + \frac{h^\nu}{\Gamma(\nu)} \sum_{j=0}^n \frac{\Gamma(n-j+\nu)}{\Gamma(n-j+1)} (0.5x(j + 1) - y(j + 1)), \end{cases} \quad (5)$$

where  $x(0), y(0)$  are the initial states. Here, the implicit system given in (5) is employed to explore the chaotic behavior of the Ushio system in its fractional order. When  $(x(0), y(0)) = (0.1, -0.3)$  and  $d = 1.9$ , then the fractional-order Ushio system will show chaotic behaviour. Figure 1, however, shows the chaotic attractor obtained by simulating the system (5) with the predictor-corrector method, along with the Largest Lyapunov Exponents (LLEs) and the bifurcation diagram that are obtained.

## 3 Chaos Stabilization Scheme

This section intends to prove a novel result established for stabilizing the dynamics of the fractional Ushio system at zero through establishing a linear control law. When we refer to stabilization, what we are talking about is adding a new time varying parameter  $\mathbf{C}(t)$  to one of the system's states and finding a closed form adaptive formula for these parameters to force the system states to zero in sufficient time. Before stating the proposed control law and establishing its stability, it is important to state the following theorem, which is essential for our proof. Interested readers are referred to [15] for the proof of this result.

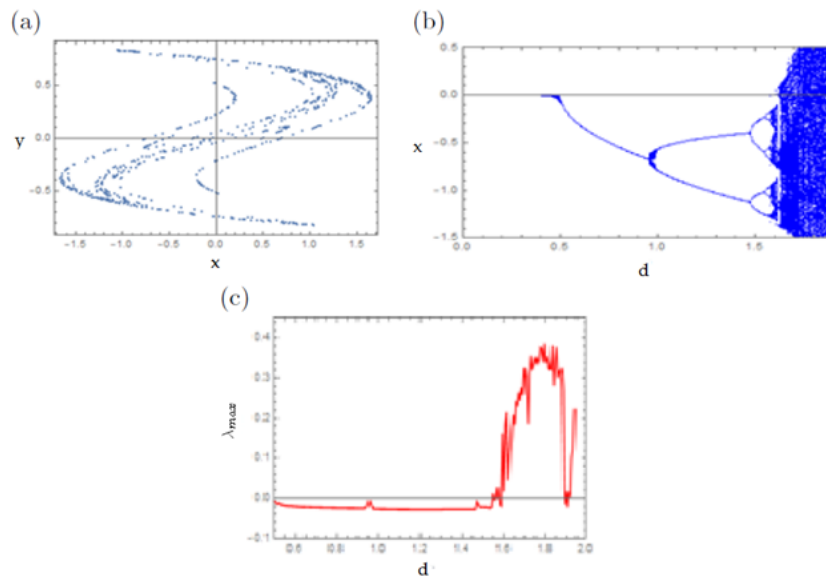


**Figure 1:** (a) Phase portrait of the Ushio system for  $\nu = 0.95$  and  $d = 19$ , (b) The bifurcation diagram versus  $d$ , (c) the largest Lyapunov exponents corresponding to (b).

**Theorem 3.1** Let  $x = 0$  be an equilibrium point of the nonlinear discrete fractional system

$${}^C_h \Delta_a^\nu X(t) = f(t + \nu h, X(t + \nu h)), \quad t \in (h\mathbb{N})_{a+(1-\nu)h}. \quad (6)$$

If there exists a positive definite and decrescent scalar function  $V(t, X(t))$ , such that  ${}^C_h \Delta_a^\nu V(t, X(t)) \leq 0$ , then the equilibrium point is asymptotically stable.

In the following, a useful inequality for Lyapunov functions is introduced.

**Lemma 3.1** [15] For any discrete time  $t \in (h\mathbb{N})_{a+(1-\nu)h}$ , the following inequality holds:

$${}^C_h \Delta_a^\nu X^2(t) \leq 2X(t + \nu h) {}^C_h \Delta_a^\nu X(t), \quad 0 < \nu \leq 1. \quad (7)$$

**Theorem 3.2** The two-dimensional fractional Ushio system can be stabilized under the one-dimensional control law

$$\mathbf{C}(t) = -dx(t) - 1.5y(t), \quad t \in (h\mathbb{N})_{a+(1-\nu)h}. \quad (8)$$

**Proof.** The controlled fractional Ushio system involves the time-varying control parameter  $\mathbf{C}(t)$  and is given by

$$\begin{cases} {}^C_h \Delta_a^\nu x(t) = (d-1)x(t + h\nu) - x^3(t + h\nu) + y(t + h\nu) + \mathbf{C}(t + h\nu), \\ {}^C_h \Delta_a^\nu y(t) = 0.5x(t + h\nu) - y(t + h\nu), \end{cases} \quad (9)$$

where  $t \in (h\mathbb{N})_{a+(1-\nu)h}$ . Substituting the proposed control law (8) into (9) yields the simplified dynamics

$$\begin{cases} {}^C_h \Delta_a^\nu x(t) = -x(t + h\nu) - x^3(t + h\nu) - 0.5y(t + h\nu), \\ {}^C_h \Delta_a^\nu y(t) = 0.5x(t + h\nu) - y(t + h\nu). \end{cases} \quad (10)$$

Now, we should prove that the trivial solution of (10) is globally asymptotically stable. If so, we will deduce immediately that all the states of the controlled system given in (9) will definitely converge towards zero. Actually, this task can be performed using the Lyapunov method that was summarized earlier by Theorem 3.1. To see this, the following Lyapunov function has to be considered:

$$V(x(t), y(t)) = \frac{1}{2} (x^2(t) + y^2(t)), \quad t \in (h\mathbb{N})_{a+(1-\nu)h}. \tag{11}$$

Consequently, applying the fractional Caputo  $h$ -difference operator to (11) leads us to the following assertion:

$${}_h^C \Delta_a^\nu V(x(t), y(t)) = \frac{1}{2} ({}_h^C \Delta_a^\nu x^2(t) + {}_h^C \Delta_a^\nu y^2(t)). \tag{12}$$

Using Lemma 1 yields

$$\begin{aligned} {}_h^C \Delta_a^\nu V(x(t), y(t)) &\leq x(t + \nu h) {}_h^C \Delta_a^\nu x(t) + y(t + \nu h) {}_h^C \Delta_a^\nu y(t) \\ &= -x^2(t + h\nu) - x^4(t + h\nu) - 0.5x(t + \nu h)y(t + h\nu) \\ &\quad + 0.5y(t + h\nu)x(t + h\nu) - y^2(t + h\nu) \\ &= -(x^2(t + h\nu) + x^4(t + h\nu) + y^2(t + h\nu)) \\ &< 0. \end{aligned}$$

This means that an efficient stabilization for all states of system (1) occurs at the origin when using the linear control law (8).

For the purpose of confirming the validity of the established controller, the phase-space and the evolution of all states of the controlled system (9) are plotted as shown in Figure 2. Such plots clearly show a stabilization at zero occurs for all chaotic dynamics of the fractional Ushio system given in (1) when using the linear control law given in (8).

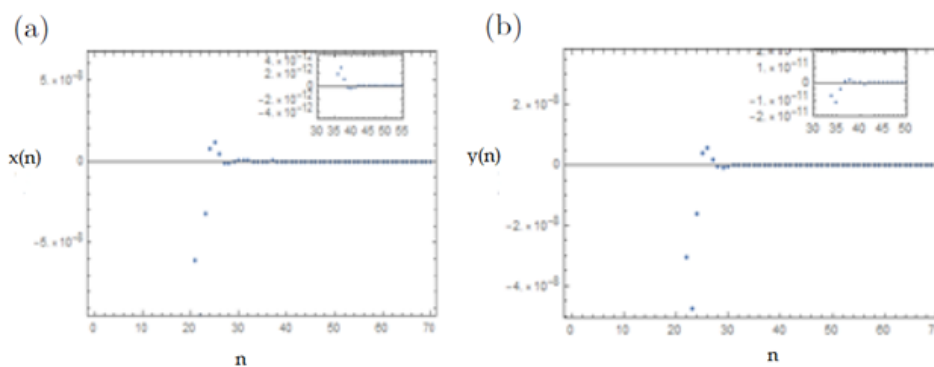


**Figure 2:** Stabilization of all states of the fractional chaotic Ushio system (1) by using the control law (8) with  $\nu = 0.95$  and  $d = 1.9$ .

### 4 Conclusion

This work has made a contribution to this research field by proposing simple linear control laws for stabilizing the dynamics of some types of those fractional maps which have been

established in view of the Caputo  $h$ -difference operator. The objective has been achieved by proving a new theorem based on assuming suitable Lyapunov functions. Since the designed control law is one-dimensional and linear, it is inexpensive and easy to implement. Finally, simulation findings have been implemented with the aim of highlighting the validity of all proposed control schemes.

## References

- [1] C. Goodrich and A. C. Peterson. *Discrete Fractional Calculus*. Springer, Berlin, Germany, 2015.
- [2] T. Abdeljawad. Dual identities in fractional difference calculus within Riemann. *Adv. Differ. Equ.* **2013**: 36, 1–16.
- [3] G. C. Wu, M. Luo, L. L. Huang and S. Banerjee. Short memory fractional differential equations for new memristor and neural network design. *Nonlinear Dyn.* **100** (2020) 3611–3623.
- [4] M. Edelman, E. E. Macau and M. A. Sanjuan (Eds.). *Chaotic, Fractional and Complex Dynamics: New Insights and Perspectives*. Springer International Publishing, 2018.
- [5] M. Mellah, A. Ouannas, A. A. Khennaoui and G. Grassi. Fractional discrete neural networks with different dimensions: coexistence of complete synchronization, antiphase synchronization and full state hybrid projective synchronization. *Nonlinear Dynamics and Systems Theory* **21** (4) (2021) 410–419.
- [6] A. Ouannas, A. A. Khennaoui, S. Momani, G. Grassi, V. T. Pham, R. El-Khazali and D. V. Hoang. A Quadratic Fractional Map without Equilibria: Bifurcation, 0–1 Test, Complexity, Entropy, and Control. *Electronics* **9** (5) (2020) 748.
- [7] A. Ouannas, A. A. Khennaoui, S. Bendoukha, Z. Wang and V. T. Pham. The Dynamics and Control of the Fractional Forms of Some Rational Chaotic Maps. *Journal of Systems Science and Complexity* (2020) 1–20.
- [8] A. A. Khennaoui, A. Ouannas, S. Bendoukha, G. Grassi, R. P. Lozi and V. T. Pham. On fractional-order discrete-time systems: Chaos, stabilization and synchronization. *Chaos, Solitons & Fractals* **119** (2019) 150–162.
- [9] A. A. Khennaoui, A. Ouannas, S. Boulaaras, V. T. Pham and A. T. Azar. A fractional map with hidden attractors: chaos and control. *Eur. Phys. J. Special Topics* **229** (2020) 1083–1093.
- [10] A. Zarour, A. Ouannas, C. Latrous and A. Berkane. Linear Chaos Control of Fractional Generalized Henon Map. *Nonlinear Dynamics and Systems Theory* **21** (2) (2021) 216–224.
- [11] T. Ushio. Chaotic synchronization and controlling chaos based on contraction mappings. *Physics Letters A* **198** (1) (1995) 14–22.
- [12] T. Abdeljawad. On Riemann and Caputo fractional differences. *Computers & Mathematics with Applications* **62** (3) (2011) 1602–1611.
- [13] G. Anastassiou. Principles of delta fractional calculus on time scales and inequalities. *Math. Comput. Model.* **52** (3–4) (2010) 556–566. (2010)
- [14] D. Mozyrska and E. Girejko. Overview of fractional  $h$ -difference operators. In: *Advances in Harmonic Analysis and Operator Theory*. Birkhäuser, Basel. (2013) 253–268.
- [15] D. Baleanu, G. C. Wu, Y. R. Bai and F. L. Chen. Stability analysis of Caputo-like discrete fractional systems. *Communications in Nonlinear Science and Numerical Simulation* **48** (2017) 520–530.